High-resolution regional modelling of changing extreme precipitation

Dissertation
zur Erlangung des Doktorgrades
der Mathematisch-Naturwissenschaftlichen Fakultät
der Christian-Albrechts-Universität zu Kiel

vorgelegt von
Edmund P Meredith

Kiel, Oktober 2015

GEOMAR Helmholtz-Zentrum für Ozeanforschung Kiel
Forschungsbereich 1
– Maritime Meteorologie –

Erster Gutachter: Prof. Dr. Mojib Latif
Zweiter Gutachter: Prof. Dr. Douglas Maraun

Tag der mündlichen Prüfung: 3. Dezember 2015
Zum Druck genehmigt: 3. Dezember 2015

gez. Prof. Dr. Wolfgang J. Duschl, Dekan

Contents

Abstract

Extreme precipitation is of interest because of the often dramatic effects that it can have on society and the environment. Observed changes in the frequency and strength of intense precipitation events in some regions since the mid 20th century have underlined the importance of understanding how extreme precipitation responds to a changing climate. In particular, identification of fine-scale processes which modulate the regional-scale response of extreme precipitation to climate change may be key to this understanding. Of similar importance is the identification of specific forcings which may amplify regional precipitation extremes. For example, over the Black Sea and Mediterranean (BSM) region the potential for extreme summertime convective precipitation has grown alongside substantial sea surface temperature (SST) increase since the early 1980s. Due to often insufficient data, however, extreme precipitation is difficult to study using observations alone. Physically based numerical models of the climate system are a vital tool for studying extreme precipitation and its climate change signal. How extreme precipitation is represented in climate models, and how this may be improved, is thus also an important topic. Climate model resolution, for example, is known to affect both the climate change signal and present-day representation of extreme precipitation. In this thesis, high-resolution regional modelling experiments are used to study these topics, with a focus on the BSM region.

The added value of high-resolution regional models, at up to convection-permitting resolution, compared to coarser resolution global models for reproducing observed extreme precipitation events is first established (chapter 3). This then serves as a basis for convection-permitting ensemble sensitivity experiments with a regional atmospheric model which study the role of SST increase in the amplification of convective precipitation extremes in the BSM region (chapter 4). The July 2012 precipitation extreme in the Black Sea town of Krymsk is taken as a showcase example and simulated under a range of SST forcings representative of past, present and future SST regimes. The crucial role of recent SST increase in the intensity of the event is revealed, allowing the extremeness of the precipitation to be attributed, conditional on the given synoptic pattern, to the observed changes in SSTs. The enhancement of lower tropospheric instability due to the current warmer Black Sea allows deep convection to be more easily triggered, increasing simulated precipitation in the Krymsk region by more than 300% relative to simulations with SSTs

characteristic of the early 1980s. Additionally, a highly nonlinear precipitation response to incremental SST increase suggests that the Black Sea has exceeded a regional threshold for the intensification of convective extremes. The nonlinear response is manifested as an initially sharp increase in precipitation intensity as higher SSTs trigger deep convection, which then levels-off with further SST increase. The physical mechanism identified indicates that BSM coastal regions may face abrupt amplifications of convective precipitation under continued SST increase, and illustrates the limitations of thermodynamical bounds for estimating the temperature scaling of convective extremes.

In light of the highly nonlinear precipitation response to incremental SST increase found in the convection-permitting sensitivity simulations of the Krymsk extreme, the added value of convection-permitting models for simulating changes in convective extremes is explored in chapter 5. This is done by comparing how the intensity of the Krymsk event responds to increasing SSTs in simulations with explicit and parametrized convection. Compared at the same spatial scale, the strongly nonlinear extreme precipitation response to SST increase in the convection-permitting simulations is not evident when convection is parametrized. The physical mechanisms behind the different responses are the focus of chapter 5, revealing that the flattened response in the convection-permitting simulations results from an improved representation of convective downdraughts and near-surface cooling, which damp the further intensification of precipitation by stabilizing the lower troposphere locally and affecting how and where subsequent convection is triggered. These features are not well represented in the parametrized convection simulations, resulting in precipitation intensity having a much more linear response to increasing SSTs.

Zusammenfassung

Extremniederschlag hat oft dramatische Auswirkungen auf Gesellschaft und Umwelt und ist deshalb von großem Interesse. Beobachtete Änderungen in Starkregenhäufigkeit und -intensität seit Mitte des 20. Jahrhunderts zeigen, wie wichtig es ist zu verstehen, wie Extremniederschlag auf den Klimawandel reagiert. Kleinskalige Prozesse zu identifizieren kann entscheidend zum Verständnis, wie Extremniederschlag auf regionaler Skala vom Klimawandel beeinflusst wird, beitragen. Ähnlich wichtig ist es, Klimaantriebe zu identifizieren, die regionale Niederschlagsextreme verstärken können. So geht beispielsweise über der Schwarz- und Mittelmeerregion (BSM) ein Anstieg des Potentials für konvektiven Extremniederschlag im Sommer mit dem erheblichen Anstieg der Meeresoberflächentemperatur (SST) seit den frühen 1980er Jahren einher. Durch eine oft unzureichende Datenlage ist es allerdings schwierig, Extremniederschlag nur anhand von Beobachtungen zu untersuchen. Physikalisch basierte numerische Modelle des Klimasystems sind deswegen ein wichtiges Werkzeug, um Extremniederschlag und dessen Klimawandelsignal zu erforschen. Wie Extremniederschlag in Klimamodellen dargestellt ist und wie dies verbessert werden kann, ist somit ebenfalls ein wichtiges Thema. Die Auflösung des Klimamodells ist beispielsweise dafür bekannt, sowohl das Klimawandelsignal als auch die Darstellung gegenwärtigen Extremniederschlags zu beeinträchtigen. In dieser Dissertation werden hochauflösende Simulationen mit einem regionalen Klimamodell genutzt, um diese Themen mit einem Schwerpunkt auf der BSM-Region zu untersuchen.

Zunächst wird der Mehrwert von hochaufgelösten regionalen Modellen bis hin zu konvektionszulassender Auflösung gegenüber gröber aufgelösten globalen Modellen, um beobachtete Extremniederschlagsereignisse zu reproduzieren, nachgewiesen (Kapitel 3). Dies dient als Grundlage für konvektionszulassende Sensitivitätsexperimente mit einem regionalen atmosphärischen Modell, welche die Rolle der Meereserwärmung auf die Verstärkung konvektiver Extremniederschlagsereignisse in der BSM-Region untersuchen (Kapitel 4). Hier dient das Niederschlagsextrem im Juli 2012 in der Stadt Krymsk an der Schwarzmeerküste als Fallbeispiel. Dieses wird über ein breites Spektrum unterschiedlicher SST-Antriebe simuliert, welche repräsentativ für vergangene, gegenwärtige und zukünftige SST-Regime sind. Die entscheidende Rolle des jüngsten SST-Anstiegs für die Intensität des Ereignisses wird aufgezeigt. So kann der extreme Niederschlag, unter der Voraussetzung der gegebenen Wetterlage, dem beobachteten SST-Anstieg zugeschrieben werden. Aufgrund der

verstärkten Instabilität in der unteren Troposphäre durch das derzeit wärmere Schwarze Meer kann Tiefenkonvektion einfacher ausgelöst werden. Dadurch hat das simulierte Starkniederschlagsereignis in der Krymskregion eine um mehr als 300% erhöhte Intensität verglichen mit Simulationen, welche mit kühleren SSTs, die charakteristisch für die frühen 1980er Jahre sind, angetrieben wurden. Ferner deutet ein stark nicht lineares Verhalten des Niederschlags bei schrittweiser Erhöhung der SSTs darauf hin, dass das Schwarze Meer einen regionalen Schwellwert für die Intensivierung konvektiver Extreme überschritten hat. Dieses nicht lineare Verhalten äußert sich durch einen zunächst starken Anstieg der Niederschlagsintensität mit steigenden SSTs, da höhere SSTs Tiefenkonvektion auslösen. Dieser Anstieg flacht dann trotz weiterem SST-Anstieg ab. Dieser physikalische Mechanismus deutet darauf hin, dass in BSM-Küstenregionen abrupte Konvektivsniederschlagsverstärkungen bei weiterem SST-Anstieg möglich sind. Weiterhin illustriert dies, dass die Abschätzung der Temperaturskalierung konvektiver Extreme durch thermodynamische Grenzen nur begrenzt möglich ist.

In Anbetracht der stark nicht linearen Reaktion des Niederschlags auf eine schrittweise SST-Steigerung, die durch die konvektionszulassenden Sensitivitätsexperimente aufgezeigt wurde, wird der Mehrwert konvektionszulassender Regionalmodelle für die Simulation von Änderungen konvektiven Extremniederschlags in Kapitel 5 untersucht. Hierzu wird verglichen, wie das Krymsk-Ereignis auf ansteigende SSTs mit expliziter und parameterisierter Konvektion reagiert. Verglichen auf derselben räumlichen Skala ist diese stark nicht lineare Reaktion des Niederschlags auf steigende SSTs aus dem konvektionszulassenden Modell im Modell mit parameterisierter Konvektion nicht ersichtlich. Die physikalischen Prozesse, welche verantwortlich für diese unterschiedlichen Modellergebnisse sind, sind der Fokus in Kapitel 5. Die abflachende Niederschlagsintensität in der konvektionszulassenden Simulation ist eine Folge der verbesserten Darstellung konvektiver Fallböen und obenflächennaher Abkühlung, welche durch lokale Stabilisierung der unteren Troposphäre die Intensivierung des Niederschlags dadurch weiter dämpfen, dass eine weitere Verstärkung der lokalen Konvektion verhindert wird, und ferner beeinflusst wird, wie und an welcher Stelle anschließende Konvektion ausgelöst wird. Diese Prozesse sind in den Simulationen mit parameterisierter Konvektion nicht gut dargestellt. Dies führt dazu, dass die Niederschlagsintensität deutlich linearer auf ansteigende SSTs reagiert.

1 Introduction

Extreme weather and climate events have the potential to seriously affect society. Understanding the causes of extreme meteorological phenomena and the mechanisms by which they may be amplified is thus an important challenge. In particular, extreme precipitation events often rapidly develop and intensify, limiting the efficacy of early-warning systems and wreaking havoc on communities. For example, in July 2012 the Black Sea town of Krymsk suffered over 170 deaths following the development of an intense convective system which brought record precipitation [Kotlyakov et al., 2013].

In a changing climate, it is most likely to be changes in the extremes, rather than the mean, that will have the most dramatic effects on society. Weather and climate extremes, however, are by definition rare meteorological events and are thus difficult to study using observational records, which often cover insufficiently long time periods. In this respect, physically-based numerical models of the climate system are an invaluable tool for assessing how the characteristics of extreme events may respond to a changing climate. Evaluation of how the physical mechanisms causing extremes are represented in such models, and how their representation may be improved, is thus also an important challenge. Climate models which realistically reproduce the physical process chains that cause observed extremes offer confidence that they will also realistically capture the response of such extremes to changes in the climate system. This is particularly true for extreme precipitation, which is one of the most difficult meteorological variables to accurately model. Indeed, due to insufficient horizontal resolution the current generation of global climate models need to parametrize many of the processes which lead to precipitation, based on rather generalised assumptions. As a result, extreme precipitation is often poorly represented, casting doubt on how well the response of extreme precipitation to climatic changes is modelled.

1.1 Changes in (Extreme) Precipitation under Climate Change

Precipitation, both mean and extreme, is expected to become more intense in a warmer climate [Allen and Ingram, 2002; Trenberth et al., 2003]. In particular, the character of precipitation - as opposed to the global mean total - is most likely to change in a changing climate; this includes characteristics such as frequency, intensity and event duration [Trenberth et al., 2003]. Such changes are made possible by the enhanced levels of atmospheric moisture that can be achieved at higher temperatures. As temperature increases, so too does the saturation vapour pressure of water, allowing higher levels of water vapour to feed into precipitating systems. Absent significant changes in circulation patterns or relative humidity, higher temperatures result in an overall stronger hydrological cycle - enhanced evaporation in areas with net evaporation and enhanced precipitation in areas with net precipitation [Trenberth, 2011; Held and Soden, 2006].

The saturation vapour pressure of water increases exponentially with temperature, at a rate of roughly 6.5% K^{-1} following the Clausius-Clapeyron (CC) relation. This relationship is observed to approximately hold on a global scale, though much more closely over the oceans than over land ($\sim$5.9% K^{-1} vs. $\sim$4.3% K^{-1}) [Dai, 2006]. The scaling of atmospheric water vapour with increasing temperature is limited by the availability of evaporable water. While this is not an issue over the oceans, the lower observed scaling over land is attributable to the often limited availability of evaporable water in inland areas [Ye and Fetzer, 2010]. This fact implies that the risk of intensified precipitation extremes due to thermodynamic effects should be greatest in areas with a strong maritime influence.

Despite the scaling of atmospheric moisture at up to the rate implied by the CC relation, it has been shown in GCM studies that global mean precipitation scales at about half this rate, as the strength of the overall hydrological cycle is limited by the ability of the troposphere to radiate away latent heat released during precipitation [Allen and Ingram, 2002]. Extreme precipitation events though, it has been argued, are likely to result from instances in which the greatest percentage of available moisture is converted to precipitation and should thus scale close to the CC rate [Allen and Ingram, 2002], significantly faster than the mean. Indeed, observed extremes of daily precipitation brought about by large-scale stratiform precipitation have been found to scale at approximately the CC rate [Berg et al., 2013]. The scaling of sub-daily precipitation extremes, however, may be even higher.

Aside from broad thermodynamical considerations, extreme precipitation also responds sensitively to dynamical changes, such as in circulation patterns or storm dynamics [Emori and Brown, 2005; Berg et al., 2013], with local factors such as orography also potentially influencing the response of extreme precipitation to warming. In particular, convective extremes - which typically occur at sub-daily timescales - are strongly influenced by mesoscale dynamics and may scale above the CC rate [Lenderink and van Meijgaard, 2008; Berg et al., 2013]. This most likely results from the increased latent heat release that will be found in convective events occurring in warmer, and hence moister, environments; increased latent heat release drives stronger updraughts and increased compensating horizontal moisture convergence, both leading to more intense precipitation. Such feedbacks and the observed super-CC scaling imply that factors other than increased moisture availability can also impact changes in precipitation extremes. Changes in static stability can also play an important role. Observed and projected warming trends are not homogeneous across the different levels of the atmosphere. Under the RCP4.5 scenario, for example, the CMIP5 ensemble mean shows stronger warming in the upper troposphere than in the lower troposphere, with the exception of in the polar latitudes [Bayr, 2013 (Fig. 1.1)]. This is strongest in the tropics, where the altered lapse rate should increase static stability. In the polar regions, however, higher low-level warming primarily due to melting sea ice - which also increases moisture availability from the oceans - should have the opposite effect on static stability. To a lesser extent, higher low-level warming is also evident in parts of the higher mid-latitudes. In short, the response of extreme precipitation to a changing climate is likely determined by the net contribution of factors which in some regions may have opposing effects on extreme precipitation.

For well over a decade there has been strong evidence that the nature of precipitation is changing [Trenberth et al., 2003], as expected from theory. Globally averaged indices of extreme precipitation and average daily precipitation intensity show upward trends over the last 60 years [Groisman et al., 2005; Donat et al., 2013; Seneviratne et al., 2012]. While trends in temperature extremes over the same period are widespread and significant, trends in precipitation extremes are much more spatially heterogeneous and are robust mostly only over the extratropics, in particular in North America (east of the Rockies) and eastern Europe [Groisman et al., 2005; Donat at al., 2013]. Trends also vary seasonally. In eastern Europe, for example, significant increases in precipitation intensity and extremes are evident during summer, despite a slight drying tendency in parts of this region during winter [Moberg et al., 2006 (Fig. 15 e,f)]. Intense precipitation in this region usually occurs during the summer and is of a convective nature, with stratiform precipitation dominant in the winter [Groisman et al., 2005]. This highlights how different classes of precipitation can respond differently to a changing climate.

Into the future, global climate models also project an increase in heavy precipitation, robust mainly over the tropics and high latitudes [Semenov and Bengtsson, 2002; Kharin et al., 2007; Orlowski and Seneviratne, 2012]. Modelling of changes in extreme precipitation, however, is not straightforward and questions remain in particular over the ability of current coarser resolution climate models to accurately simulate changes in convective precipitation. The intensity of modelled extreme precipitation, for example, appears to deviate further from observations as temperatures increase, suggesting poorer model performance as precipitation of a convective nature begins to dominate, as is the case at higher temperatures [Lenderink and van Meijgaard, 2008 (Fig. 1)]. This can undoubtedly be improved by increasing model resolution, especially to resolutions that no longer require that convective processes be parametrized [e.g. Kendon et al., 2014] (referred to as 'convection-permitting resolution'), or with improved model parametrizations. This is an issue that will be explored later in the thesis.

1.2 Studying Extreme Precipitation using Regional Models

This topic is explored in more detail in subsequent chapters, but is discussed here briefly to help provide a context for the research foci presented in §1.3.

Unlike many common meteorological variables, for instance temperature, sea-level pressure or humidity, precipitation is highly variable in both space and time. Due to its high spatial variability, the accurate simulation of precipitation, especially extreme precipitation, stands to benefit greatly from higher model resolution. Increased resolution not only adds small-scale detail to simulated precipitation, but importantly also more realistically simulates the physical processes that can play a crucial role in amplifying or damping the intensity of precipitating systems. Higher resolution, however, comes with the drawback of increased computational expense, often making the desired resolution simply not feasible. To achieve higher model resolution while limiting the increase in computational expense, regional models - alternatively referred to as 'limited area models' (LAMs) - are a useful tool. As the name suggests, regional models can be run over a small portion of the globe, allowing a much higher resolution than would be computationally affordable in a global model. At the edges of the regional simulation domain, coarser global model data is interpolated to the resolution of the LAM in order to provide lateral boundary conditions, which can be regularly updated. Improvements in simulated precipitation - both mean and extreme - offered by this technique have been demonstrated in several studies, see for example the reviews by Maraun et al. [2009] and Rummukainen [2010]. The level of value added to the simulation of precipitation provided by increased LAM resolution, however, varies considerably depending on factors such as region, topography, season, type of precipitation, and accumulation period. Increased LAM resolution also affects the simulation of changes in precipitation extremes, which is important in the context of a changing climate. Different resolution models can produce quite different climate change signals for certain types of extreme precipitation, most notably for summertime convective precipitation when convection-permitting resolutions are reached. The known scope of the added value for studying extreme precipitation obtainable from regional climate models

(RCMs) has been extended in a number of recent studies [e.g. Kendon et al., 2014; Ban et al., 2015; Torma et al., 2015], and will be further built on in this thesis.

1.3 Research Foci and Thesis Outline

Preceding the research foci outlined below, **chapter 2** introduces some key background and concepts which are important for understanding the subsequent chapters where the research foci are addressed.

The added value of RCMs for simulating observed extreme precipitation events

Simulation of extreme precipitation remains a considerable challenge for numerical models, with models often needing to capture a complex chain of processes which produce the extreme precipitation, such as moisture convergence, condensation, and the triggering of deep convection. The ability of models, particularly global models, to accurately capture these processes is often hampered by insufficient model resolution, meaning that key mechanisms by which extreme precipitation is caused cannot be resolved by the model. Where this is the case, such processes need to be accounted for by model parametrization schemes. Convective parametrization schemes, for example, are designed to take account of sub-grid scale convective processes, i.e. those not resolved by the model. Without the parametrization of convection in models with horizontal resolution coarser than about 5 km, convective potential energy would build up over too large an area and too long a time period, producing unrealistically intense grid-scale precipitation when convection eventually is triggered, and overly active low-level cyclogenesis.

The priority of such schemes, however, is to perform well under the most common atmospheric conditions, meaning that they often perform poorly under extreme conditions. Increased resolution in RCMs thus allows an increasing fraction of key processes to be resolved by the model, adding value to the simulation of extreme precipitation. The range of resolution increase over which value continues to be added to the simulation of extreme precipitation varies depending on the nature of the precipitation; extreme precipitation brought about by large-scale systems in the mid- to high-latitudes is often reasonably well represented in relatively coarse global models, especially in winter [Volosciuk et al., 2015]. For localized precipitation extremes of a convective nature, however, RCMs can continue to add value even as convection-permitting resolution is reached (finer than 4 km).

These aspects of RCM added value are explored in **chapter 3**, where the ability of a regional model to accurately simulate two recent extreme precipitation events is tested. Two recent summertime precipitation extremes - one resulting from mesoscale forcings and the other from synoptic scale forcings - are selected, presenting quite different challenges for the model and thus necessitating different modelling strategies.

Identification and understanding of mechanisms by which extreme precipitation events may be amplified

Under global climate change, fine-scale processes are expected to play an important role in modulating the climate change signal of extreme events at the regional scale [Diffenbaugh et al., 2015], which could result in either an enhancement or diminution of the large-scale signal. Identifying such processes, the specific forcings that drive them, and the mechanisms by which they regulate extreme precipitation events is thus important for regional planning and adaptation. Such information is difficult to obtain from standard transient climate simulations though, as increasing carbon-dioxide levels affect multiple components of the climate system and their individual impacts on extreme precipitation can be difficult to disentangle.

Regional sensitivity studies are an efficient manner in which to identify the contribution of changes in individual forcings to observed extreme events. In such studies, an observed event is studied under two different scenarios - first simulated with all forcings as observed during the event, and then again with recent trends removed from one of the forcing fields. The limited area setup enables the event to be simulated at the most appropriate resolution, however high that may be. Studies adopting this approach have looked at, for example, the impact soil moisture anomalies on the 2003 heatwave in Europe [Fischer et al., 2006] or the impact of unusually warm sea surface temperatures (SSTs) on the intensity of Hurricane Juan [Fogarty et al., 2006]. While this binary sensitivity approach, i.e. the difference between present and past, can be highly instructive, it also potentially misses out on any nonlinearity in the relationship between event intensity and forcing strength.

Focusing on extreme precipitation in coastal regions, in **chapter 4** the July 2012 Krymsk precipitation extreme (§3.2) is taken as a showcase example to study the role of increasing SSTs in amplifying convective precipitation extremes. The intensity of the event is examined over 11 different SST states, representative of past, present and future climate states, which allows any nonlinear relationships to be revealed.

Attribution of recent extreme precipitation events to changes in the climate system

High profile extreme events often illicit a public demand to know whether or not the event was a result of global warming. While general trends in extreme precipitation due to climate change can be straightforwardly studied using climate model simulations, the contribution of climate change to an individual event can be more difficult to pinpoint and quantify. The field of extreme event attribution (discussed in detail in §2.3) seeks to address this question. One approach is to use global coupled models to simulate present and past climates, i.e. how the climate would have looked without humans, and compare the relative probabilities of a certain event in both climates [e.g. Lott et al., 2013]. Another approach is that of 'conditional event attribution' [Trenberth et al., 2015] which asks how, given an observed circulation pattern which accompanied an extreme, the intensity of the extreme was affected by known changes in the climate system's thermodynamic properties.

The latter approach is ideal for regional modelling experiments, and is used in **chapter 4** to examine whether the intensity of the July 2012 Krymsk precipitation extreme can be attributed to the warming that has been observed in the Black Sea since the early 1980s.

The added value of convection-permitting models for studying changes in extreme precipitation

Convection-permitting models (CPMs) represent the cutting-edge in modelling of extreme precipitation, for both weather and climate applications. In such models, the very-high horizontal resolution (under 4 km) allows convective processes to be explicitly resolved, thus removing the need for convective parametrizations. As supercomputers become more powerful, the use of CPMs is becoming more prevalent, even at decadal timescales. With this, the added-value of CPMs for simulating extreme precipitation, and the corresponding climate change signal, is a topic of active research. Studies to date have shown the added value of CPMs for (i) weather forecasts of extreme precipitation [e.g. Lean et al., 2008], (ii) improving the accuracy of the simulated climatology of summertime sub-daily extreme precipitation, and (iii) for projections of summertime sub-daily extreme precipitation based on roughly decade-long past and future integrations [e.g. Kendon et al., 2014; Ban et al., 2015]. Lacking in the literature have been studies examining the physical mechanisms by which models with explicit and parametrized convection can produce differing responses of extreme precipitation to warming.

This gap is addressed in **chapter 5**, where the response of extreme coastal precipitation to

SST increase is compared between simulations using parametrized and explicit convection. To again study any nonlinearities in the relationship, this is done across 11 different SST states using the Krymsk precipitation extreme as a showcase example. The physical mechanisms behind the shapes of the extreme precipitation responses to SST increase in the two different resolution models, and any differences which may exist, are also explored with the goal of pinpointing the sources of the added value that CPMs provide.

2 Concepts and Methods

In this chapter, concepts and methods important for understanding of the subsequent chapters are introduced. This includes an overview of the limited area modelling technique, how limited area modelling adds value, and how/when it can be used as a tool for sensitivity experiments - all with an emphasis on extreme precipitation. Additionally, the limited area model (LAM) used throughout this thesis is introduced, alongside its basic setup. Attribution of extreme events is also discussed.

2.1 Regional Modelling and Extreme Precipitation

2.1.1 Development of Regional Modelling

The development of numerical weather prediction (NWP) with computers in the 1950s and 1960s from single-level barotropic models, to multi-level baroclinic models, to the Deutscher Wetterdienst's pioneering implementation of operational primitive-equation models in 1966 saw a constant improvement in the simulation and prediction of synoptic-scale atmospheric fields, such as geopotential height and sea-level pressure [Lynch, 2006]. Improvements in the modelling of synoptic-scale meteorological fields, though, were not matched at the smaller scales at which impactful weather is often experienced (mesoscale). In particular, precipitation exhibits a high level of spacial variability at mesoscales and improvement of forecasts was thus very slow [Anthes, 1983]. The need for higher resolution models to improve the representation of mesoscales was constrained by the associated increase in computational expense, thus motivating increased research into the development of regional, or limited-area, NWP models [Anthes, 1983]. By the early 1970s, the first limited-area fine-mesh model became operational in the U.S., running at horizontal resolutions of up to 127 km on a 6-level domain covering roughly one eight of the globe [Shuman, 1989]. These limited-area models (LAMs) were initially integrated over short 12-hour cycles, taking initial conditions from observations and without any update of the lateral boundary conditions. From these beginnings the nested regional modelling approach evolved, involving taking large-scale atmospheric conditions simulated by a global model and using them to provide regularly updated lateral boundary conditions for a higher resolution LAM over a domain of interest. Nested modelling can be either one-way or two-way, with the solution of the nested model feeding back to its parent in the latter[1]

2.1.2 Basic Principles of Regional Modelling

The nested regional modelling approach relies on the prescription of lateral boundary conditions taken from a coarser model, which may be global or regional. The solution of the coarser parent model is interpolated to the resolution of the nested model along the nested domain's outermost rows and columns, i.e. the lateral boundaries. Nesting ratios (i.e. the resolution increase from the parent domain) in the range of 3:1 to 5:1 are typical, though ratios of up to 12:1 have been shown to be workable [Denis et al., 2002]. The interpolation of coarse data to higher resolution at the lateral boundaries can lead to the generation of spurious gradients and noise, potentially generating inertial gravity waves that can rapidly propagate into the model interior [Warner, 1997]. To reduce these effects, relaxation or 'sponge' zones are typically implemented adjacent to the nested model's lateral boundaries, usually 5-10 grid cells wide. Within the sponge zone, the nested model's solution is relaxed towards that of the parent model via a weighting function. The weight given to the coarse model's solution decreases towards the internal edge of the sponge zone, where the so-called 'free zone' begins. The requirement to balance the model solution with that of it's parent domain at the lateral boundaries can often lead to areas of strong precipitation or other sharp gradients across the sponge zone at the domain outflow boundary, depending on how much the nested solution has deviated from that of its parent. In contrast to within the sponge zone, the model solution within the free zone is not an intrinsic function of the coarse model solution, unless interior nudging is applied. Standard atmospheric variables specified at the lateral boundaries are terms for humidity, pressure, temperature, geopotential height and horizontal winds. More sophisticated models may also communicate microphysical information, such as precipitate type, at the lateral boundaries.

While fixing the lateral boundary conditions generally reduces the sensitivity to initial conditions, especially for longer simulations, the location of the lateral boundaries, and thus the size of the domain, can have a strong influence on the model solution over the area of interest. To a first approximation, the bigger the domain the more freedom the nested model has to develop its own small-scale features and deviate from the solution of its parent. Depending on the application, the latter may or may not be desirable. Jones et al. [1995], studying the sensitivity of the climate change signal over Europe to the lateral boundary location in a nested RCM, propose the following criteria for producing realistic

---

[1] Unless stated otherwise, a 'nested' model is taken to be a one-way nested model throughout this document.

downscaled regional climatologies:

1. The coarser parent model must realistically reproduce the (large-scale) climate over the region of interest;
2. The RCM domain must be sufficiently small that the synoptic-scale flow does not deviate too far from that of the parent model;
3. The RCM domain must be sufficiently large that features on scales that cannot be realistically resolved by the parent model are free to develop over the region of interest.

While point one is essentially a truism, the implementation of points two and three can vary depending on factors such as season and region of the globe.

The strength of the lateral boundary forcing, i.e. how strong the cross-domain flow is, is a key determinant in how much the synoptic scale flow in the nested domain will deviate from that of it's parent. Rinke and Dethloff [2000] investigated this effect in a regional climate model with a pan-Arctic domain, centred on the north pole. As the strong zonal flow associated with the jet stream tends to circle the poles, regional domains centred on or near the poles typically experience a relatively weak forcing at the lateral boundaries, compared to similar domains centred in the mid-latitudes. Due to the slow speed at which boundary information transited through their circumpolar domain, Rinke and Dethloff observed a strong error growth in synoptic fields (relative to analyses), which took up to three weeks after initialization to stabilize, when a sort of quasi-equilibrium was reached between physically induced internal error growth and laterally induced internal error reduction. As they point out, this timescale depends strongly on the strength of advection from the lateral boundaries, as shown by Giorgi [1990]. Repeating the same experiment with a smaller domain, they were able to reduce error-growth by an order of magnitude, despite the still-weak lateral forcing. Returning to point two of Jones et al., sufficiently small is thus highly case-dependent. Analogous environments - where weak lateral forcing would be expected to cause stronger domain size sensitivity - could be expected in the tropics, as well as during mid-latitude summer [Seth and Giorgi, 1998].

An opposing situation to that presented in Rinke and Dethloff would be a mid-latitude domain during winter, when strongly zonal jet streams of up to 120 m s^{-1} are possible. In such a set-up, a rapid domain through-flow could be expected, quickly sweeping any small-scale deviations out of the domain before they had a chance to become developed mesoscale features. This would greatly reduce the potential of the higher-resolution RCM to add value to the forcing model. The inflow boundary of such a domain would thus need to be extended far upstream of the area of interest in order to satisfy point three of Jones et al.

How and where small-scale features develop in regional simulations is strongly related to the large-scale environment. An accurate representation of the large-scales is thus a prerequisite for realistic small-scale features to develop [Diaconescu et al., 2007]. To overcome the tendency of the large-scales in RCMs to drift from those of their parent, the spectral nudging technique [Waldron et al., 1996] has been applied to regional climate modelling [von Storch et al., 2000]. The application of this technique is based on the view that regional models cannot be relied on to consistently reproduce the evolution of sections of planetary scale features within their domain when they only receive lateral boundary information over much smaller areas. When spectral nudging is applied, the solution in the RCM interior is relaxed towards that of its parent model. Spectral nudging is applied at long wavelengths expected to be better represented in the parent model than in the nested model. Dynamic atmospheric variables - zonal and meridional winds, geopotential - are typically chosen for nudging, though thermodynamic variables such as temperature and humidity can also be nudged. Spectral nudging is most effective when applied in the middle and upper atmosphere, leaving the solution in the lower atmosphere free to benefit from the more realistic surface forcing (orography, sea surface temperature, etc.) that the higher-resolution RCM provides [von Storch et al., 2000]. The spectral nudging technique has been shown to be a highly effective tool for reducing the sensitivity of regional climate simulations to domain size and lateral boundary location [Miguez-Macho et al., 2004], resulting in a much-improved representation of local processes and a more accurate precipitation climatology [Miguez-Macho et al., 2005].

Aside from the strength of the boundary forcing, another relevant factor when designing a regional modelling experiment is the frequency at which the lateral boundary conditions are updated. This, too, can have a varying range of impacts on the internal solution. As the large-scale atmospheric components in RCMs tend to be slowly varying, updating daily is likely sufficient for large domains or domains with weak boundary forcing, though not necessarily optimal [Denis et al., 2002]. Improvement in RCM fields from increasing the temporal update frequency can be expected to come primarily at smaller scales, namely in features that vary rapidly over space and time, such as precipitation or vorticity. The limiting factor in the benefit gained from increasing the update frequency is thus the spatial resolution of the boundary data. Low-resolution boundary data are likely to well represent only large-scale features, which tend to travel slowly in space [Denis et al., 2002]. For higher-resolution driving data, benefit can be expected from a higher update frequency. Indeed, if nesting is run 'inline', i.e. if the driving model and nested domain are run concurrently, boundary information can be communicated at every time-step of the driving model. Smaller regional domains benefit in particular from a higher update frequency in situations with a rapid domain through-flow or a strong diurnal cycle. The former is most relevant in winter, for example fast moving storms, while the latter is more important in summer, when the daily convective cycle dominates [Giorgi and Mearns, 1999].

While downscaling is the motivation behind the RCM concept, where the nested model is used to reveal small-scale features that cannot be resolved in the forcing data [Rummukainen, 2010], the ability (or lack thereof) of unnudged regional models to improve simulation of the large-scale flow is also worth considering. Although research has focused almost exclusively on the improved simulation of small-scales in regional models, there are a handful of studies asking the opposite question [e.g. Mesinger et al., 2002; Veljovic et al., 2011; Diaconescu and Laprise, 2013]. Veljovic et al. [2011] demonstrated an improved placement of the jet stream in regional weather forecasts over the US, which they attributed to a combination of the improved representation of the Rocky Mountains and the use of the Eta coordinate system in the regional model. Focusing on multi-year simulations over North America, i.e. on timescales more akin to climate experiments, Diaconescu and Laprise [2013] found that, for RCMs driven by boundary conditions with only small errors, no improvement can be expected at the large-scales and that added value comes only at the small-scales. For RCMs driven by coarse boundary data with relatively large errors, however, some reduction in large-scale errors is possible when using very large domains. This improvement was only investigated for winter simulations; it's doubtful that similar improvements would be found in summer, when the zonal forcing is much weaker.

As a concluding remark, it should be remembered that nested regional models are no panacea. In the absence of quality lateral forcings, the RCM cannot be expected to produce quality downscaled results; this is the so-called garbage in, garbage out problem.

2.1.3 Internal Variability in Regional Climate Models

As there is no unique RCM solution to a given set of lateral boundary conditions, internal variability (IV; i.e. sensitivity to initial conditions) is an inherent feature of regional climate modelling. Quantification of RCM IV is thus important when seeking to understand regional climate sensitivity and feedbacks. Unlike in global modelling, though, RCM IV is constrained by the lateral boundary conditions, which place an upper limit on the impact of stochastic effects and hence the IV, dependent on many of the factors discussed in §2.1.2 (i.e. domain size, season, region, etc.). The existence of suitably large RCM IV, such that the growth of local features due to initial state perturbations, stochastic effects or changed surface forcings is not too strongly damped by the lateral boundary forcing, is thus also a prerequisite for carrying out regional sensitivity experiments. Without this, the internal RCM solution cannot respond realistically to changes in forcings.

Without considering the impact of domain size, Christensen et al. [2001] demonstrated that RCM IV for variables primarily influenced by local processes, such as summertime precipitation and evaporation, can be comparable to that found in atmospheric general circulation models (AGCMs). As discussed in §2.1.2, a larger domain and weaker throughflow give the RCM freedom to develop a more independent solution from that of its driving model. The existence of this freedom is directly related to RCM IV (Box 2-1). Using particularly large domains, Lucas-Picher et al. [2008] demonstrated that IV reaches a maximum close to the outflow boundary. This implies that the greater the transit time through a regional domain, the greater the IV. Even in situations with strong lateral boundary forcing, sufficiently large domains can therefore generate strong IV. It thus follows that the larger the RCM domain, the larger the ensemble size necessary to eliminate artefacts of IV from RCM climatologies.

For smaller mid-latitude domains, a clear annual cycle of IV exists, with greater IV found during the summer. As the domain size grows, however, this annual cycle steadily diminishes, already becoming indistinct for continental-scale domains [ibid.].

An additional influence on RCM IV may be found in the choice of physical parametrization schemes. In the case of regions where convective precipitation dominates, the convective parametrization can modulate the IV of the precipitation field, even on seasonal timescales [Cretat and Pohl, 2012]. Convective parametrization schemes which employ an ensemble approach to their convection trigger appear to produce less IV in the precipitation field [ibid.].

Box 2-1 | RCM Internal Variability

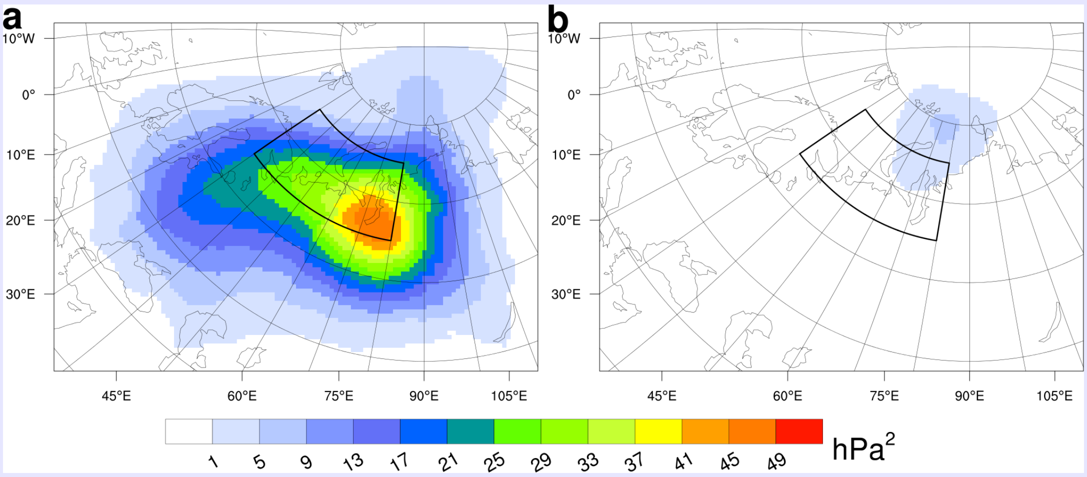

Figure 2.1: **Impact of Lateral Boundary Forcing on RCM IV.** Regional sensitivity experiments with the WRF model investigating the relative importance of local (i.e. surface) and large scale (i.e. lateral) forcings in the development of Eurasian winter blocking anticyclones. In panel **a**, a 20-member ensemble is created for winter 2005/06, a winter characterised by (then) record-low Barents-Kara sea ice cover and a strong blocking event over Eurasia which brought anomalously cold temperatures to Europe in January and early February [*Pethoukov and Semenov*, 2010]; variance of the sea-level pressure field during the period (see Figure 2.2) of peak anticyclone intensity is shown. Despite the strong internal variability within the regional domain, applying sea ice forcing from the winters of 1991 and 1969 - winters with moderate and high Barents-Kara sea ice levels, respectively - results in no statistically significant changes in anticyclone intensity (not shown). This is in contrast to similar experiments using global models [*Pethoukov and Semenov*, 2010; *Semenov and Latif*, 2015], suggesting a limited role for *local* sea ice feedbacks in the intensification of such blocking events. In panel **b** an identical model setup is employed as in panel **a** (including surface forcings), except that lateral boundary forcings are taken from the winter of 1988/89, a winter characterized by a particularly high Arctic Oscillation index and hence strong zonal flow. As can be seen, internal variability over the same time period virtually disappears from the domain under such strong lateral forcing. The anomalously low sea ice cover, as compared to that present in winter 1988/89, has little impact on the large-scale circulation under the RCM setup. Area averages over the region outlined in black are shown in Figure 2.2.

Continued on next page →

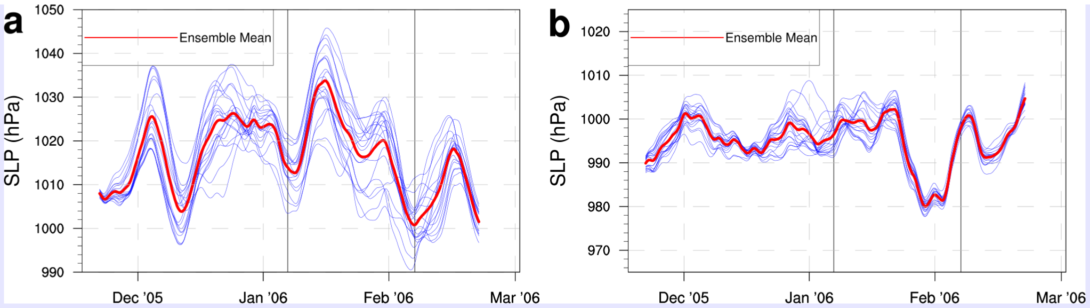

Figure 2.2: **RCM IV over extended period.** Area averaged sea level pressure over 65-75°N, 30-80°E (marked in Figure 2.1). Panel **a** shows all members of the ensemble described in Figure 2.1 (a), with panel **b** showing the same for Figure 2.1 (b). The period of winter 2005/06 peak anticyclone intensity is marked by black vertical lines and also corresponds to the period of maximum intra-ensemble spread in **a**. In contrast, little intra-ensemble spread is evident in **b** as any developing independent features are quickly swept out of the domain by the strong zonal flow.

2.1.4 Added Value of Regional Models for Simulating (Extreme) Precipitation

Precipitation, particularly convective precipitation, is highly variable in space and often generated through a chain of complex localized processes. This makes it one of the most difficult meteorological variables to model and accurately forecast. As such, precipitation is also one of the variables which most stands to benefit from the increased spatial resolution that regional models can provide. For the simulation of precipitation, the potential of higher-resolution regional models to add value to AGCM output varies according to season, geography, and temporal scale [Di Luca et al., 2012]. In addition, the level of added value (AV) gained for a given resolution increase will vary depending on whether means or extremes are being considered.

Surface or near-surface forcings - orography, land-sea contrasts, planetary boundary layer (PBL) turbulence, etc. - often play a crucial role in the initiation and maintenance of precipitation. The enhanced representation of surface forcings that can be achieved in regional models is thus a key source of AV. Simulation of precipitation in regions of complex topography benefits strongly from higher resolution, regardless of the season or temporal scale over which the statistics are calculated [Di Luca et al., 2012]. A higher horizontal resolution gives a more realistic orography field, and hence better represents orographically forced vertical motions, resulting in more accurate precipitation climatologies in regions where orographically enhanced precipitation plays an important role [Heikkilä et al., 2011].

Importantly, this added value is also observed at the same spatial scale as resolved by the driving AGCM [Torma et al., 2015]. Where such orographic precipitation is prevalent, the extra AV obtained from increasing to relatively high horizontal resolutions of close to 10 km is most apparent in the extremes [Heikkilä et al., 2011], though for convective extremes this is likely still too coarse [e.g. Hohenegger et al., 2008]. At coarser resolutions, local orographic features are mostly smoothed-out. The improved representation of surface altitude, and hence near-surface temperatures, also adds value over mountainous terrain by better determining the precipitate category, i.e. liquid or frozen.

A distinct seasonal variation in AV is also evident, with maximum AV coming during the warm season when convective precipitation plays a greater role [Di Luca et al., 2012]. The high mesoscale variability provided by regional models allows convective systems to develop and evolve in response to more localised forcings, in addition to any large-scale forcings from the background environment. Due to the more transient nature of convective systems and their associated triggers, as compared to large-scale stratiform precipitation, the AV at shorter temporal scales (i.e. sub-daily) is consequently much higher than the AV over longer accumulation periods (i.e. supra-daily) [ibid.].

While the aforementioned AV provided by high-resolution regional models marks a significant improvement on AGCMs, regional models which parametrize convective processes still have a tendency to misrepresent precipitation extremes. Convective processes generally need to be parametrized in models with horizontal resolution lower than about 4 km (convective parametrization is discussed in more detail in chapter 4.). In particular, models with parametrized convection create precipitation extremes that are too spatially widespread, not locally intense enough, and too temporally persistent, regardless of season [Kendon et al., 2012]. In this respect, convection permitting models (CPMs) that is, models which explicitly simulate convective processes provide additional AV. CPMs give an improved representation of important convective features, such as bow-echoes, squall-lines and mesoscale vortices [Weisman et al., 2008]. This in turn leads to more realistic local precipitation intensities [Lean et al., 2008]. The more realistic convective dynamics generated in CPMs also give a much improved simulation of the diurnal convective cycle [Prein et al., 2013], helping to make less persistent extremes. As a caveat, it should be noted that the primary AV of CPMs (for simulating precipitation) is not expected to come in terms of improved precipitation totals at point locations, though these may still be improved, in particular for intense events. Rather, the main AV can be expected to come in the form of improved area average precipitation totals, for example over a river catchment [Roberts, 2008].

Finally, it must be noted that the AV of RCMs is not limited to the representation of observed events and the present-day climate, but also includes the representation the corresponding climate change signal. This is explored in detail in chapter 5.

2.2 Model Description

All regional model simulations described in this thesis have been carried out with the Weather Research and Forecasting (WRF) Model [Skamarock et al., 2008], version 3.4.1.

The WRF model is a state-of-the-art mesoscale NWP model designed for both research and operational purposes. While WRF can be run globally, it is primarily used as a LAM at spatial resolutions ranging from mesoscale to sub-kilometre. The dynamical core solves the fully compressible nonhydrostatic equations, meaning that vertical velocity is explicitly calculated as a prognostic variable, unlike in coarse resolution AGCMs. The WRF horizontal grid uses Arakawa C-grid staggering. In the vertical, a terrain-following dry hydrostatic-pressure coordinate system is used, described as follows:

$$\sigma = \frac{p_h - p_{ht}}{p_{hs} - p_{ht}} \tag{2.1}$$

where $\mathrm{p_h}$ is the hydrostatic component of pressure and $\mathrm{p_{ht}}$ (constant) and phs are the values at the model top and surface, respectively. The model top is defined by a constant pressure level. Model levels are by default more concentrated at lower levels, but can also be explicitly defined. Lateral boundary conditions are specified at the outermost rows and columns of the model grid, which are separated from the free-zone by a relaxation zone, after Davies and Turner [1977], of user-defined width. Within the relaxation zone, the model prognostic variables are relaxed towards the coarse model data based on a weighting function which decreases (either linearly or exponentially) towards the innermost row/column of the relaxation zone. The WRF model includes a wide array of physical parametrization options. Unless stated otherwise, the physical parametrizations used in all of the presented experiments are as given in Table 2.1. Further details of the WRF model can be found in Skamarock et al. [2008].

Parametrization	Scheme	Reference
Cumulus Physics	Kain-Fritsch	Kain (2004)
Cloud Microphysics	WSM6	Hong and Lim (2006)
Shortwave Radiation	CAM SW	Collins et al. (2004)
Longwave Radiation	RRTM LW	Iacono et al. (2008)
Planetary Boundary Layer	Yonsei University scheme	Hong, Noh and Dudhia (2006)
Land Surface Physics	Unified Noah LSM	Tewari et al. (2004)
Surface Layer	MM5 Similarity scheme	Multiple (see § in References)

Table 2.1: Parametrization schemes used in WRF experiments

2.3 Attribution of Extreme Events

Extreme weather events often have serious societal and economic impacts. The 2003 European heat wave, for example, saw mortality rates increase by 54% in France during early August that year [Schär and Jendritzky, 2004]. Indeed, the beginning of the 21st century was marked by a number of notable meteorological extremes [Coumou and Ramstorf, 2012], many of which saw record precipitation totals. There is strong evidence of trends in certain types of extreme weather due to anthropogenic warming, for example intense precipitation [e.g. Zhang et al., 2007; Min et al., 2011] or temperature maxima and minima [e.g. Brown et al., 2008; Klein Tank and Können, 2003].

Whether individual extreme events are attributable to a warmer climate is also a topic of great public concern and has become an area of active research [e.g. Peterson et al., 2012], though remains a challenging question. How the risk of such extreme events may change in the future is of similar interest. Based on theoretical considerations, mechanisms linking internal or externally forced climate variability to changes in certain types of extremes can be deduced. The most straightforward manner in which to test such hypotheses would be using classical statistical analysis of meteorological time series to test whether the likelihood of an observed event increases as certain forcings increase, for example carbon-dioxide levels or regional SSTs. Observational data, however, are often too temporally limited to study changes in extremes associated with natural or forced variability in the climate system. Climate models are thus usually required to assess how the likelihood of a particular event changes in a changing climate.

The most common approach to understanding changes in extremes is with global model experiments. In such experiments, large ensembles representative of the present-day climate and a counterfactual climate where some forcing signal has been removed are simulated.

In this way, the impact of changes in a certain forcing on observed meteorological trends, or on the likelihood of an individual extreme, can be isolated. For the latter, the changed (or not) likelihood of an event similar to one observed is compared between the two simulated climates and quantified in terms of a 'fraction of attributable risk' [Allen, 2003] due to the additional (anthropogenic) forcing. Increased public demand for such information, often highest in the wake of an extreme event [Stott et al., 2013], has seen this and similar modelling approaches to event attribution develop into a coordinated international effort with annual bulletins investigating the meteorological extremes of the previous year [e.g. Peterson et al., 2012, 2013; Herring et al., 2014].

This attribution approach has been criticized for relying on the null hypothesis of no anthropogenic global warming effect [Trenberth, 2012]. It is argued that, by having to re-establish an anthropogenic effect on an event from first principles, this approach is inherently conservative and prone to false-negatives [Trenberth et al, 2015], as it ignores the reality that all extreme events occur in a climate system that has been affected by climate change and are thus also affected by climate change - the question should be to what extent [Tenberth, 2012]? The approach also has limitations when studying extremes that are controlled by dynamical effects, including local precipitation dynamics, due to the relatively weak climate change signal of circulation changes compared with natural variability [Trenberth et al., 2015].

An alternative approach is that of 'conditional event attribution'. Within this framework, the likelihood of the synoptic pattern which accompanied the extreme is not considered, rather the intensity of the event is assessed in light of observed changes in the climate's thermodynamic properties, such as SSTs, sea ice, or soil moisture [Trenberth et al., 2015]. This approach is amenable to regional modelling experiments, whereby a LAM is used to simulate an observed event under different boundary forcings [e.g. Fischer et al., 2007]. Fixing the large-scale boundary conditions gives a higher signal-to-noise ratio, allowing finer resolution simulations which offer better understanding of fine-scale physical processes not resolved by global models. Such regional experiments must be carefully designed based on the specific scientific question being asked, though; too small a regional domain can lead to an unrealistic response (generally too weak) to changes in internal forcings, for example soil moisture [Seth and Giorgi, 1998]. If well designed, regional studies of individual extremes can provide important insights into risk factors for enhanced extremes not only in the region under study, but also in comparable regions where similar changes have been observed or are projected.

At a more practical level, event attribution is also limited by the ability of the model to reproduce the observed event. If the model is unable to reproduce events similar to that observed, then it cannot be used to detect changes in the intensity or likelihood of such events under global warming. This limitation is highest in global models, whose often coarse resolution renders them incapable of reproducing certain types of extremes, in particular intense precipitation events which can be of a highly localised nature. The ability to fix the lateral boundary conditions and achieve much higher spatial resolutions makes LAMs more suitable for attribution studies of localised precipitation extremes.

3 Added Value of Regional Models for Simulating Precipitation Extremes

In this chapter, the ability of the WRF regional atmospheric model to reproduce two recent extreme precipitation events - the June 2013 Central Europe floods and the July 2012 Krymsk flooding - is studied and discussed in the context of the concepts presented in chapter 2, in particular the added value with respect to the driving model. The Central Europe and Krymsk precipitation extremes were primarily caused by large- and local-scale forcings respectively, presenting quite different challenges for the model.

3.1 The June 2013 Central Europe Flooding

A (brief) model sensitivity study assessing the role of anomalous SST and soil moisture in the severity of the precipitation experienced during the June 2013 Central Europe flooding can be found in Appendix 3A.

The June 2013 Central Europe floods brought some of the most serious flooding witnessed in the past two centuries to the Upper Danube Basin. Over a four day period, precipitation totals reached up to 300 mm in parts of the northern Alps, with at least 100 mm recorded in the same period across large swathes of the northern Austrian Alps [Blöschl et al., 2013]. Near the northern Austrian village of Lofer, 48-hour precipitation of 173 mm was recorded the highest since records began in 1961 and corresponding to a return period of 70 years (based on a Gumbel distribution) [ibid.]. A nearby stream gauge also recorded the highest river runoff on record (since 1959), corresponding to a return period of 100 years; the differences in the two return periods point to a contributory role of high pre-existing soil moisture in the magnitude of the flooding [ibid.]. Indeed, the preceding weeks had been characterised by unusually cool and wet weather in Central Europe, with some regions experiencing over 75 mm of rain in the fortnight prior to the floods [Grams et al., 2013]. Outside of the Alps, the highest precipitation totals were recorded in the mountainous regions along the German-Czech border.

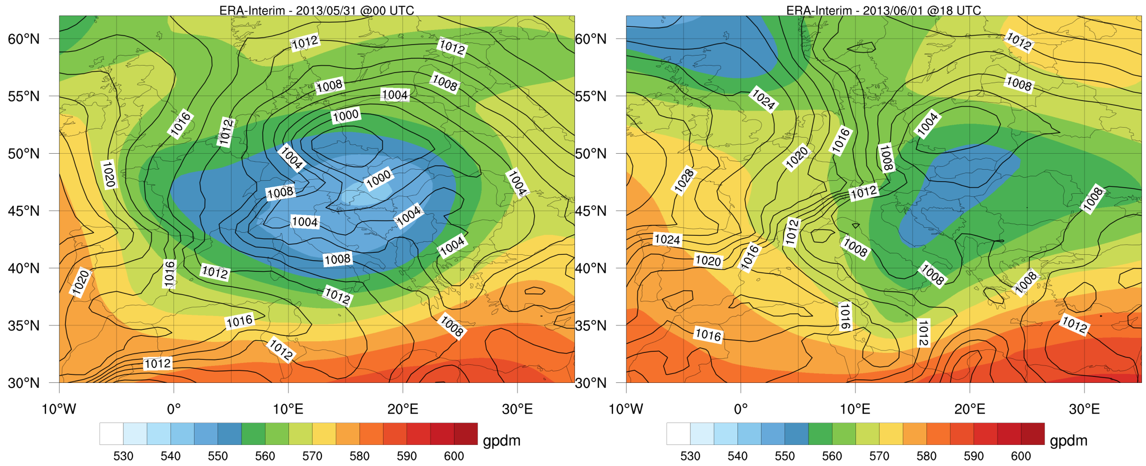

Figure 3.1: **Synoptic situation accompanying the 2013 Central Europe floods.** Geopotential heights (shading) show a quasi-stationary cut-off low over Central Europe, which steered successive low pressure systems (contours, hPa) westward towards Germany, which transported moisture rich air southwards towards the Alps.

3.1.1 Synoptic Discussion

On the 30th May 2013, a cut-off low centred over eastern France formed at the 500 hPa level, with a weak surface low further east over Hungary. The cut-off low edged eastwards thereafter, to be centred over western Hungary 24 hours later (Figure 3.1, left). During this time the surface low tracked slowly north-westward to western Czech Republic and deepened (Figure 3.1, left), following the steering flow, before moving north-eastwards into Poland as the upper low weakened. The surface low filled and dissipated by June 1st, though as the upper low, centred north of the Balkans on June 1st, remained slow moving, a new surface low was steered westwards across Poland and into the Czech Republic, carrying further precipitation (Figure 3.1, right). During the entire period of precipitation, a ridge extended north-eastwards from the Azores into Western Europe. The presence of this ridge ensured a high pressure gradient across Central Europe, enhancing southward moisture advection towards the northern Alps.

It is clear that the persistence of the cut-off low played a key role in the high 4-day precipitation accumulations. This instigated an atypical sequence of westward tracking cyclones, which brought the intense precipitation and associated moisture-rich southward warm conveyor belts [Grams et al., 2013]. The upper-level latent heating accompanying the intense precipitation ultimately resulted in a negative feedback, weakening the cut-off low and causing it to disintegrate [ibid.].

3.1.2 Simulation Design

To simulate the June 2013 Central Europe floods, the WRF regional model is used with a horizontal resolution of 0.15° (roughly 16.5 km) and 38 vertical levels up to 10 hPa. Lateral boundary and initial conditions are updated 6-hourly and come from the 0.75° ERA-Interim reanalysis [Dee et al., 2011], giving a nesting ratio of 5:1. Spectral nudging of the zonal and meridional wind fields is applied above the PBL, to keep the large-scale dynamics consistent with those of the driving model. Spectral nudging takes place at spatial scales greater than domain-relative wavenumber 3, roughly 7.0°.

3.1.3 Results and Discussion

The WRF model succeeds in well reproducing the extreme precipitation experienced during the event (Figure 3.2 a,c), which is not surprising as the event is also reasonably well represented in the driving model (Figure 3.2 b). Importantly though, the regional model also succeeds in capturing the observed locally intense precipitation (Figure 3.2 a) that is missed by the driving model (ERA-Interim). The concentration of the most intense (observed) precipitation around the complex terrain of the northern Alps and the Ore Mountains (Erzgebirge) suggests that, for this particular precipitation extreme, the enhanced topographic detail provided by the 0.15° WRF simulation is the main source of AV with respect to the driving model, which has a horizontal resolution five times lower (0.75°). The AV from additional small-scale detail is also evident in the atmospheric fields, where independent fine-scale structures develop to give local areas of enhanced water vapour relative to the driving model (Figure 3.3). While convective processes still need to be parametrized at 0.15° degree resolution, larger-scale precipitation extremes resulting from persistent synoptic forcing can generally be well captured with parametrized convection, especially as accumulation periods increase beyond sub-daily [Chan et al., 2014a].

The simulation domain shown in Figure 3.2 is relatively small, increasing the control of the lateral boundary conditions on the area of interest. Nevertheless, the use of the weak spectral nudging described above still plays an important role in the high quality reproduction of the event, which is consistent across multiple members and initialisation times (Appendix 3B). An identical simulation, except for the absence of spectral nudging, is shown in Figure 3.4. Here the precipitation maxima, though less intense, are still correctly located over the northern Alps. The heavy precipitation over Bavaria and the western Czech Republic is missing from this simulation though. A spurious local precipitation maximum located over Sachsen-Anhalt suggests that the absence of spectral nudging allowed at least one of the precipitation-bringing cyclones to deviate from its correct path.

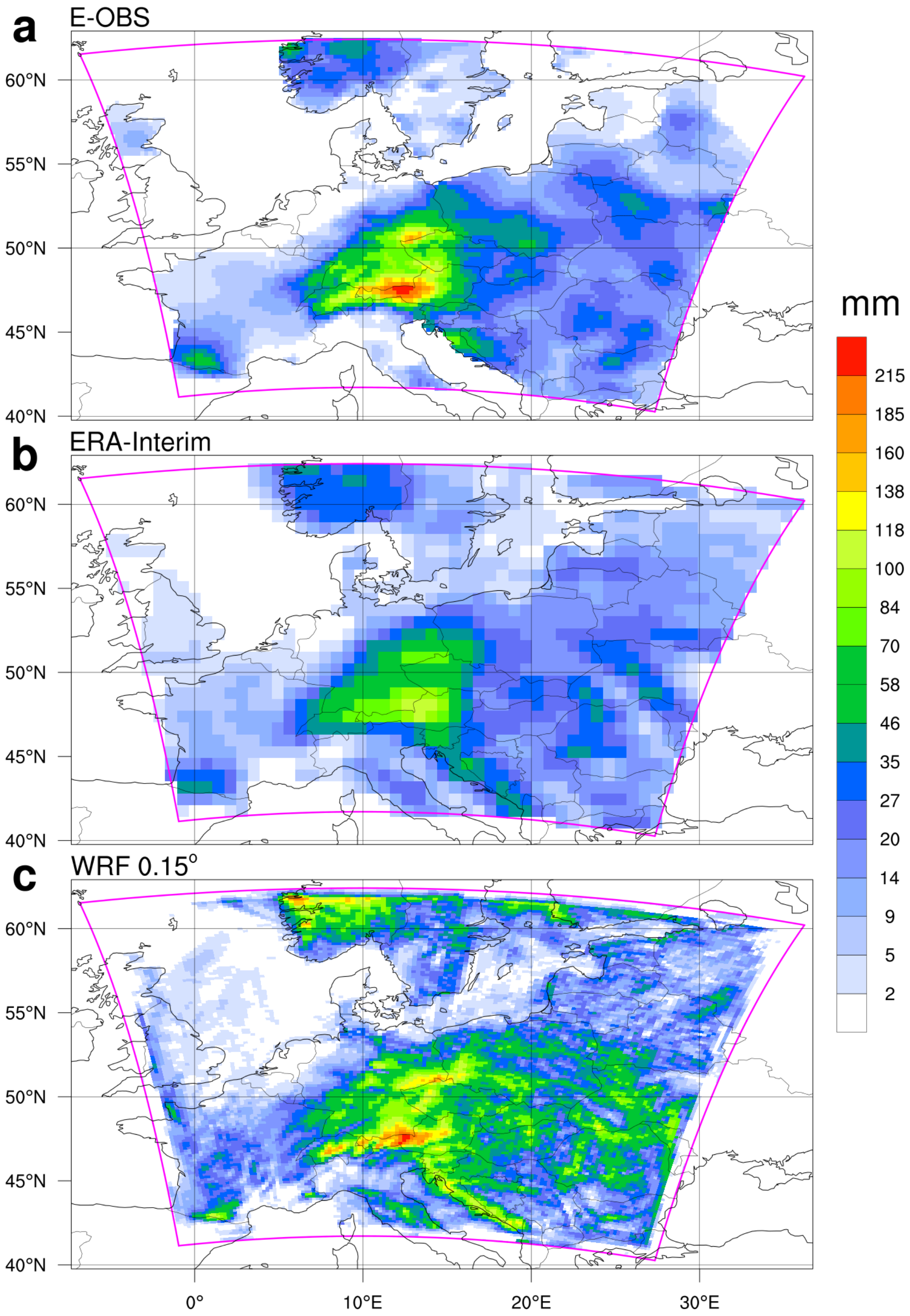

Figure 3.2: **Precipitation Accumulations.** Four day precipitation totals covering May 30th - June 2nd 2013 inclusive. **(a)** E-OBS observational dataset, **(b)** ERA-Interim [*Dee et al.*, 2011], **(c)** WRF 0.15°resolution simulation. For ease of comparison, the WRF domain is marked in all plots with a magenta coloured boundary and no values outside of the WRF domain are shown in (a) and (b). All data are plotted on their native grids.

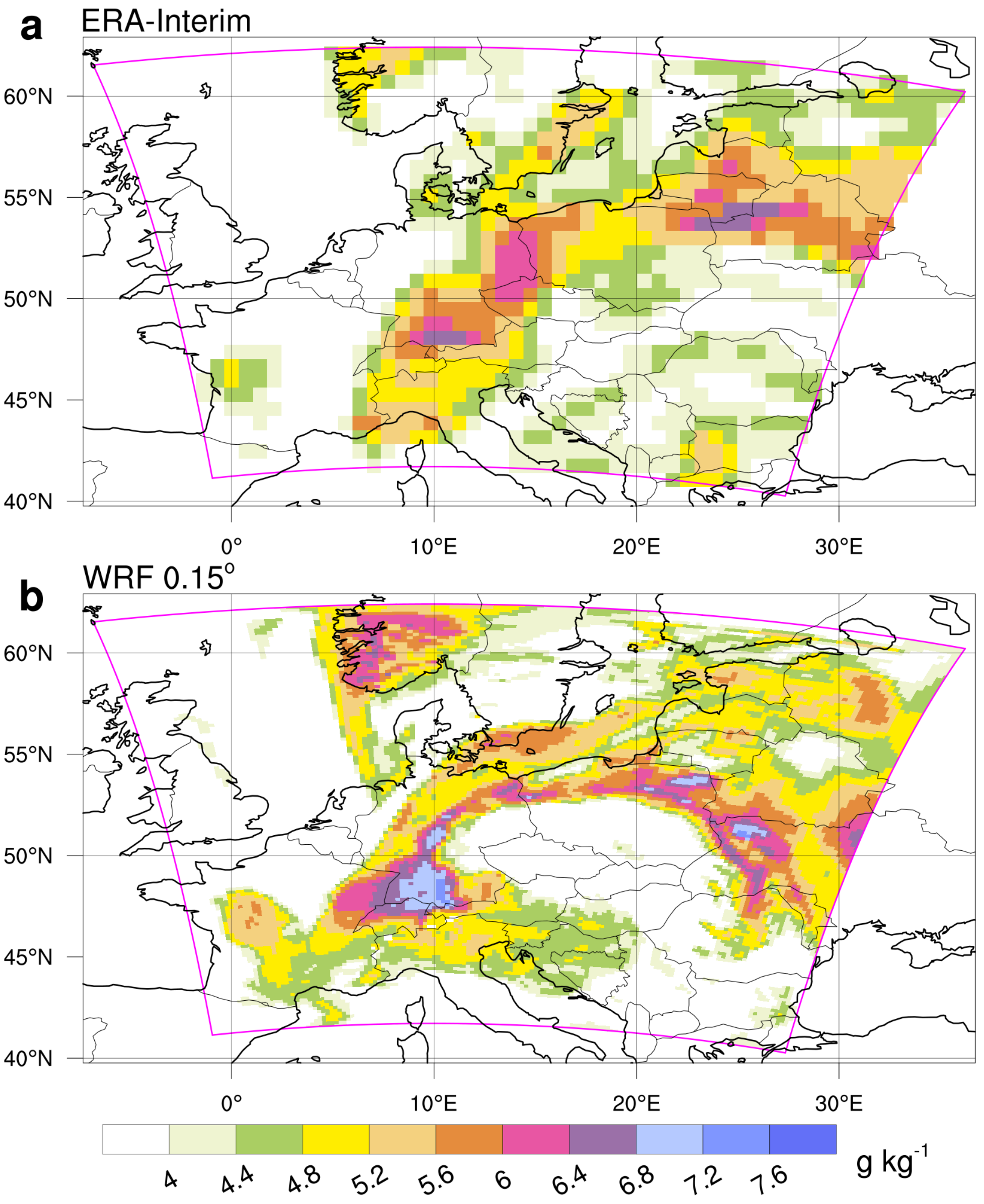

Figure 3.3: **Fine-scale Structures.** Snapshot of 750 hPa specific humidity on June 1st 2013 at 1800Z. **(a)** ERA-Interim, **(b)** WRF 0.15°resolution simulation.

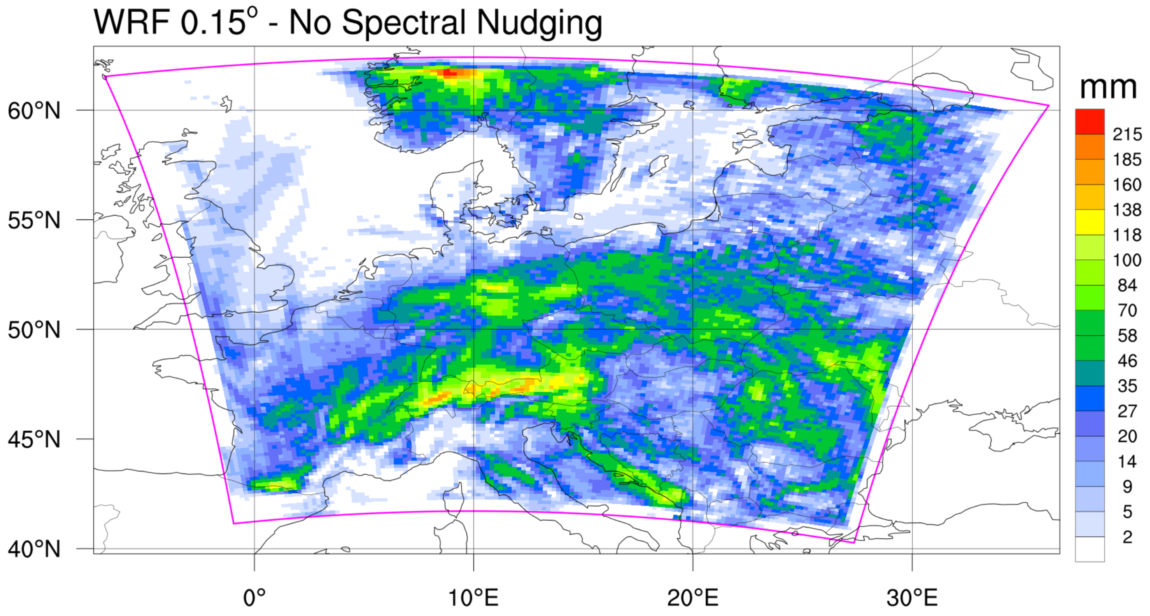

Figure 3.4: **Deterioration without Spectral Nudging.** As in Figure 3.2 (c), except without the use of spectral nudging (initial and lateral boundary conditions are the same)

Even increasing the domain size by 160% (i.e. 2.6 times bigger), spectral nudging still allows for the accuracy of the precipitation field to be maintained (Figure 3.5 a), also across multiple members (Appendix 3C). Without spectral nudging, such a large domain sees a greater deterioration in the faithfulness of the precipitation field than seen in the smaller domain (Figure 3.5 b).

3.2 The July 2012 Krymsk Precipitation Extreme

The Krymsk precipitation extreme [Kotlyakov et al., 2013; Meredith et al., 2015] occurred on the 6th/7th July 2012, along the north-eastern coast of the Black Sea. The precipitation affecting the Krymsk region was associated with two waves of convection, the first coming early on the 6th of July and the second the following night. Total precipitation of 171 mm fell in 24 hours at Krymsk, a station where daily precipitation had previously not exceeded 80 mm, resulting in over 170 deaths; the nearby station at Novorossiysk recorded almost twice as much precipitation in the same period [Kotlyakov et al., 2013]. The Krymsk event was Europe's deadliest weather-related flash-flooding since the early 1970s [EM-DAT].

3.2.1 Synoptic Discussion

In the presence of a quasi-stationary cold upper low, a slow moving cyclone tracked across the eastern Black Sea, advecting warm and moist air towards the foothills of the Caucasus

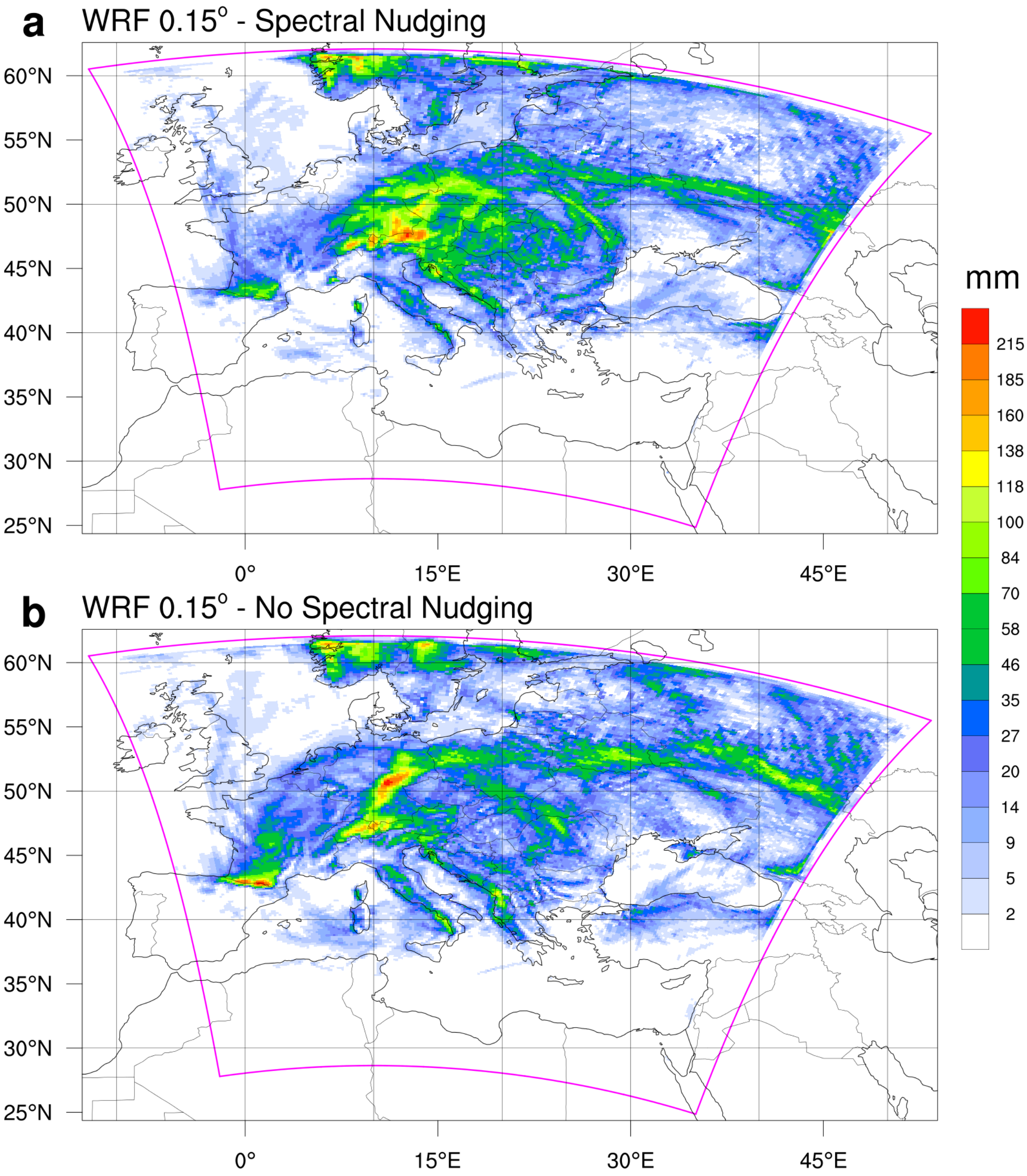

Figure 3.5: **Impact of Increased Domain Size. (a)** As in Figure 3.2 (c), except with the domain size increased 2.6 times (initial conditions are the same). Spectral nudging of the U and V fields is carried out above the PBL and at wavelengths of approximately 6°. **(b)** As in (a), except without spectral nudging. Compared to the smaller domain in Figure 3.4, the precipitation field in the bigger domain deteriorates more in the absence of spectral nudging.

mountains (Figure 3.6). The atmospheric profile early on the 6th, from the down coast station of Tuapse (44.10°N/39.07°E), shows the lower atmosphere to be saturated at most levels below 500 hPa and primarily conditionally unstable below 750 hPa (Figure 3.7). Analysis of the lower troposphere reveals the development of a south-westerly low-level jet in the vicinity of Krymsk. Maximum wind speeds of over 13 m s^{-1} at the 925 hPa level (Figure 3.8) provided a rich source of shoreward moisture advection, giving rise to the first wave of convection as thunderstorms formed mostly on the maritime side of the coastal topography.

Later that night, convective cells formed at the head of an equivalent potential temperature (theta-e) ridge before merging into a larger organized mesoscale convective system (MCS). A steady infusion of warm and moist air was fed along the theta-e ridge axis towards the developing MCS, where its high energy content fuelled vigorous convection and the subsequent second wave of intense precipitation. The most intense precipitation was centred over a coastal topographical ridge exceeding 500 m elevation, with orographic uplift acting as a key convective trigger.

3.2.2 Simulation Design

The extreme precipitation experienced in the Krymsk region was a mesoscale phenomenon. The simulation of such localized convective extremes can be greatly improved by using convection-permitting resolution [Weisman et al., 2008]. A modelling strategy involving the explicit representation of convection is thus adopted to reproduce the Krymsk event. While no consensus exists on exactly when convection-permitting resolution begins, it is generally taken to be at horizontal resolutions finer than 4 km [e.g. Prein et al., 2015]. Even at 1 km horizontal resolution though, many internal dynamical cloud processes are still under-resolved. A horizontal resolution of 0.6 km is thus selected for the WRF model, far higher than is currently used in operational weather forecasting.

To achieve this resolution, a triply nested regional domain is configured over the Black Sea (Figure 3.9). A nesting ratio of 5:1 is used, giving domains with horizontal resolutions 15-, 3-, and 0.6 km for the three WRF nests; these are referred to as D15, D3 and D0.6, respectively. Lateral boundary and initial conditions come from 1° resolution NCEP Final Analyses, with the exception of sea surface temperatures (SSTs). SSTs are taken from NOAA's 0.25° optimal interpolation data set, to provide surface forcings at resolutions closer to the simulation resolution. A weak spectral nudging of the horizontal and meridional winds is applied in D15, though only at wavelengths greater than 300 km and above the PBL. Parametrizations are as given in Table 2.1, with the exception of the convective

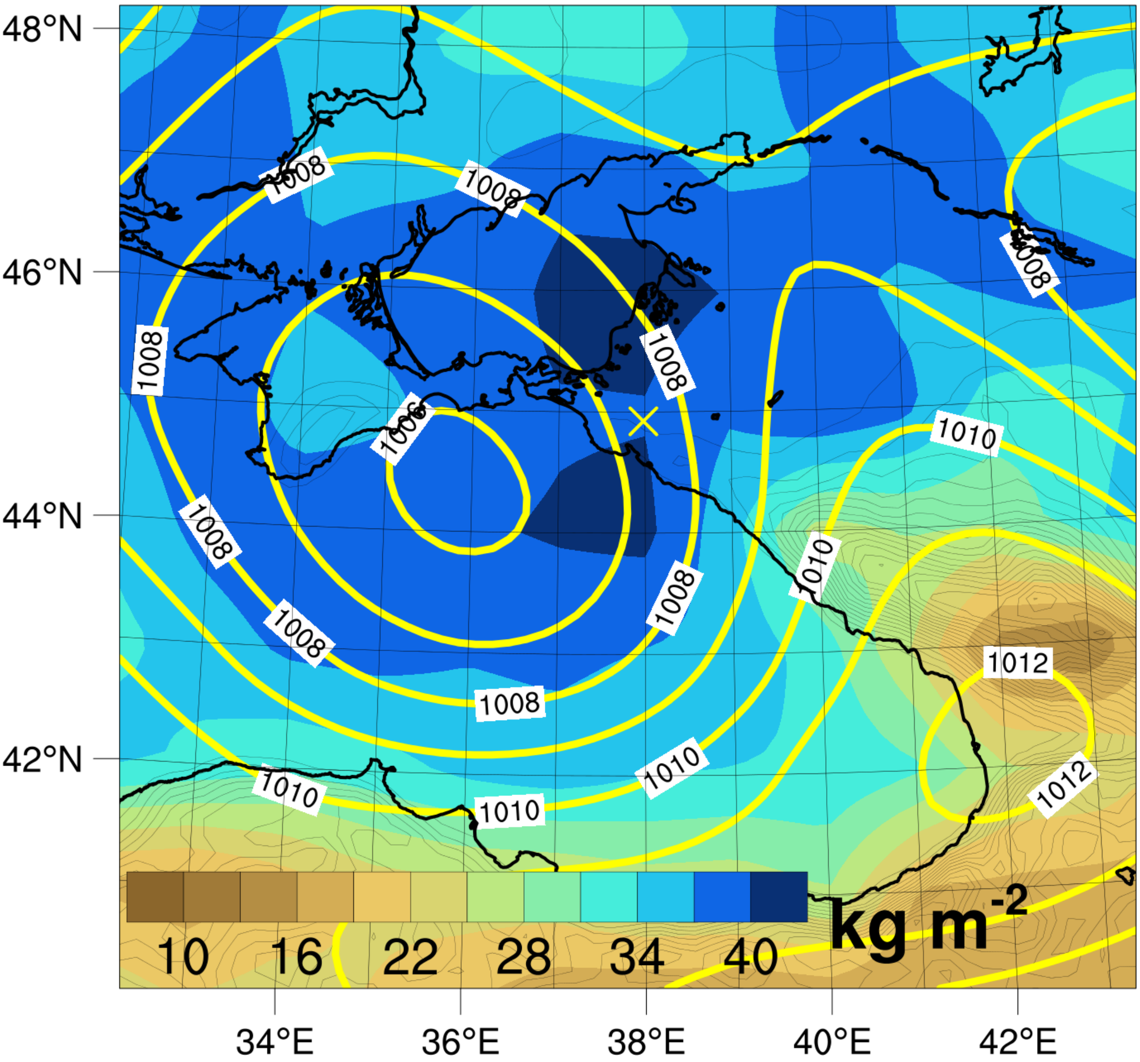

Figure 3.6: **Synoptic pattern.** Column integrated precipitable water (shading, kg m^{-2}) and sea level pressure (hPa, contours) on the 6th of July, 2012, at 18Z. Based on NCEP Final Analyses. Krymsk is marked with an 'x'. Adapted from Meredith et al., 2015.

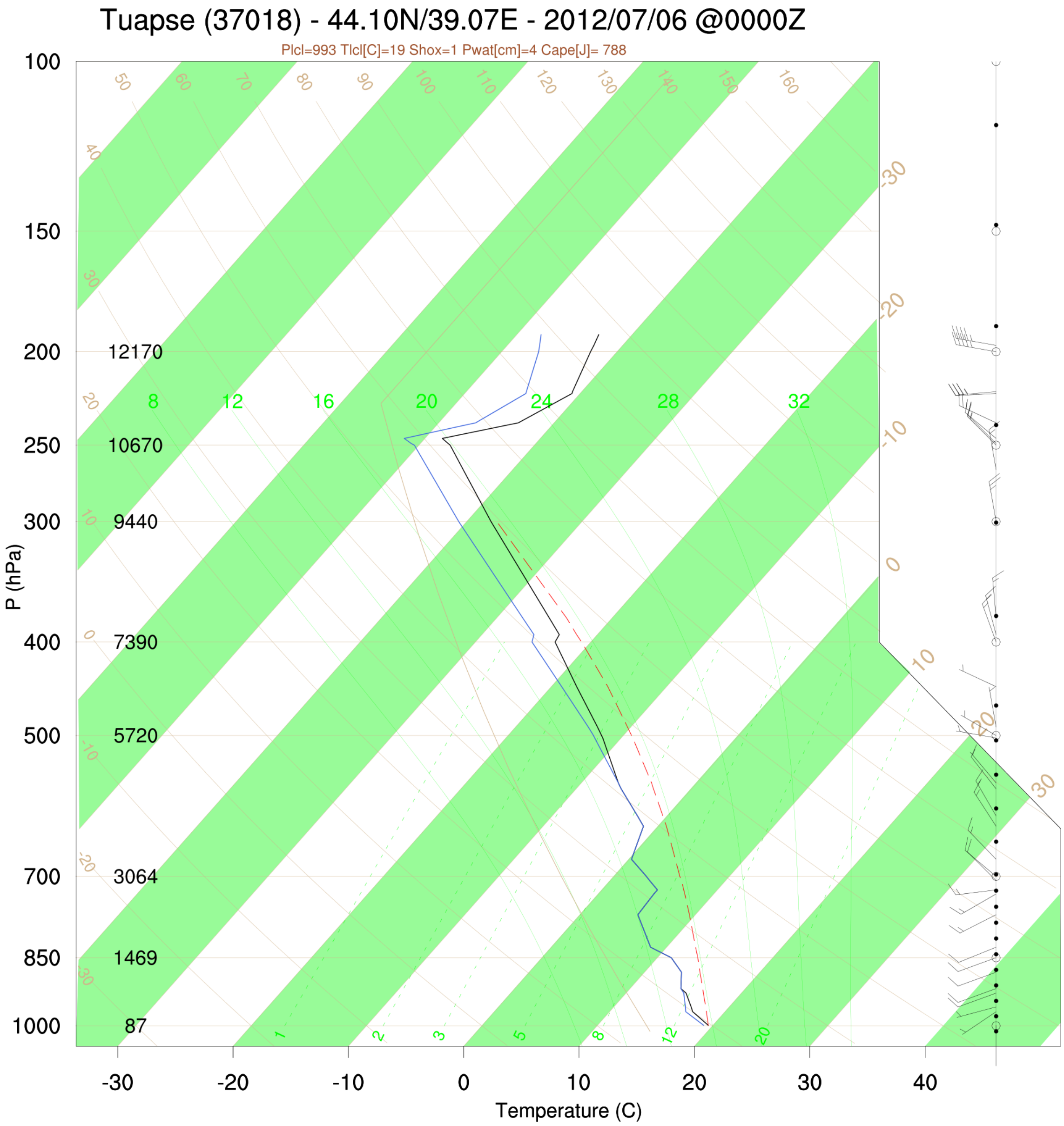

Figure 3.7: **Atmospheric Sounding.** Skew-T log-P diagram based on radiosonde data from Tuapse (44.10N/39.07E) on July 6th 2012 at 00Z.

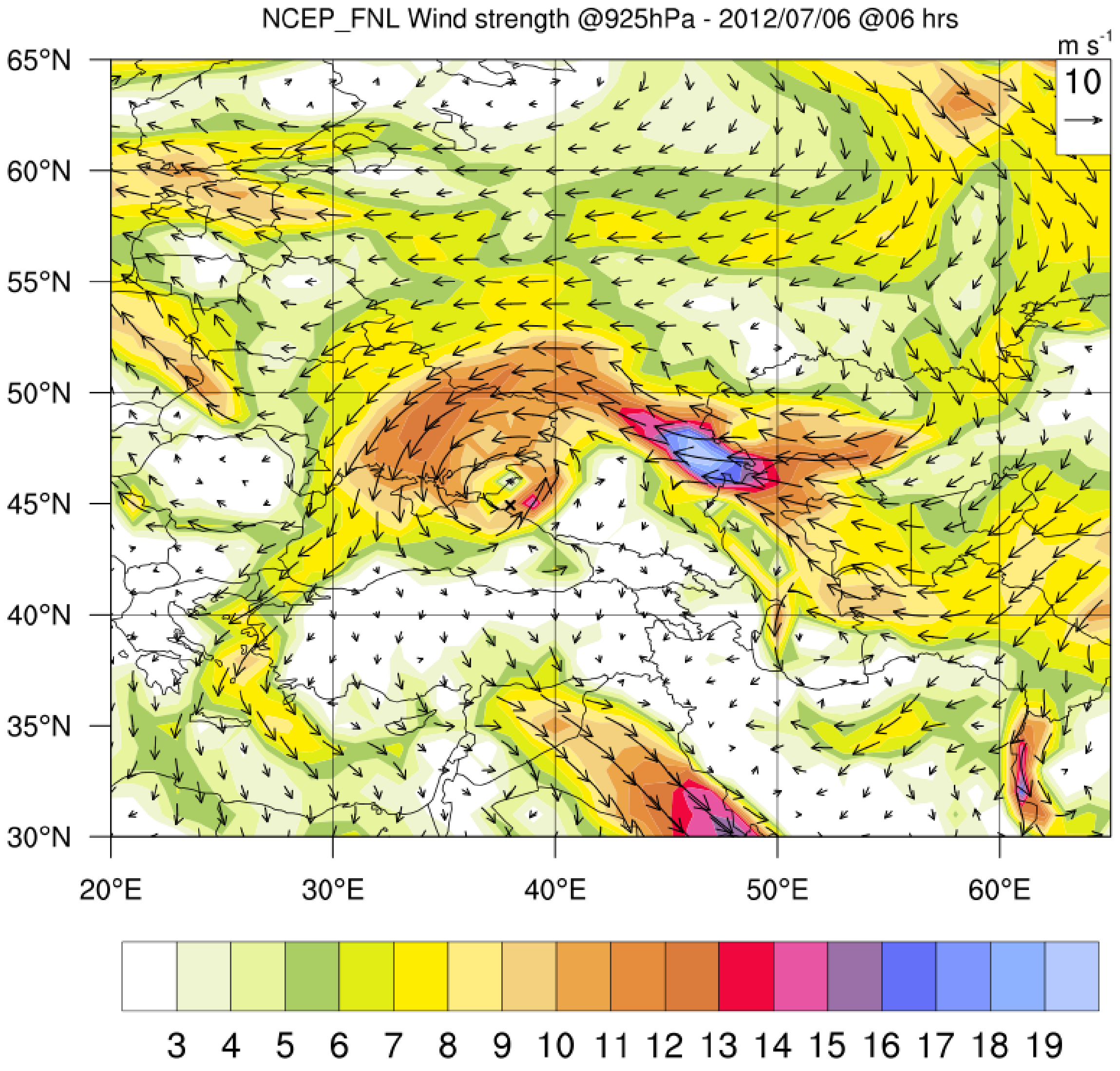

Figure 3.8: **Low-level winds.** Wind direction (vectors) and strength (shading or vectors) at 925 hPa on July 6th 2012 at 06Z. Based on NCEP Final Analyses.

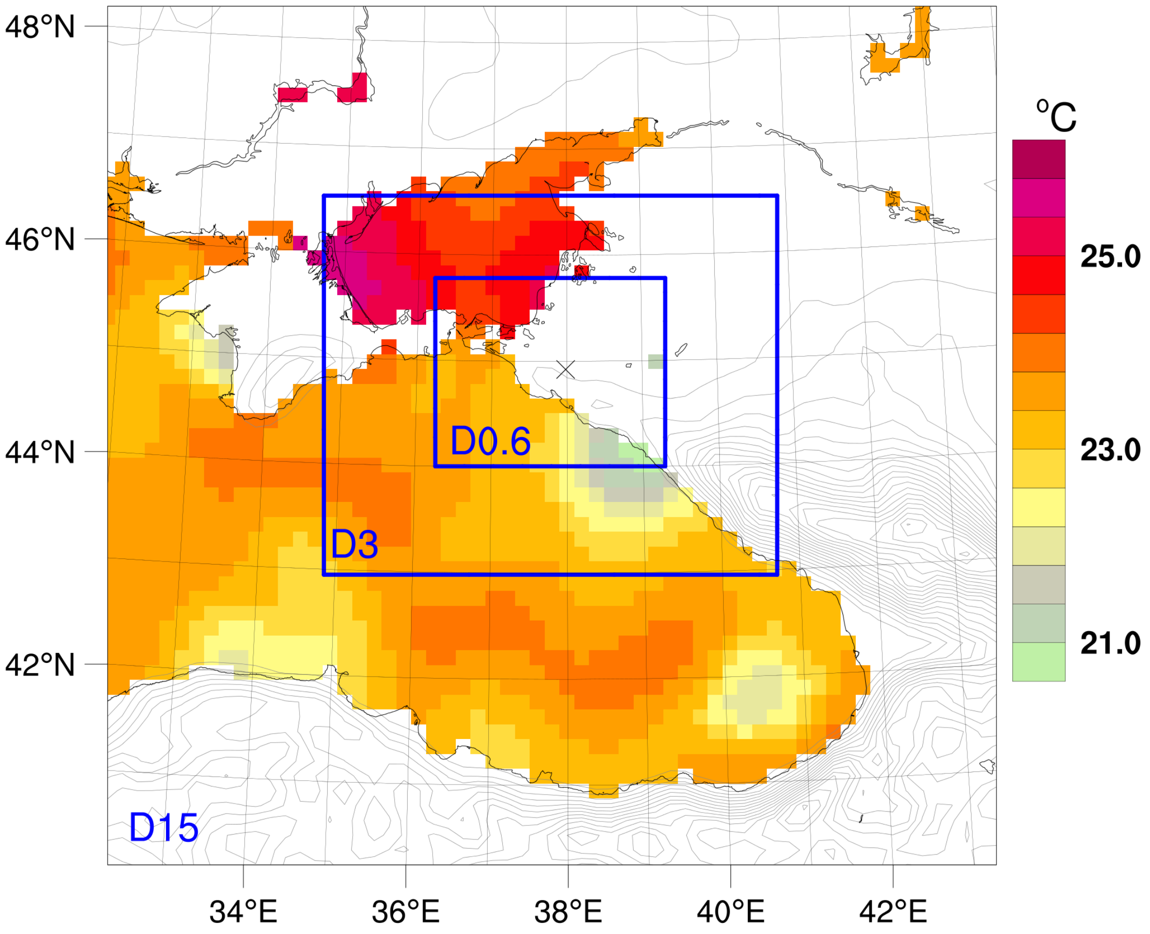

Figure 3.9: **Nested Domains.** WRF simulation domains D15, D3 and D0.6 (blue). Sea surface temperature in the eastern Black Sea on July 5th 2012 (shading), based on the 0.25° NOAA Optimum Interpolation dataset [*Reynolds et al.*, 2007]. Krymsk is marked with an x; light black contours denote the D15 orography field, at 150 m intervals.

parametrization scheme which is turned off in the 3- and 0.6 km resolution domains. A six-member ensemble is created, using staggered initialisation times from July 4th at 00 UTC to July 5th at 06 UTC. This gives at least 21 hours of model integration time before the first wave of precipitation, which is sufficient for small-scale dynamics in D0.6 to spin up from the coarse-model interpolated initial conditions (Figure 3.10).

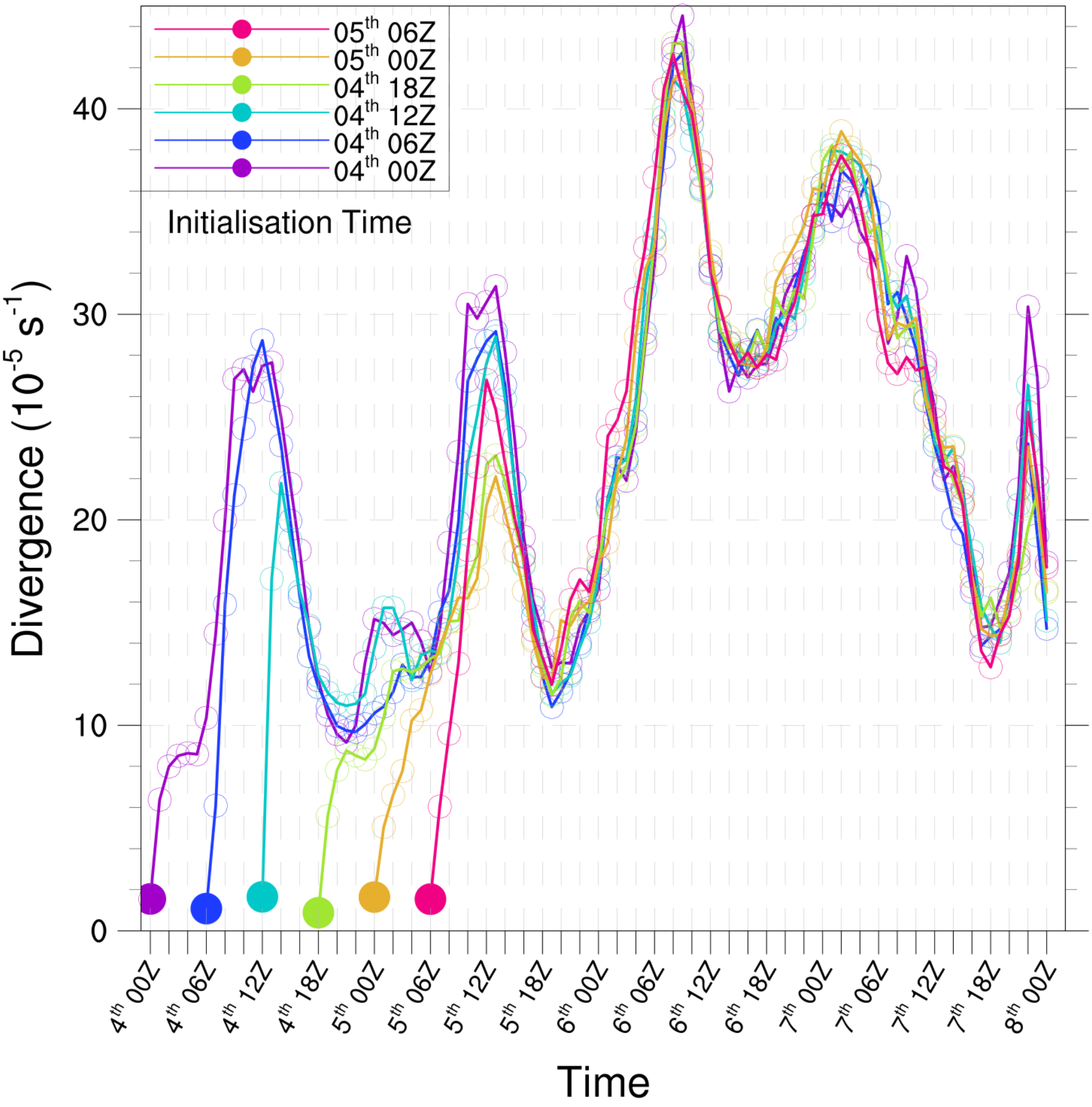

Figure 3.10: **Spinup.** D0.6 domain averaged divergence magnitude (i.e. absolute value of divergence) versus time, for all ensemble members. Divergence is shown here for model level 10, roughly equivalent to 800 hPa. The small-scale dynamic features resolvable in the D0.6 simulation can be seen rapidly developing after the model is initialized with initial conditions interpolated from the coarse global model, which are devoid of such mesoscale detail. In all cases it takes less than 6 hours from initialization for the level of mesoscale detail to match that in the earlier initialized members.

3.2.3 Results and Discussion

The convection-permitting WRF simulation adds value by producing precipitation intensities (Figure 3.11) much closer to observations[1] [Kotlyakov et al., 2013] than those simulated in lower-resolution forecast models run at the time of the event (Figure 3.12). While the relatively high 15 km resolution WRF simulation produces 24 hour rainfall totals in excess of 75 mm (Figure 3.13), these maximum intensities are shifted slightly south-west and still fall well short of those observed. This is in contrast to the WRF simulation of the 2013 Central Europe flooding (§3.1), which was driven by synoptic-scale forcing at supra-daily timescales and hence reproducible at coarser resolutions. While the background synoptic situation was of course also important for the Krymsk event, the most intense precipitation resulted from a localized MCS. Separate sensitivity simulations (not shown) applying the D15 orography field to the D0.6 domain indicate that the more detailed orography at 0.6 km resolution is not a key factor in the higher precipitation intensity that the convection-permitting simulations produce. Rather, as demonstrated by Prein et al. [2013], the added value comes from the more realistic deep-convective dynamics produced when convection is explicitly resolved. It should also be recalled that, as mentioned in §2.1.4, the added value of convection-permitting models is not expected to be found in terms of point scale precipitation totals, but rather in area averages over, for example, a watershed or drainage basin [Roberts, 2008]. The six-member WRF ensemble gives a mean 24 hour precipitation total of 182 mm (s.d. 27 mm) at Krymsk station, as opposed to 171 mm in the observations. While this represents a good result, there is a considerable random component in point-scale precipitation intensities and, as such, a less-close match would not necessarily constitute a 'poorer' simulation.

Further validation of the model simulation can be carried out using other standard meteorological variables recorded at local weather stations in the Krymsk region. Sea level pressure, for example, provides a good proxy for circulation; likewise two metre relative humidity for saturation within the boundary layer. Two metre temperature can provide a good indication of temperature drops associated with intense thunderstorm activity. In Figures 3.14-3.16, 3-hourly observations from four stations in the Krymsk region are compared with WRF model output at equivalent locations. Model output is at a temporal frequency of 1 hour and all six ensemble members are shown, as well as the ensemble mean. Due to the very high resolution of the convection-permitting setup, the degree of precision of the weather station coordinates creates some uncertainty as to which model cell best corresponds to the exact station location. For example, station coordinates with

---

[1] The density of stations used to create the E-OBS data set, which was used for comparison in §3.1, is insufficient in the Krymsk region to capture the Krymsk precipitation extreme.

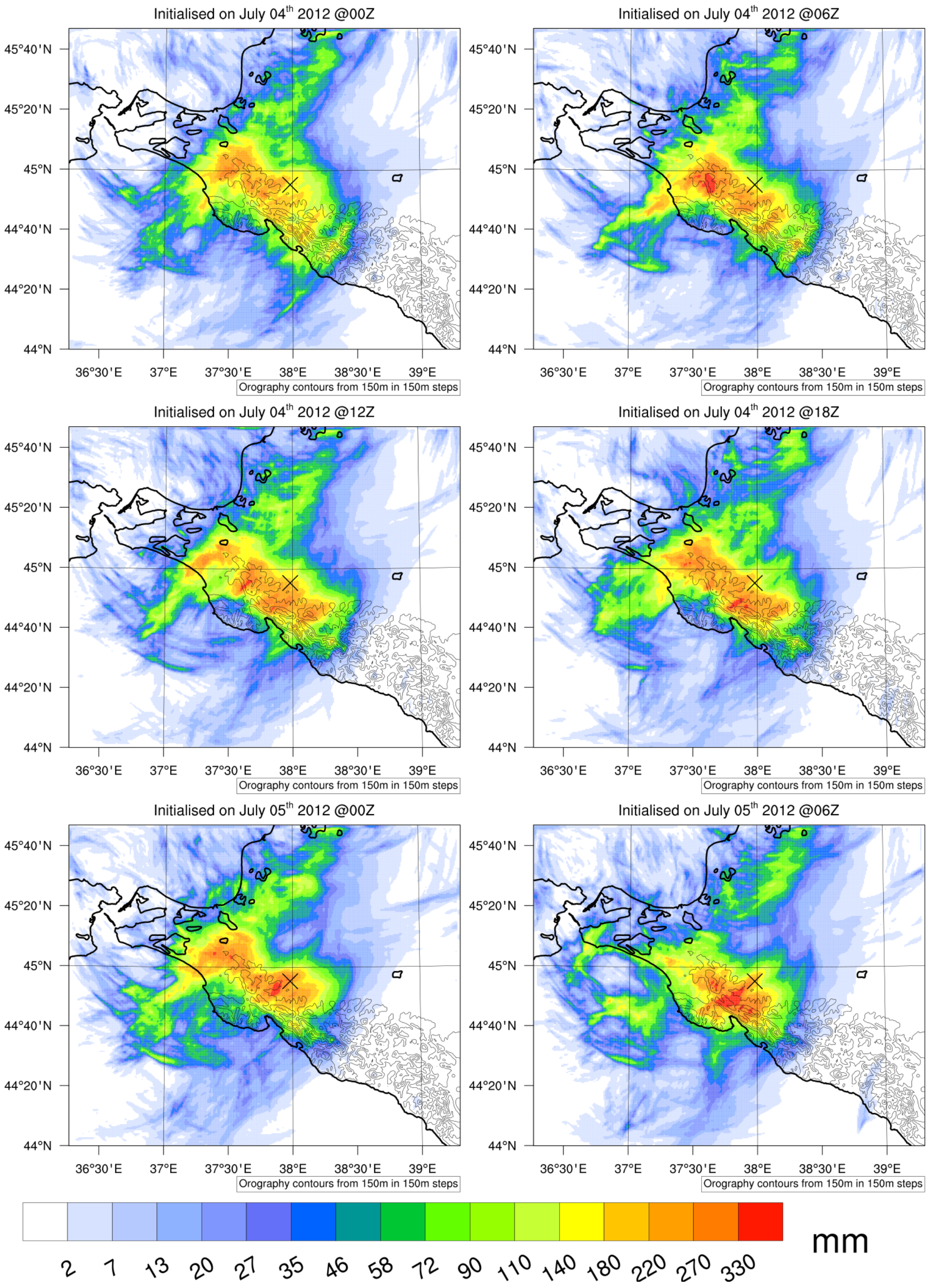

Figure 3.11: **Simulated 24 hour precipitation totals** (mm), from July 6th 2012 at 03Z to July 7th 2012 at 03Z (24 hours), for all six ensemble members. Members are initialised at 6 hour intervals from July 4th 2012 at 00Z to July 5th 2012 at 06Z. Krymsk is marked with an 'x' and orography contours are shown at 150 m intervals. Note the detail of the D0.6 orography field compared to that in D15 (Figure 3.9,3.11)

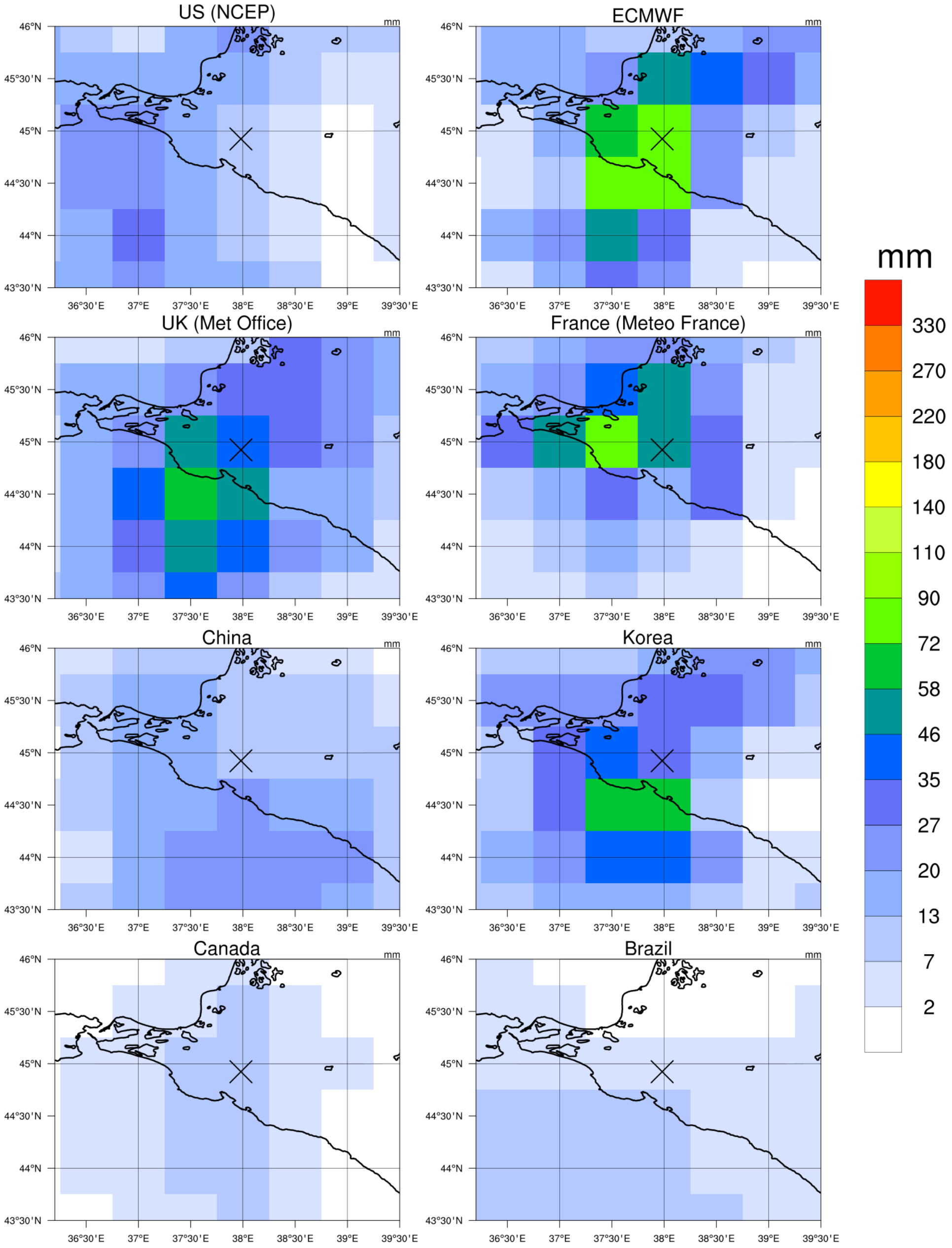

Figure 3.12: **Krymsk Forecasts from TIGGE Database.** Total simulated precipitation (mm) from 6th July 2012 at 00Z to 7th July 2012 at 06Z by the forecast models of national agencies within the TIGGE database [*Bougeault et al.*, 2010]. The totals are sums of 6-12 hour precipitation forecasts, from the nearest model initialisation time. Krymsk is marked with an 'x'. As the TIGGE database only provides precipitation totals at 6-12 hour frequency, the accumulation period is six hours longer than that shown for the WRF simulations, which was chosen to match the local station data. Despite this extra accumulation time, precipitation totals are still well below observations.

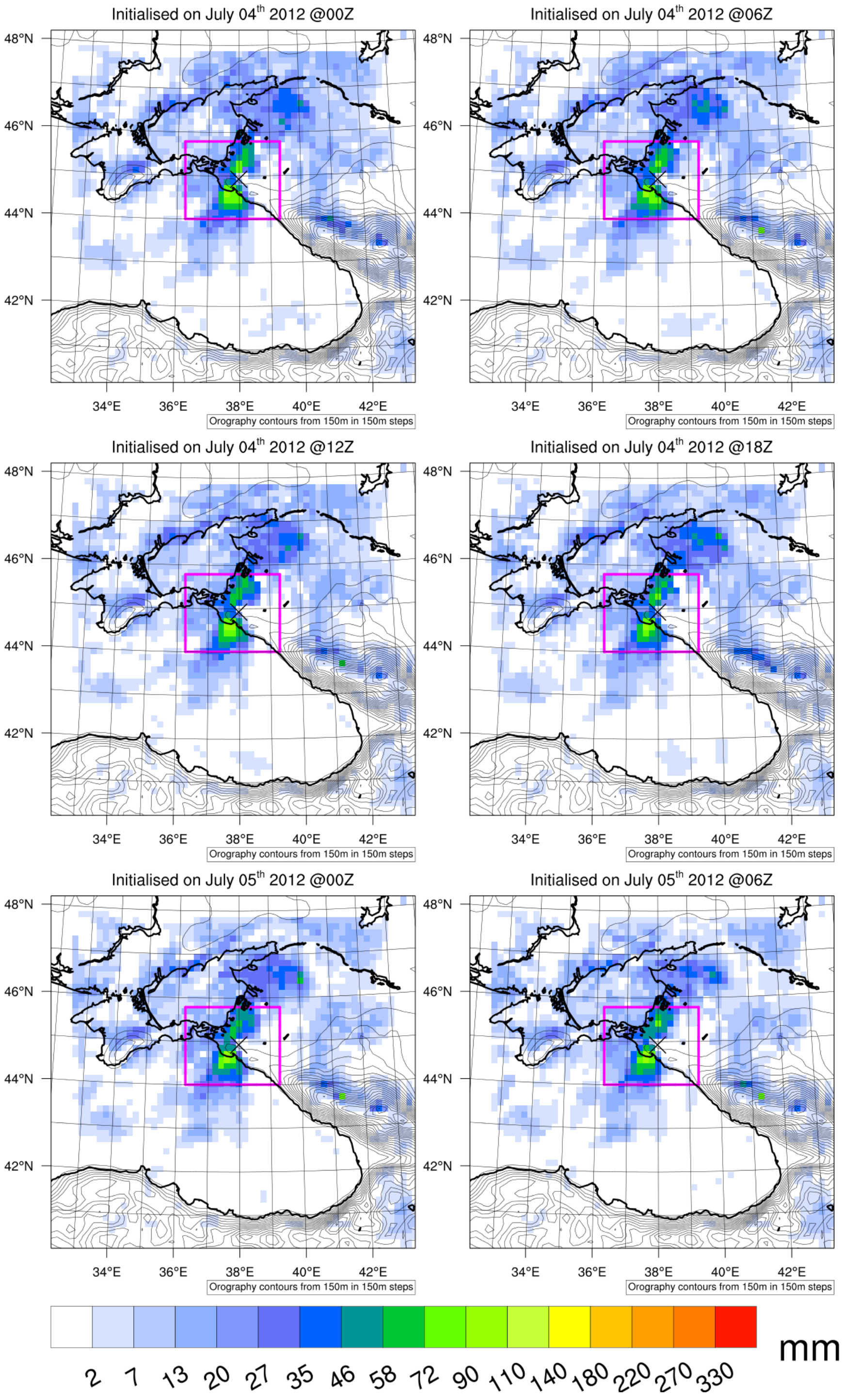

Figure 3.13: **D15 Ensemble.** As in Figure 3.11, except for D15. The area covered by D0.6 is marked by a magenta box.

0.1 precision would have an uncertainty of roughly 18 model grid cells. In a simulation over a mountainous region with high resolution topography, this can have considerable impact on the terrain and altitude of the grid cell being compared with the station data. As only 0.1 precision coordinates are available for 2 of the 4 weather stations, the anomaly of each thermodynamic variable during the period July 6th 2012 at 00Z to July 7th 2012 at 12Z is therefore analysed. The mean over this period serves as the reference value.

As can be seen in Figures 3.14-3.16, the model setup well reproduces the temporal evolution of the meteorological conditions observed during the Krymsk event, with in general good agreement between all members. This lack of sensitivity to initial conditions brought about by the spectral nudging is clear from the similarity of the intra-ensemble precipitation fields, which is in contrast to those created in simulations without spectral nudging (Figure 3.17).

3.3 Concluding Remarks

As has been shown in this chapter, LAMs provide an effective tool for studying extreme precipitation events. The higher resolution afforded by such models more realistically simulates mesoscale processes and gives a better representation of surface forcings, both of which can be poorly represented in coarser global models. High resolution LAM simulations not only add small-scale detail to coarse model output, but can also add value at the spatial scale of the driving model. This is particularly true for the simulation of precipitation, both mean and extreme, due to its high level of spatial variability and tendency to often be triggered and/or maintained by localized dynamical processes. The AV of LAMs for studying precipitation extremes extends beyond just more accurate simulations though, and also includes how extreme precipitation responds to changes in external forcings, which will be demonstrated and discussed in detail in chapter 5.

In addition to the improved simulation of extreme precipitation events, the internal variability that can be generated in regional models (§2.1.3) also makes LAMs a useful tool for regional sensitivity experiments. If the regional domain is carefully designed for the specific scientific question, then the IV generated in regional models can be comparable to that found in global models, for variables influenced by mesoscale processes [Christensen et al., 2001]. When this IV is present, LAMs have the freedom to respond realistically to perturbations of the surface forcing [Seth and Giorgi, 1998], for example sea ice cover, soil moisture or SST. In this way, the contribution of observed changes in such surface forcings to the intensity of individual weather events can be revealed, which is exploited in the next chapter.

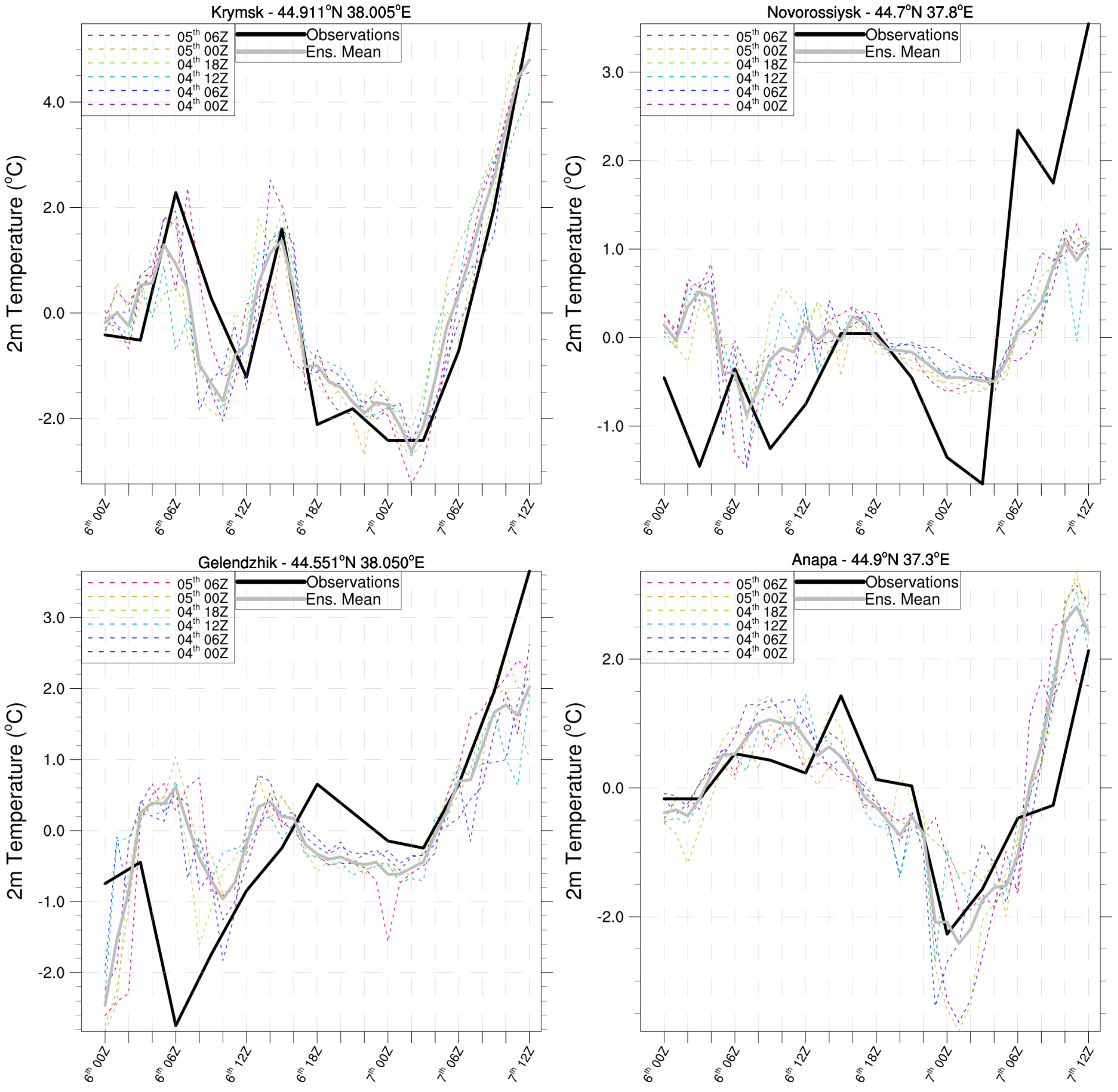

Figure 3.14: **Observed and Modelled Temperature (2m).** Thick black line shows observations from meteorological stations around the Krymsk region. Modelled totals at equivalent locations are shown for the D0.6 ensemble mean (thick grey line) and individual members (dashed coloured lines), with initialisation times of the latter indicated in the legend.

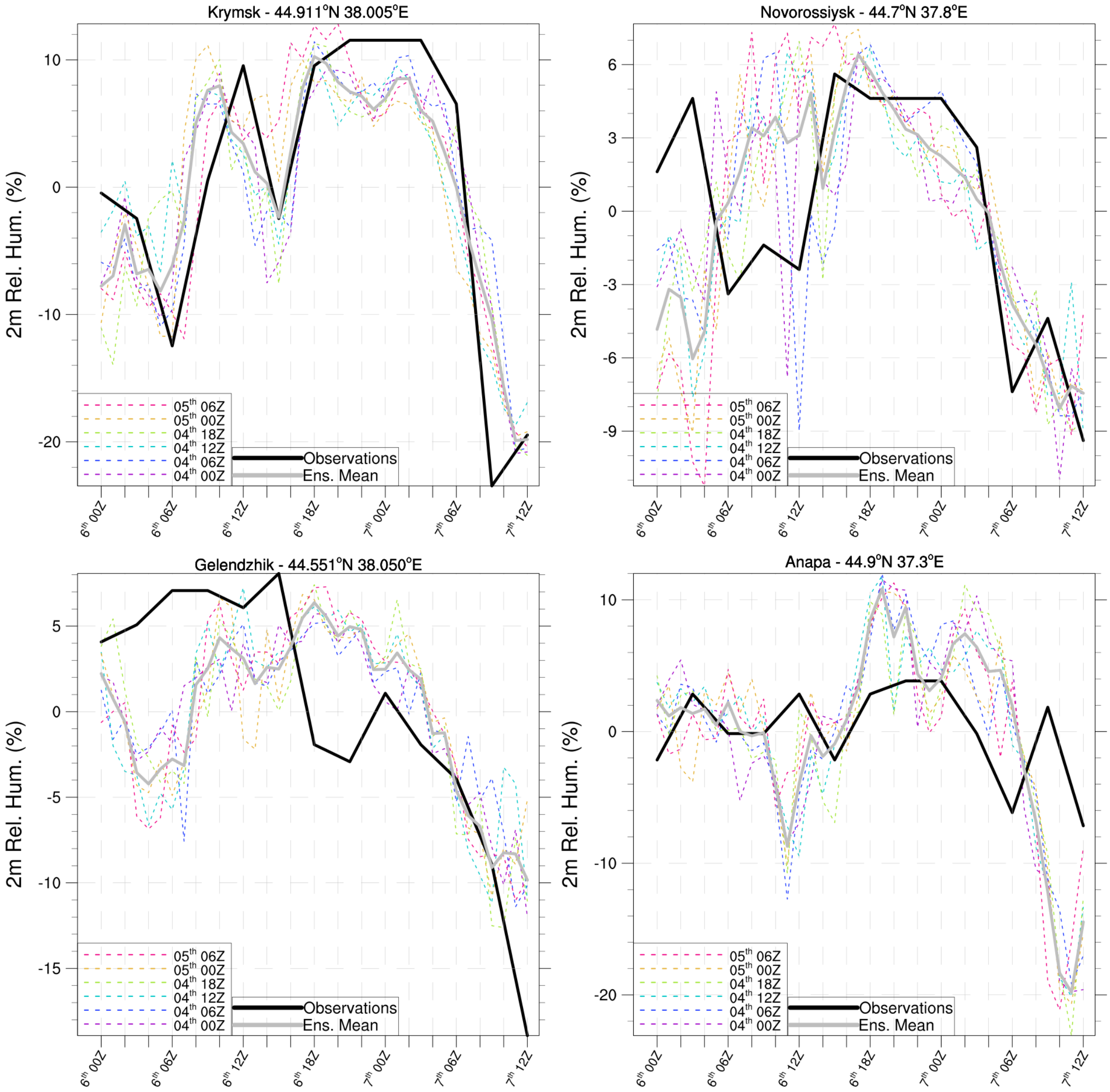

Figure 3.15: **Observed and Modelled Relative Humidity (2m).** Lines coloured as in Figure 3.14.

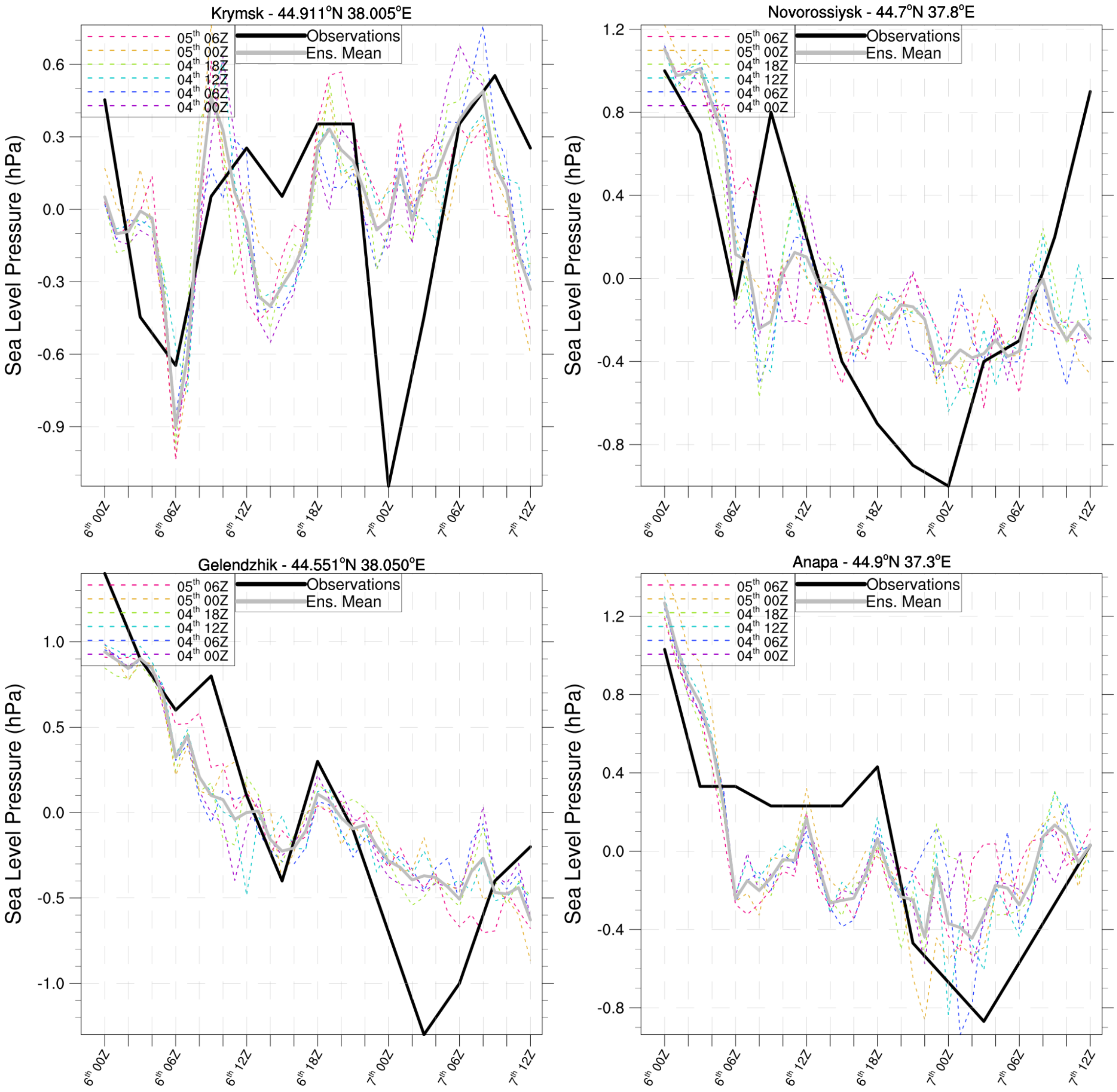

Figure 3.16: **Observed and Modelled Sea Level Pressure.** Lines coloured as in Figure 3.14.

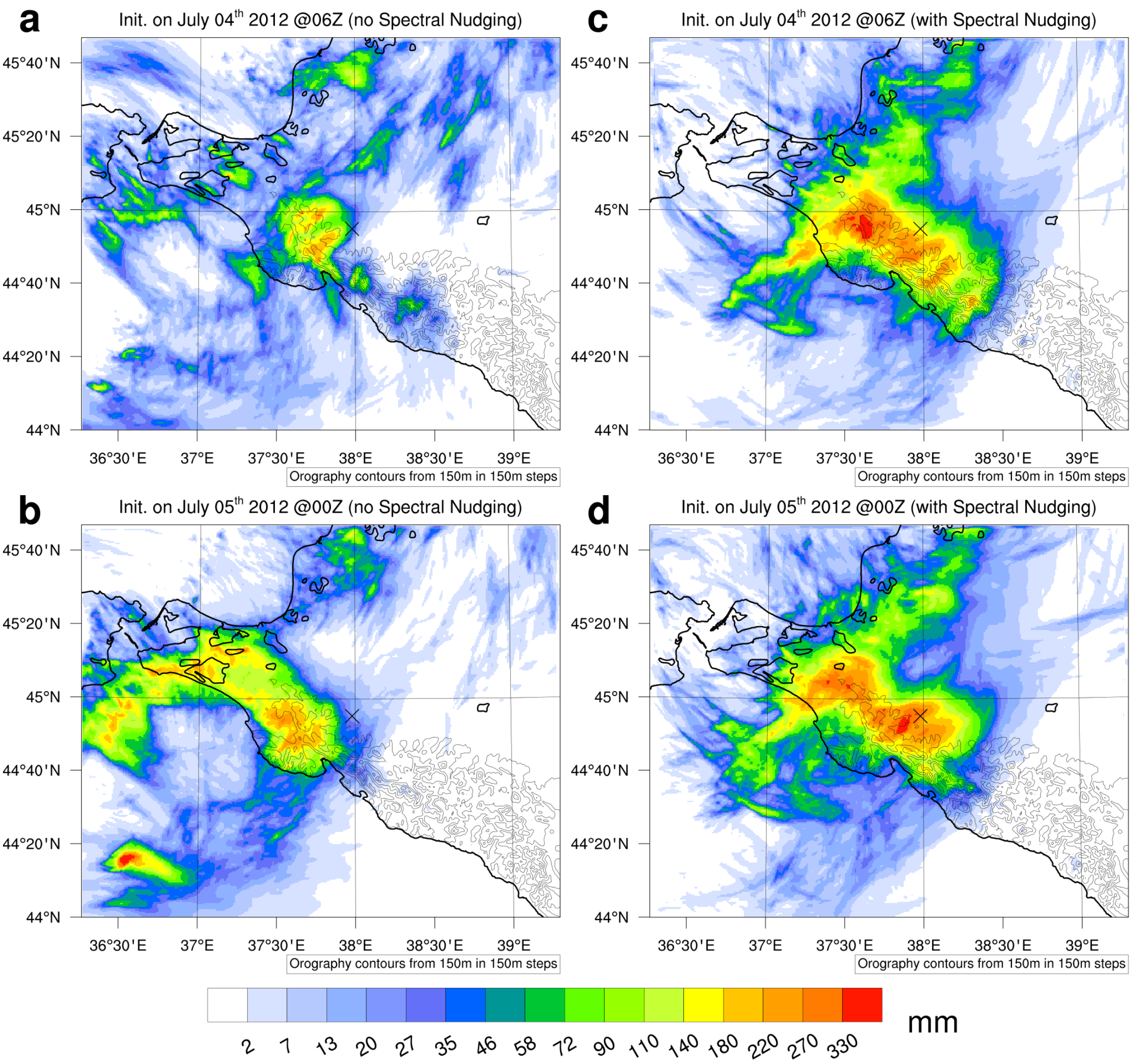

Figure 3.17: **Utility of Spectral Nudging.** Simulated 24 hour precipitation totals within ensembles with (right) and without (left) spectral nudging. Ensemble members on the top and bottom rows are initialised just 18 hours apart, though produce quite different precipitation fields in the unnudged simulations (a, b), which is not evident when nudging is employed (c, d). Additionally, the unnudged simulations (a, b) shift the strongest precipitation north-westwards, missing out on the intense precipitation at Krymsk (marked with an 'x').

3.4 Appendix

3A Sensitivity of 2013 Central Europe floods to SST and soil moisture

In figure 3.18, the Central Europe floods have been re-simulated in an ensemble with altered SSTs. The 1979-2013 trend of summer SSTs have been subtracted from the observed SST field over the Mediterranean and Black Seas, to assess the impact of the warming over recent decades on the precipitation intensity. To allow the model solution freedom to develop independently, the larger of the two domains shown in §3.1 is used. Figure 3.21 shows the same simulation using unaltered SSTs. As can be seen, the differences in SSTs leads to no discernible difference in differences in precipitation totals, indicating that the event's intensity was not dependent on increased moisture availability from the Mediterranean (or Black) Sea.

Late June 2013 was also marked by anomalously high soil moisture levels in much of Eastern Europe, primarily due to a wet period during early June. Another factor may have been an unusually cold spring delaying the melt of snow. Similar sensitivity experiments using reduced soil moisture levels also had no discernible effect on precipitation totals. As an extreme case, figure 3.19 shows a simulation where soil moisture has been reduced by 50% across the whole simulation domain, but the precipitation is still unaffected.

Together, these results suggest that the June 2013 Central Europe floods were not dependent on a critical moisture source. Instead, the key factor was the persistence of the cut-off low over Central Europe, which brought successive cyclones into Central Europe. Surface runoff may also have been enhanced by soil that was already very wet, as discussed in §3.1.

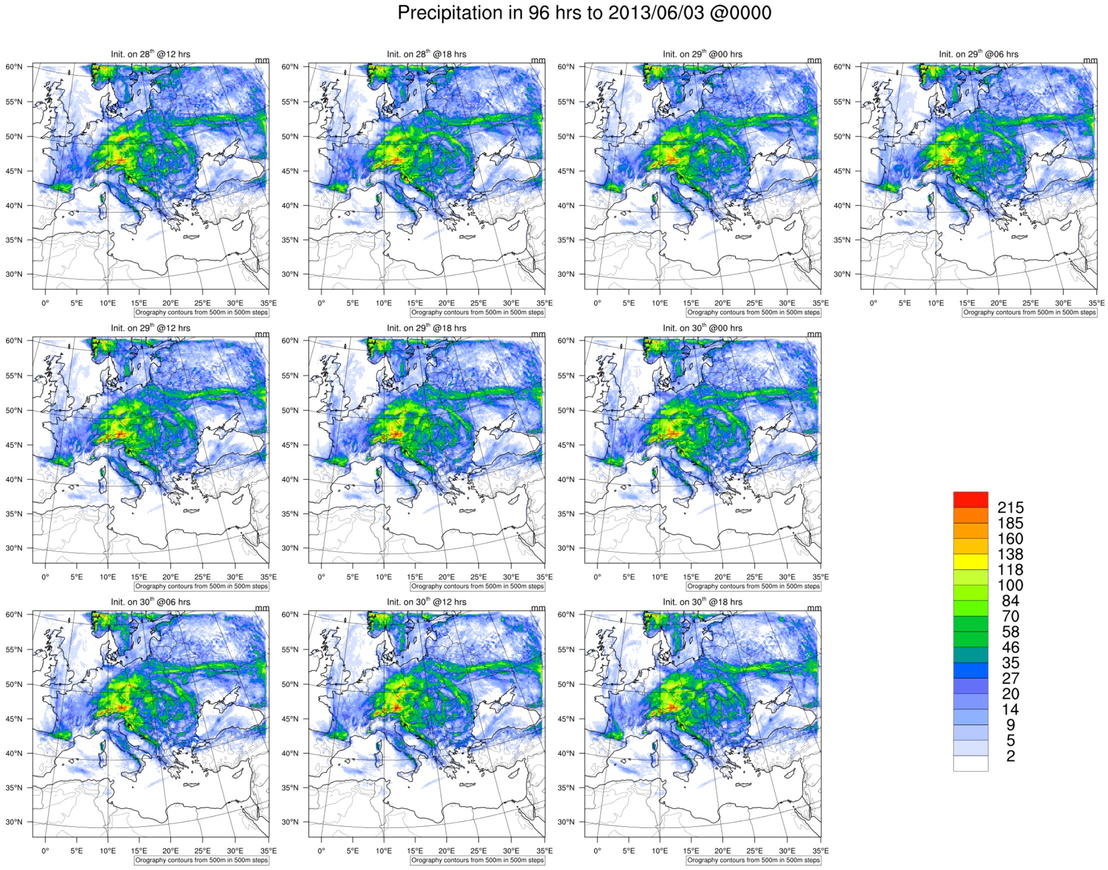

Figure 3.18: **Sensitivity to anomalous SSTs.** As in Figure 3.2 c, except across multiple initialisation times and using WRF's native grid. Initialisation time are staggered by 6 hours, and indicated at the top of each picture.

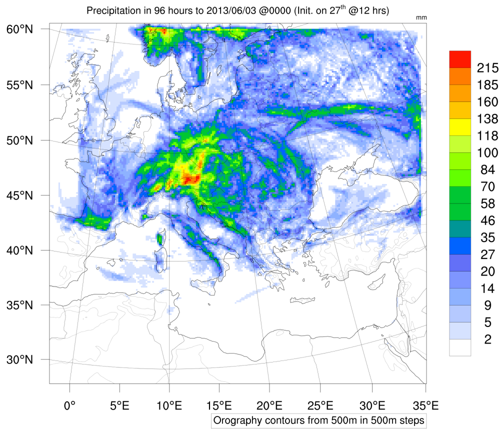

Figure 3.19: **Sensitivity to soil moisture.** As in Figure 3.2 c, except that in this simulation soil moisture has been reduced by 50% prior to model initialisation, across the whole domain.

3B

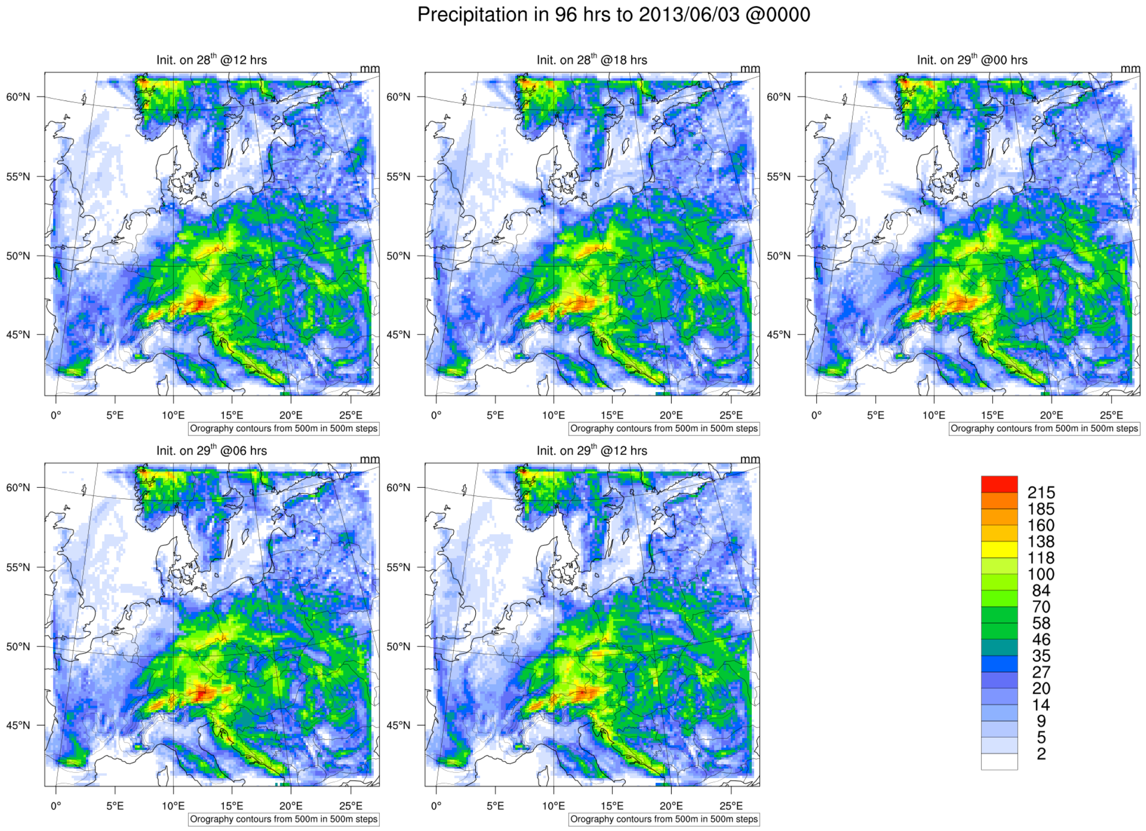

Figure 3.20: **Utility of spectral nudging.** As in Figure 3.2 c, except across multiple initialisation times and using WRF's native grid. Initialisation time are staggered by 6 hours, and indicated at the top of each picture.

3C

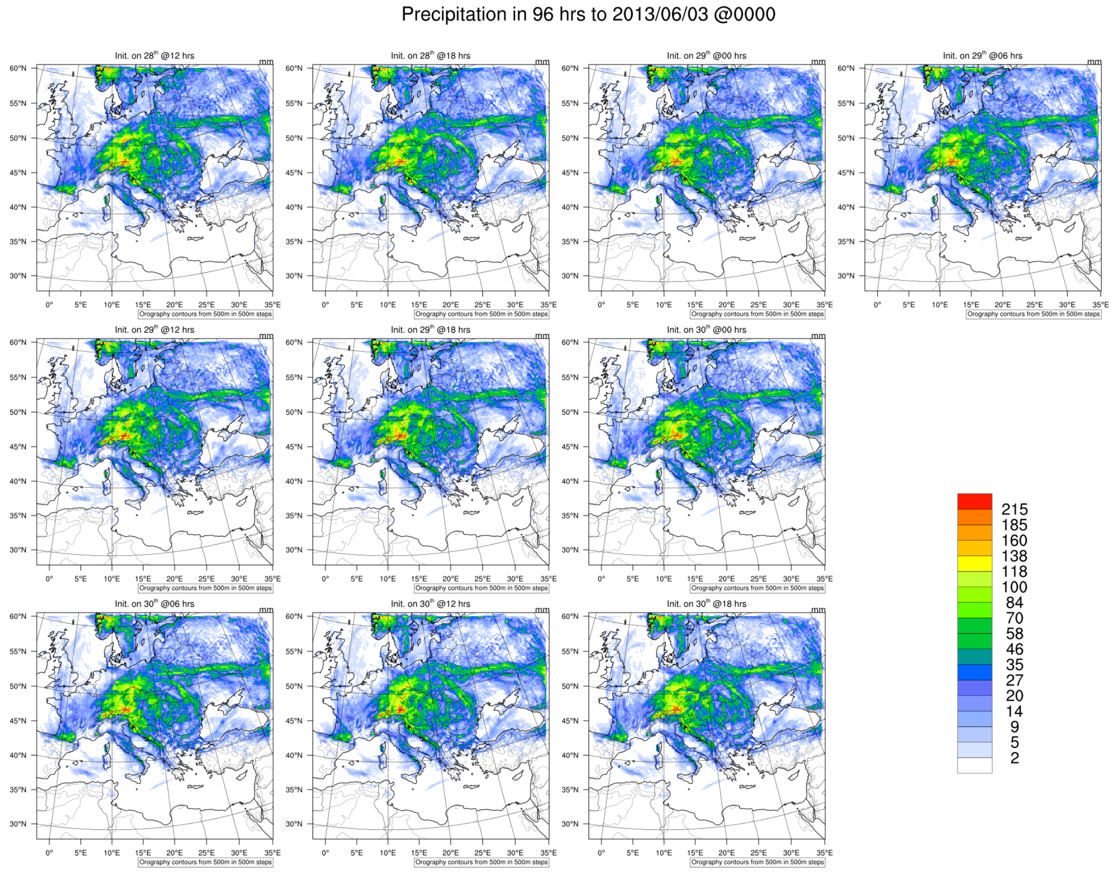

Figure 3.21: **Utility of spectral nudging.** As in Figure 3.5 a, except across multiple initialisation times and using WRF's native grid. Initialisation time are staggered by 6 hours, and indicated at the top of each picture.

4 Understanding Coastal Precipitation Extremes from a Climate Perspective

-Focus on the Black Sea and Mediterranean Region-

This chapter is motivated by the July 2012 precipitation extreme at Krymsk (§3.2), along the north-eastern Black Sea coast, and a desire to understand (i) how extreme precipitation in the Black Sea region may have been affected by recent trends in regional sea surface temperatures and (ii) whether the extremeness of the Krymsk event can be attributed to these trends. The regional modelling results presented in this chapter are based on the publication ***Crucial role of Black Sea warming in amplifying the 2012 Krymsk precipitation extreme***, by EP Meredith, VA Semenov, D Maraun, W Park and AV Chernokulsky, and published in Nature Geoscience, Vol. 8, pp. 615-619 (2015).

4.1 Introduction

One area where the potential for intense summertime precipitation has increased is the Black Sea and Mediterranean (BSM) region, a region where summertime precipitation is already dominated by intense but infrequent events [Cortesi et al., 2012]. Since the early 1980s, the BSM region has seen a substantial increase in summertime SSTs, exceeding 2 K in places. Higher SSTs lead to a moister lower atmosphere through increased surface moisture flux, and by enabling higher water vapour concentrations through sensible heating. Such heating can also reduce stability by breaking down low-level inversions. The resulting combination of increased moisture and instability provides a clear potential for enhanced precipitation. The observed summertime SST increase in the BSM region has thus mostly been co-located with a strong increase in convective available potential energy (CAPE), giving an increased risk of intense precipitation events (Figure 4.1). This is particularly true in coastal regions, where the influence of the Black and Mediterranean Seas is strongest.

The Krymsk precipitation extreme (§3.2) saw a daily precipitation total which exceeded all previous annual daily maxima since 1936 by a factor of two (Figure 4.2), when a slow moving cyclone crossing the Black Sea advected warm and moist air towards the western foothills of the Caucasus mountains (Figures 3.6, 4.7). Based on statistical evidence from

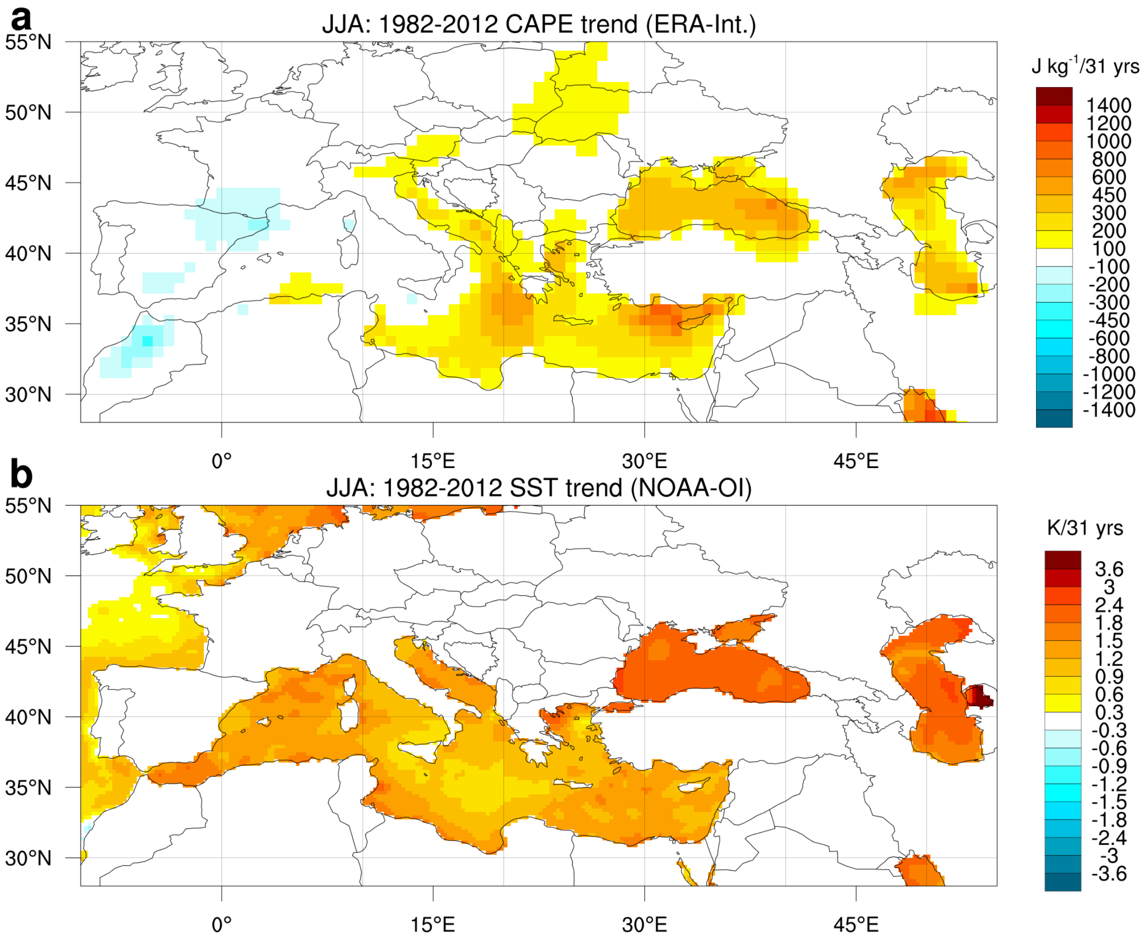

Figure 4.1: **European CAPE hotspots.** **(a)** Trend in mean summer (JJA) CAPE from 1982-2012, based on the ERA-Interim dataset [*Dee et al.*, 2011]. **(b)** Trend in mean summer (JJA) SST during the same period, based on NOAA Optimal Interpolation dataset [*Reynolds et al.*, 2007].

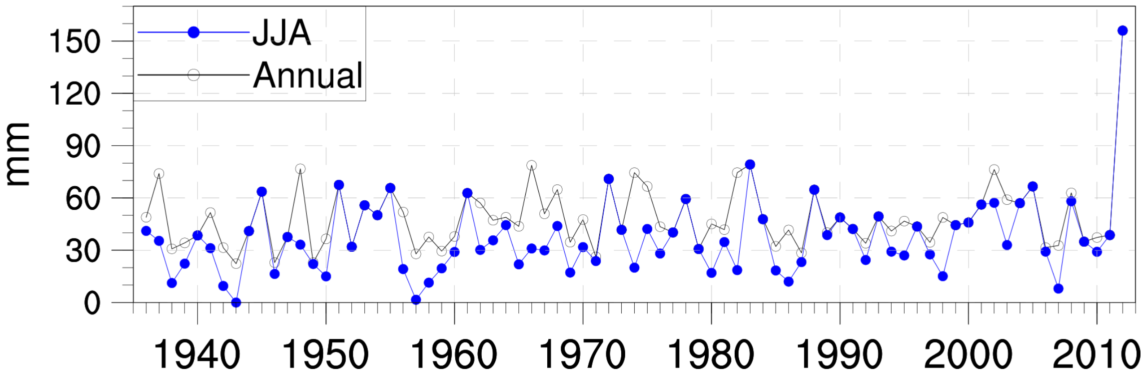

Figure 4.2: **Extremeness of the Krymsk event.** Time series of annual and summer (JJA) daily precipitation maxima at Krymsk meteorological station (44.911°N, 38.005°E) from 19362012.

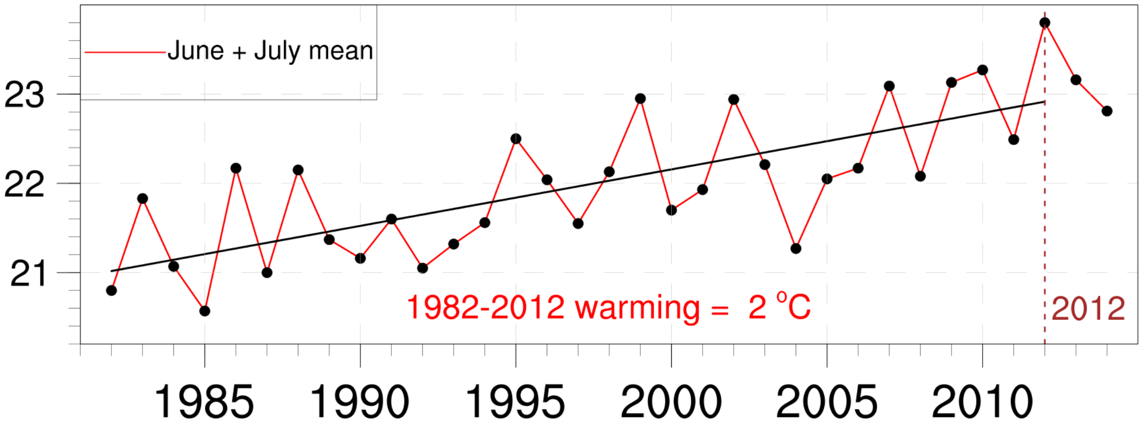

Figure 4.3: **Black Sea warming.** Time series of Black Sea area average SST for the June to July mean, from 1982-2014. The linear trend covers the 1982-2012 period.

the pre-2012 record, the magnitude of the Krymsk event should have been virtually impossible. This raises the question of whether a shift in the background climate has occurred, making such an event more likely in the present-day. Indeed, Black Sea June-July mean SSTs have steadily increased over the period 1982-2012, by 2 K (Figure 4.3); this trend is likely a superposition of anthropogenic warming and natural variability [Oguz et al., 2006]. As mentioned above, this has been accompanied by an upward trend in CAPE, greatest over the eastern Black Sea.

Understanding the Krymsk precipitation extreme is not only important because of its unprecedented magnitude [Kotlyakov et al., 2013], but also because the event is representative of a broad class of intense convective systems affecting BSM coastal regions during summertime, when precipitation is dominated by infrequent intense events [Cortesi et al., 2012]. Funatsu et al. [2009] look in detail at the large-scale environments associated with intense summer precipitation events in the Mediterranean region. Their methodology involves identifying 5 areas across the Mediterranean, from southern France to the Levant, frequently affected by heavy precipitation and then using satellite data to, first, identify heavy precipitation events (areas where rain and deep convection are co-located) and, second, identify the upper level features associated with each event. Commonalities are then identified between the upper level features of all events, using specific satellite channels (or combinations of satellite channels) for specific features, such as upper level troughs or lows (and their vertical penetration), areas of high potential vorticity and temperature anomalies. The authors show that intense summer precipitation events in the Mediterranean region are associated with an upper level trough, or low, at 200 hPa to the west of the target area, with deeper troughs for more extreme precipitation events. At the same level, they also find a potential vorticity maximum to be located in the vicinity of the area of deep convection.

For the Krymsk event, NCEP Final Analyses show the presence of a shortwave trough to the west of the Krymsk region during the precipitation event (Figure 4.4). To the east of the trough axis, a strong potential vorticity maximum can also be seen. This synoptic pattern fits with that illustrated by Funatsu et al. [2009] for intense summertime precipitation events in the Mediterranean region. It can thus be concluded that the Krymsk event is broadly representative of extreme summertime precipitation events in the BSM region.

Large stretches of the BSM region are characterised by steep orography rising from the coasts, and a densely populated coastal strip. Understanding the impact of changes in SSTs on extreme precipitation in this area is thus an important challenge. In the following sections, both global and regional modelling approaches are used to address this question.

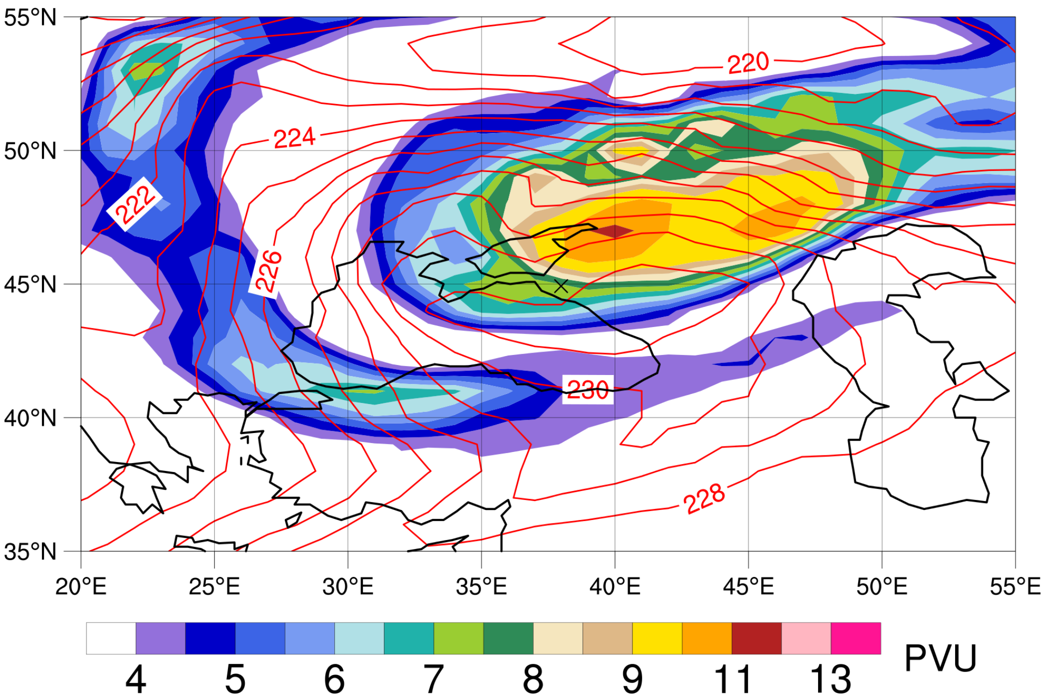

Figure 4.4: **Characteristic large-scale pattern.** Temperature (K; red contours) and potential vorticity (PVU; shading) at the 200 hPa level during July 6th 2012. Based on NCEP Final Analyses. A short-wave trough is evident to the west of Krymsk (marked with an 'x').

4.2 Global Modelling Approach

4.2.1 Experiment

To investigate the potential for more intense precipitation extremes due to SST increase in the BSM region, the ECHAM5 [Roeckner et al., 2003] atmospheric general circulation model (AGCM) is integrated over two 40-year periods[1], with each 40-year integration using a different SST climatology. In the first integration, the global SST field is based on the monthly mean 1970-1999 climatology. The second integration is the same, except that the SST field in the Mediterranean and Black Seas is based on the 2000-2012 climatology, representative of a warmer SST regime (Figure 4.5). The SST field is derived from the HadISST dataset [Rayner et al., 2003], and updated at the start of each month. The horizontal resolution is T159, roughly 0.75° and there are 31 vertical levels.

---

[1] The ECHAM5 simulations described in this section were performed by Vladimir Semenov, of the AM Obukhov Institute for Atmospheric Physics, Moscow.

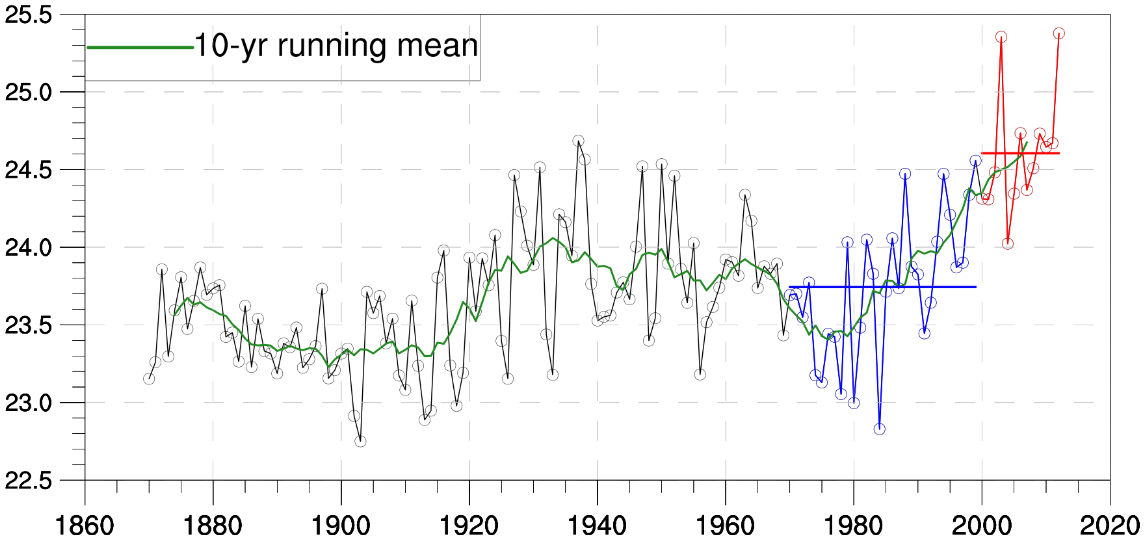

Figure 4.5: **BSM summertime SSTs.** Annual average summer SST (°C) over the Black Sea and Mediterranean, based on the HadISST dataset [*Rayner et al.*, 2007]. The periods of colder and warmer SSTs described in §4.2.1 are marked in blue and red, respectively.

For the analysis, the focus is on daily precipitation during the summer months (June, July and August; JJA). Extreme value theory [Coles, 2001] is used to compute 20-summer return levels of JJA maximum daily precipitation, the standard technique employed for such analysis [e.g. Kharin et al., 2007; Volosciuk et al., 2015]. The block-maxima approach is used, which involves taking the maximum daily precipitation for each summer in the 40-year simulation, and fitting the generalized extreme value (GEV) distribution to the resultant time series using maximum likelihood estimation. Via inversion of the GEV distribution, extreme quantiles can be obtained, e.g. the 20-summer return level [Coles, 2001]. In a given summer, the 20-summer return level of maximum daily precipitation has a probability of 5% of being exceeded.

4.2.2 Results and Discussion

The extreme value analysis of the two ECHAM5 ensembles clearly suggests that a warmer Black Sea leads to more intense summertime precipitation extremes in that region (Figure 4.6), by over 70% in the vicinity of Krymsk (§3.2). The two AGCM ensembles create their own climatologies of extreme precipitation, whose differences can be attributed to the different SST forcings. The spatially coherent structure of the changes in 20-summer return levels highlights the important role that the Black Sea plays in modulating extreme precipitation in the region. The Black Sea provides an important source of moisture for precipitating systems. More importantly though, the Black Sea can also heat and moisten

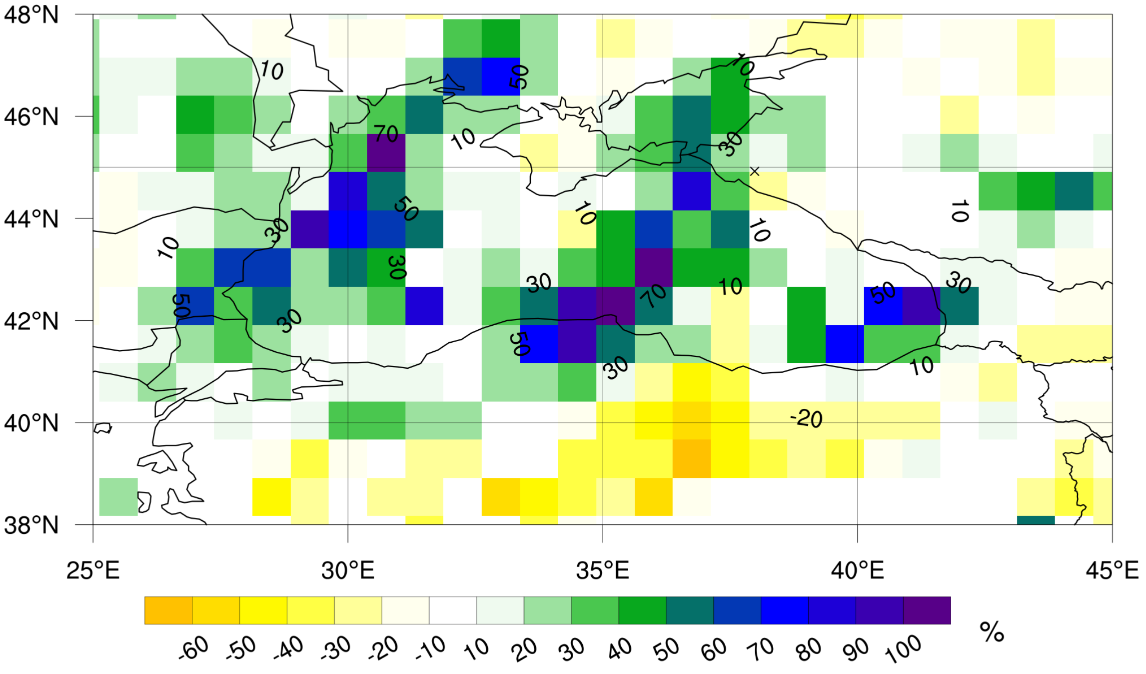

Figure 4.6: **More intense precipitation extremes.** Changes in 20-summer return levels of annual summer daily precipitation maxima due to a warmer Black Sea and Mediterranean (Figure 4.5). Krymsk is marked with an 'x'.

the lower atmosphere, increasing low-level instability and thus the potential maximum intensity of any convective systems which develop. This is reflected in the increased amount of precipitation generated by the AGCMs convective parametrization scheme in the warmer Black Sea ensemble (not shown).

While one can gain useful insights from such AGCM experiments, the coarse resolution of the global model necessitates the parametrization of convective processes that occur at unresolved scales. In a T159 model, that includes most mesoscale processes. As such, the results provide little direct information about how convective processes in the region differ under the different SST regimes. In addition to this, the ensemble-based nature of the experiment means that process analysis must be carried out based on composites of similar events; it is not possible to see how a particular system might develop under the two different SST forcings. Some of this information can, however, be obtained with a LAM setup.

4.3 Regional Modelling Approach

To simulate the response of convective extremes to climatic changes, accurately resolving local storm dynamics is essential [Kendon et al., 2014]. This is best achieved with convection-permitting resolution [Weisman et al., 2008], which comes at considerable computational cost and would make the type of experiments described in §4.2 infeasible. Another option would be to use an RCM to downscale the GCM simulations to convection-permitting resolution, though this would also be highly computationally expensive for two 40-year ensembles. To study the effect of recent sea surface warming on convective extremes within the BSM region, the devastating July 2012 Krymsk precipitation extreme (§3.2) is therefore taken as a showcase example for a range of SST sensitivity experiments at relatively low computational cost. As shown in §4.1, the Krymsk extreme provides a good proxy for studying intense summertime precipitation events affecting the BSM region.

4.3.1 Experiment

The sensitivity of the Krymsk event to recent changes in SSTs is investigated in a series of convection-permitting ensemble simulations with the WRF model [Skamarock et al., 2008]. While cyclone characteristics and large-scale atmospheric circulation have also changed over recent decades [Neu et al., 2013], including indications of increased summertime cyclonic activity in much of the BSM region [Tilinina et al., 2013], the focus of this study is solely on sensitivity to SSTs and can thus be viewed as one of conditional event attribution. In particular, it is investigated whether the extreme precipitation near Krymsk would have been possible if the same cyclone had passed over the Black Sea during a colder SST regime, characteristic of preceding decades. Potential threshold behaviour in the precipitation response to SST increase is also examined.

The synoptic and mesoscale environments which accompanied the Krymsk event are described in detail in §3.2, as is the ability of the WRF model to realistically reproduce the Krymsk event under observed SST forcings, across a 6-member ensemble. This successful reproduction provides confidence that the WRF model will also accurately simulate how the Krymsk event responds to changes in the SST field. Taking the ensemble with observed SST forcings ($\mathrm{SST_{obs}}$) as a starting point, an additional 6-member ensemble is created with identical setup, except with an SST state characteristic of the early 1980s ($\mathrm{SST_{cold}}$). For $\mathrm{SST_{cold}}$, the trend in Black Sea SSTs from 1982-2012 of an averaged 31 day period, centred on the date of the Krymsk event (6^{th} of July), is calculated. This trend, equivalent to 1.5-2.0 K over most of the eastern Black Sea and Sea of Azov (Figure 4.7), is then subtracted from the observed SST field to give the SST forcing for the SST_{cold} ensemble. NOAA's 0.25°Optimum Interpolation dataset [Reynolds et al., 2007] is used as it is the highest resolution SST dataset available that is also long enough to compute climatological trends (i.e. >30 years).

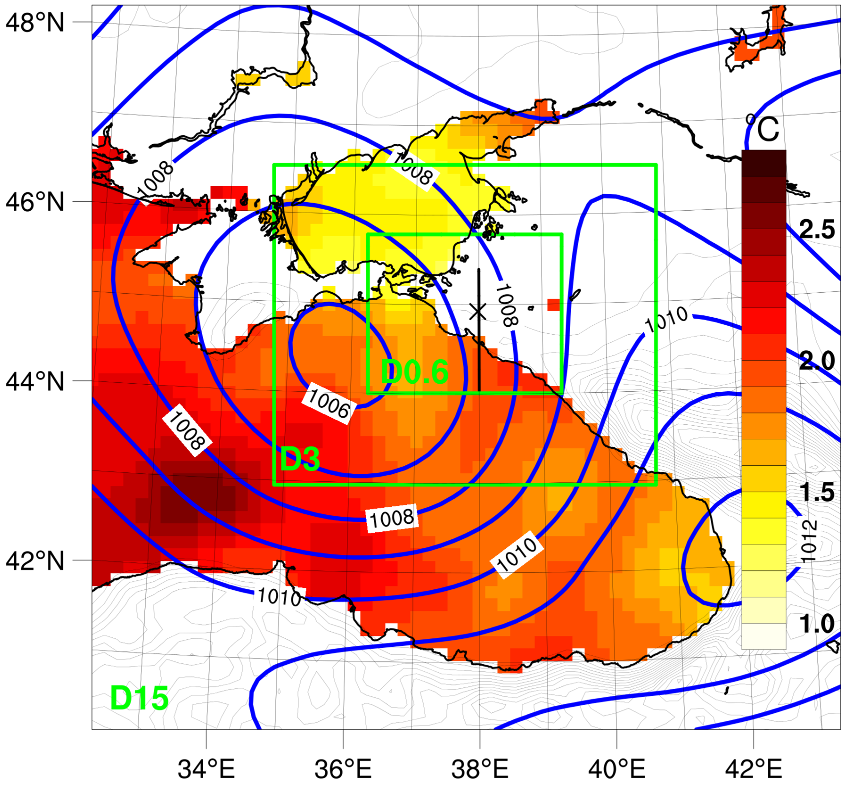

Figure 4.7: **Domains, SST anomaly and synoptic pattern.** Sea level pressure (blue contours) on July 6th 2012 at 1800 UTC, based on NCEP Final Analyses. Simulation domains D15, D3 and D0.6 (green). 1982-2012 SST trend across experimental domains (shading). Krymsk is marked with an x; light black contours denote the D15 orography field, at 150 m intervals. The black line through 38°E marks the cross-section used in Fig. 4.9.

Important aspects of the experimental setup to recall from §3.2.2 are

(i) a triply nested regional domain is used (Figure 4.7), giving horizontal resolutions of 15-, 3-, and 0.6 km (referred to as D15, D3 and D0.6, respectively);
(ii) convection-permitting resolution is used in D3 and D0.6 (remaining parametrizations are as in Table 2.1);
(iii) nesting is carried out on a 1-way basis, meaning that the higher resolution domains

do not influence the flow in their parent domains;
(iv) ensembles are created using staggered initialisation times from July 4th at 00 UTC to July 5th at 06 UTC, allowing between 21 and 51 hours prior to the first observed precipitation for the model to adjust to the imposed SST forcing, which sensitivity tests show to be sufficient;
(v) a weak spectral nudging of the U and V fields is carried out in D15 at 6-hourly intervals and at scales greater than 300 km; nudging helps to accurately maintain the large-scale circulation, without squelching the precipitation extremes [Otte et al., 2012]. This reduces sensitivity to initial conditions and thus allows the event to be consistently reproduced across staggered initialisation times; additional sensitivity studies with two-way nesting and without nudging show that the weak nudging used does not impact the precipitation response. Analyses show that the setup gives a high signal-to-noise ratio, necessitating fewer memers.

To investigate the transition behaviour of the precipitation field between a colder and warmer Black Sea, additional 6-member ensembles are created using intermediate past and extrapolated future SST states. These SST states consist of subtracting (adding) the 1982-2012 SST trend from (to) the observed 2012 SST field in 20% increments, giving a total of 11 ensembles whose SSTs differ from the observed field by between -100% and +100% of the warming trend. Each SST state can be described by

$$SST_i = SST_{obs} + \frac{i-5}{5} SST_{trend}, \text{ where } i \in [0..10] \tag{4.1}$$

All other aspects of the simulation are as described in §3.2.2. For the analysis, to what extent and through which mechanisms the increasing SSTs influence the precipitation field is investigated.

4.3.2 Results

As discussed in §3.2.3, the high resolution WRF simulation with observed SST forcing succeeds in reproducing the most intense precipitation of the Krymsk event, giving 24-hour precipitation totals in excess of 300 mm in places. Without the warmer observed Black Sea, however, the extreme precipitation is not reproducible (Figure 4.8). There is no evidence of deep convection and the extreme precipitation around the coastal hills disappears. Between the $\mathrm{SST_{obs}}$ and $\mathrm{SST_{cold}}$ ensemble means, there is an over 300% increase in the simulated precipitation around the Krymsk region (box, Figure 4.8). To understand

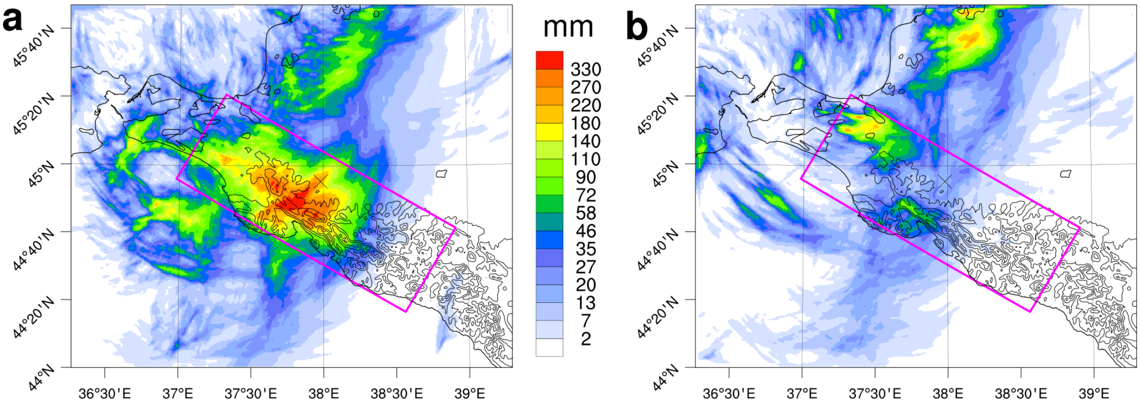

Figure 4.8: **Simulated precipitation using observed and reduced SST. (a)** Simulated 24 h precipitation total (colour scale), from 6th July at 03 UTC to 7th July at 03 UTC, using $\mathrm{SST_{obs}}$. **(b)** The same as in **a**, but using the $\mathrm{SST_{cold}}$. Both images show one member of each ensemble, initialized on 5th July at 06 UTC. Remaining members show similar patterns for both ensembles (Figure 3.11; Appendix 4A). The magenta rectangles show the area over which precipitation totals are averaged for comparison. Thin black lines show orography contours in steps of 150 m. Krymsk is marked with an 'x'.

this dramatic increase, the relative roles of thermodynamical and dynamical changes are addressed.

With observed SST forcing, the greater surface heating and moisture flux (Appendix 4B) cause average moisture content to increase by up to 20% in parts of the lower atmosphere (Figure 4.9), compared to the $\mathrm{SST_{cold}}$ ensemble. The specific humidity increase exceeds what would be expected based on temperature increase at the same level, i.e. following the CC relation, and is partly achieved through higher relative humidity around the upper PBL (Figure 4.10). With atmospheric moisture increasing on a basin-wide scale, it is clear how local precipitation increases could be magnified through moisture convergence.

These thermodynamical changes, however, clearly cannot fully account for the much larger increase in precipitation. Dynamical changes due to the triggering of deep convection play the major role in the precipitation increase. Enhanced vertical velocities over the coastal hills and increased specific humidity in the upper troposphere are evident in the $\mathrm{SST_{obs}}$ ensemble, indicating a deep convection event centred over the mountain ridge (Figure 4.9). The deep convection is made possible by changes in the thermodynamical properties of the airmass upstream of Krymsk. Higher SSTs warm and moisten the lower atmosphere, increasing the low-level conditional instability and hence the potential for intense precipitation should a source of uplift be found (Figure 4.11). Despite the same synoptic forcing,

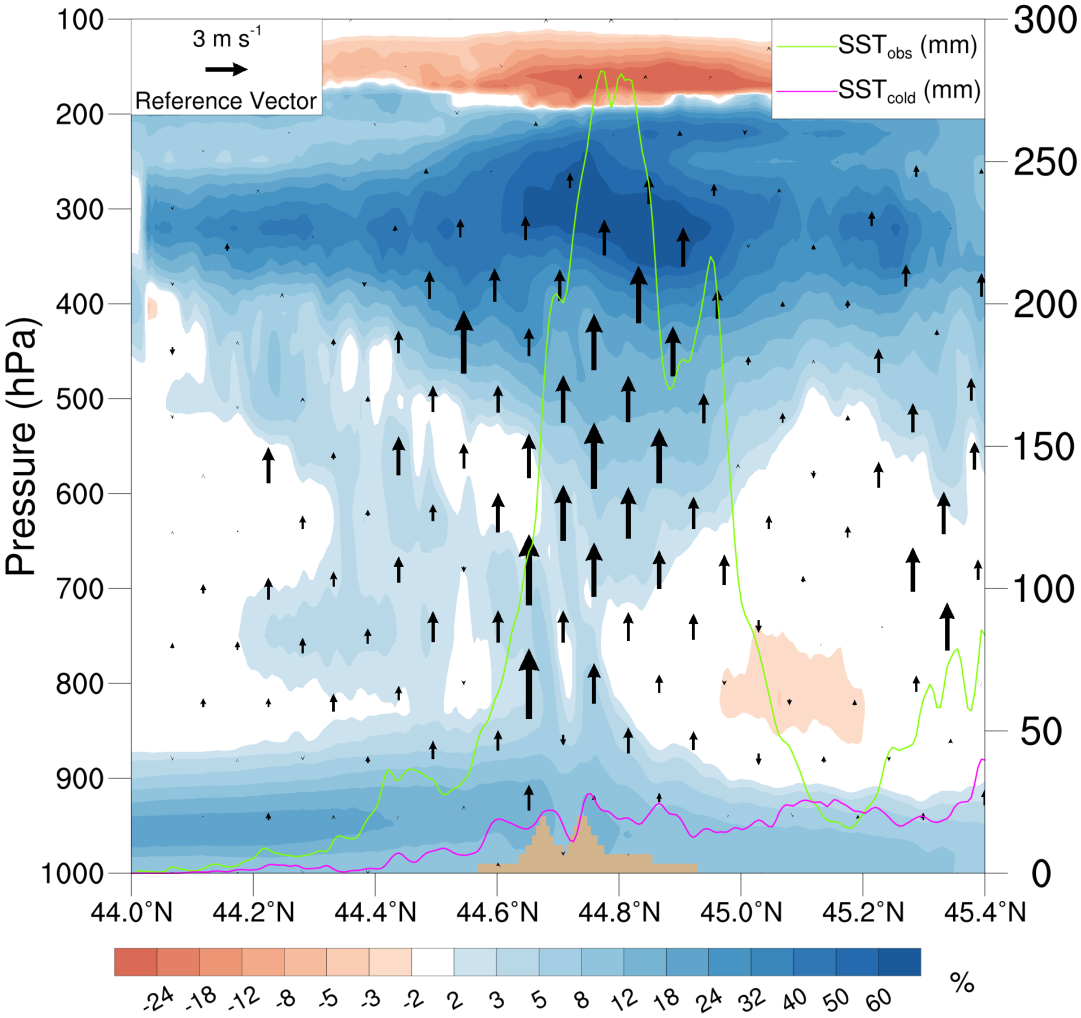

Figure 4.9: **Triggering deep convection in response to observed SST.** Cross-section through 38.0° E (as marked in Fig. 4.7) showing the percentage change in ensemble mean specific humidity between $\mathrm{SST_{obs}}$ and $\mathrm{SST_{cold}}$ in D0.6. Vectors show differences in vertical velocity maxima between the two ensemble means, calculated by taking the vertical velocity maxima of each member and then averaging this across all ensemble members. The temporal period over which these values are calculated is the same as in Fig. 4.8. The green and magenta lines are cross-sections of the precipitation in Fig. 4.8 a,b, respectively. Tan filling represents orography.

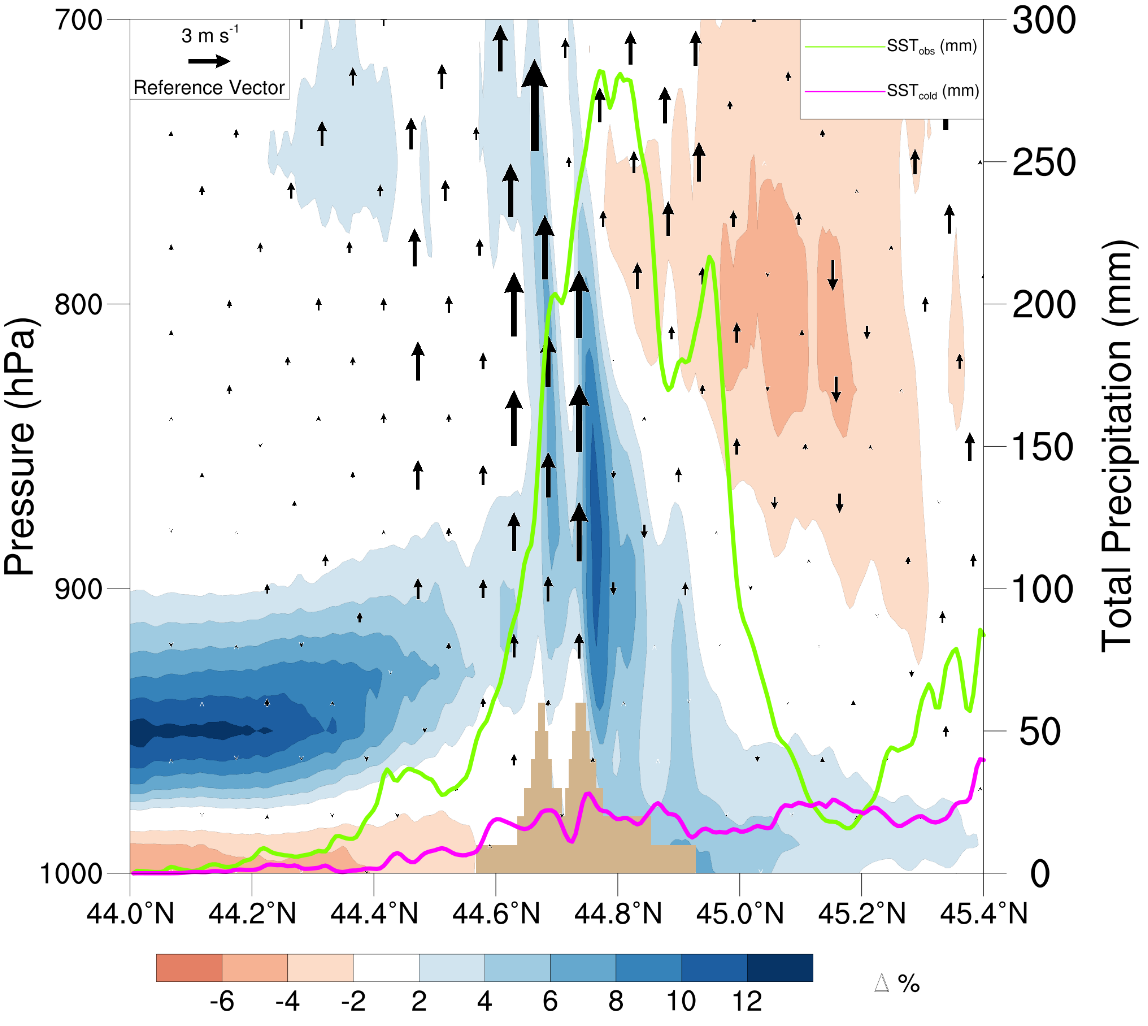

Figure 4.10: **Relative humidity change.** Cross-section showing change in ensemble mean relative humidity between SST_{obs} and SST_{cold}, through 38.0°E in D0.6. While relative humidity increases above and in the upper planetary boundary layer (PBL) in SST_{obs}, a slight decrease in the lower PBL is also evident. Note that the increase shows the change in relative humidity percentage, *not* the percentage change. The temporal period is as in Fig. 4.8. The vectors and green and magenta lines are as in Fig. 4.9.

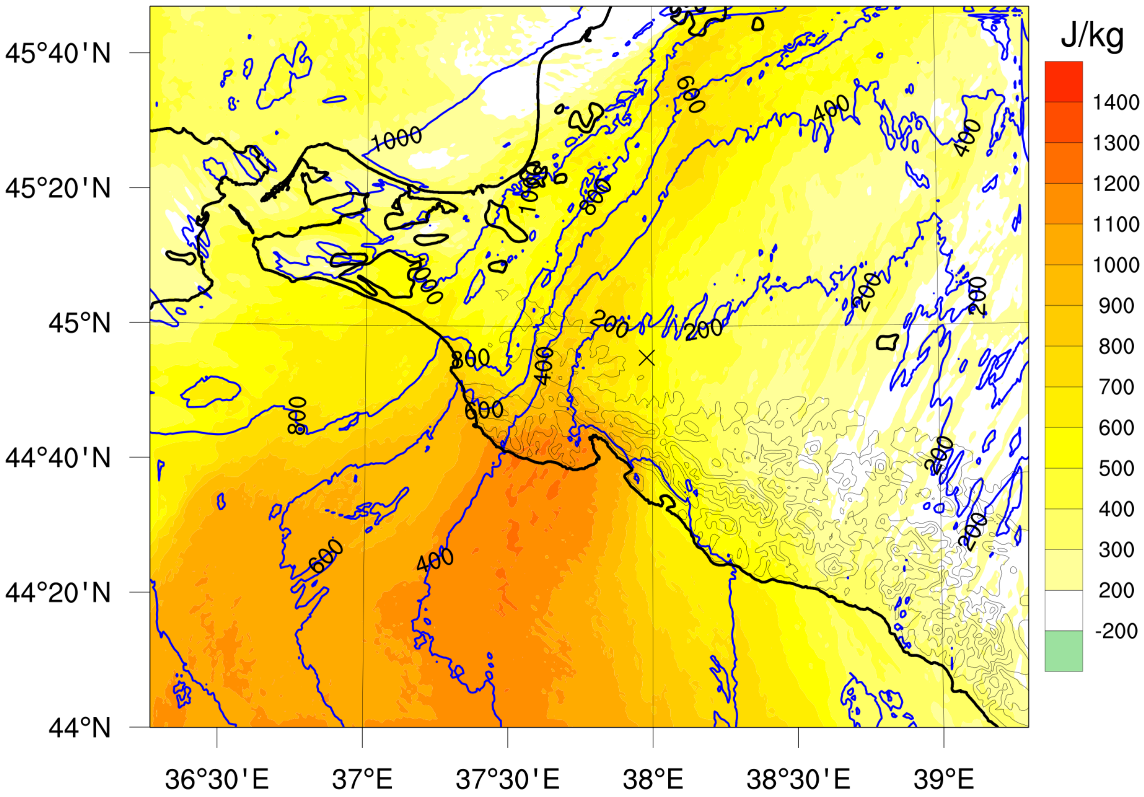

Figure 4.11: **Increased instability.** Change in CAPE maxima between the $\mathrm{SST_{obs}}$ and $\mathrm{SST_{cold}}$ ensembles. CAPE maxima during the precipitation event are calculated for each ensemble member, before averaging across all members. The blue contours show the ensemble mean CAPE maxima for $\mathrm{SST_{cold}}$. The temporal period is as in Supplementary Fig. 4.8. The thin black lines show orography contours in 150 m steps.

the higher CAPE results in a dramatically different response to orographic lifting of the onshore flow (Figure 4.9). In $\mathrm{SST_{cold}}$, orographic lifting cannot trigger deep convection due to the stability of the airmass being advected shorewards. Instead, parcels become negatively buoyant and simply restore downwards in the lee of the hills, back to their equilibrium levels (Figure 4.12). By contrast, convective latent heat release, in response to lifting moister and less stable air, drives further vertical motions in the $\mathrm{SST_{obs}}$ ensemble. These must be offset by increased convergence towards the lifting zone, fuelling further convection and intensifying the convective system. In this sense, the thermodynamic and dynamic changes are interrelated and cannot be fully separated.

The dramatic shift from a state without notable convection to one with deep convection motivates studying the transition behaviour for increasing SSTs in more detail. This is done by using the intermediate past and extrapolated future SST states described in the

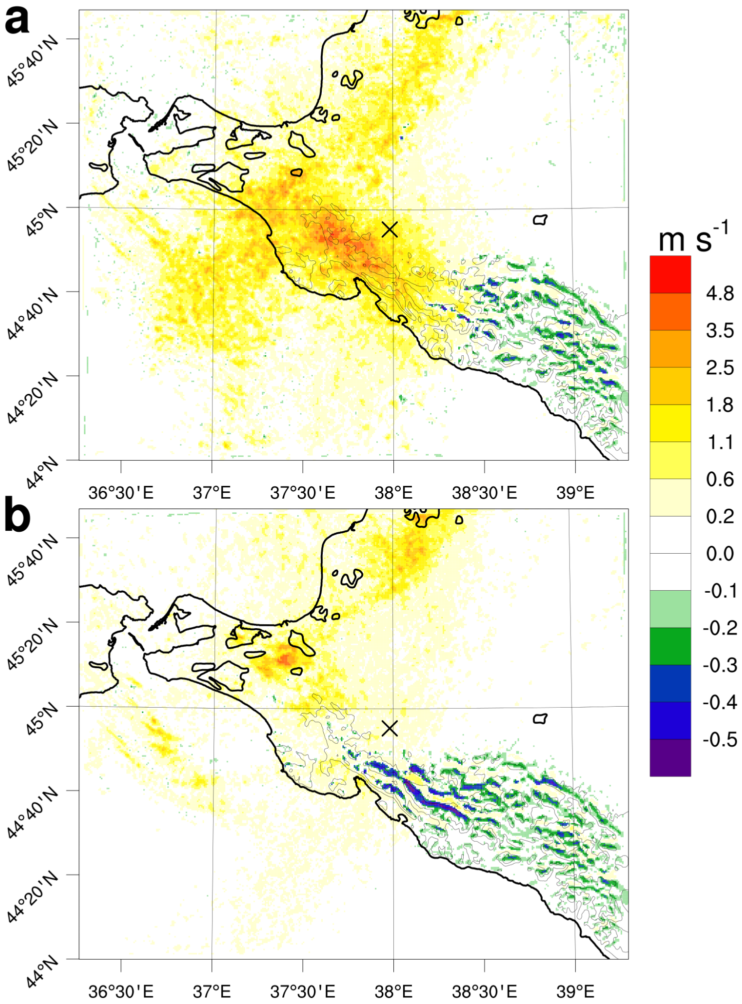

Figure 4.12: **Increased vertical velocity maxima.** Column averaged vertical velocity maxima for **(a)** SST$_{\text{obs}}$ and **(b)** SST$_{\text{cold}}$. Maxima of column average vertical velocity are taken for each ensemble member, before being averaged across all members. The temporal period is as in Fig. 4.8. Thin black lines show orography contours at 200 m and 400 m. For the SSTobs ensemble, vertical velocity maxima show strong upward motions over the coastal hills surrounding Krymsk. For the SSTcold ensemble, vertical velocity maxima are greatly reduced and, in the lee of the coastal hills, are orientated downwards. This suggests that in the SST$_{\text{cold}}$ ensemble, air parcels reaching the coastal hills were sufficiently stable that orographic lifting could not trigger any convection or additional vertical motion and instead parcels simply restored towards their equilibrium level in the lee of the hills.

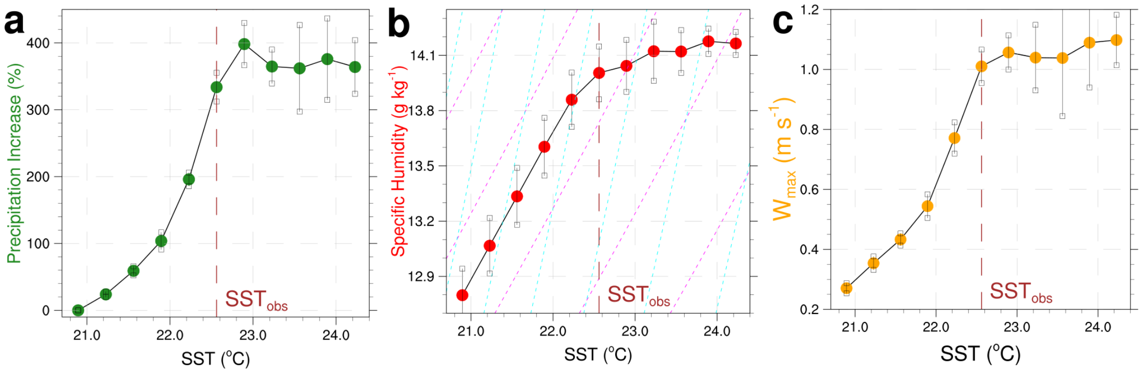

Figure 4.13: **Nonlinear response to incremental SST increase.** Two-metre specific humidity versus SST. Dashed magenta and cyan lines show the CC and double CC rates of increase, respectively. **(c)** Column average vertical velocity maxima versus SST. SST values are area averages over all sea points in D0.6. All other variables are area averaged over the rectangle marked in Fig. 4.8. Small squares denote 95% confidence intervals. The temporal period is the same as in Fig. 4.8.

Experiment section (§4.3.1). For the Krymsk event, the dramatic precipitation increase from SST$_{\text{cold}}$ to SST$_{\text{obs}}$ does not continue inexorably with further SST increase. Instead, precipitation totals stabilize once SSTs cross a certain threshold (Figure 4.13 a). The mechanisms behind this nonlinear response to SST increase are explored in depth in chapter 5, so here are discussed briefly.

As SSTs increase, low-level humidity in the Krymsk region initially increases at the CC rate, keeping relative humidity constant, before falling sub-CC (Figure 4.13 b) and decreasing the relative humidity. Lower relative humidity acts against increasing virtual temperature, thus curbing the increase in CAPE brought about by higher SSTs, which makes further intensification of the precipitation more difficult. Reduced relative humidity also inhibits latent heat release from ascending air parcels, tempering the enhancement of updraughts (Figure 4.13 c), and hence precipitation, as parcels are orographically lifted. Similar reduction in relative humidity associated with intense precipitation events occurring at higher temperatures has elsewhere been observed [Hardwick-Jones et al., 2010]; here such decreases are found primarily in the lower PBL. Across the ensembles, the decrease in low-level relative humidity results from a few factors. Higher SSTs set off vertical motions at ever faster rates, making it more difficult for the surface layer to remain saturated. More importantly, though, more intense precipitation once deep convection becomes established produces stronger convective downdraughts and low-level cooling. These downdraughts transport relatively dry air into the sub-cloud layer, locally damping low-level instability.

Additionally, increased precipitation over the sea in the warmer SST ensembles also limits the moisture that reaches the Krymsk region.

4.3.3 Discussion and Conclusions

When seeking to attribute extreme events to different forcings, two main modelling approaches have been pursued to date. The most common is probabilistic event attribution [Stott et al., 2004], in which the likelihood of a certain type of event is compared between two different climates, based on large ensembles of global climate model simulations under different forcings. This approach has been used to both identify and exclude anthropogenic contributions to recent temperature [Herring et al., 2014; Stott et al., 2004] and precipitation [Pall et al., 2011; Herring et al., 2014] extremes. An alternative approach involves using a regional model to simulate an observed event under different boundary forcings [e.g. Fischer et al., 2007]. The fixed lateral boundary conditions in the RCM setup give a higher signal-to-noise ratio, allowing finer resolution simulations which offer better understanding of local-scale processes not resolved by global models. Here, this method has been further developed to study the sensitivity of a small-scale convective extreme to long-term SST trends, using convection-permitting resolution across a spectrum of forcing strengths. In the context of extreme event attribution, this is the first study to demonstrate such nonlinear/threshold behaviour.

The results reveal a physical mechanism linking a sudden amplification of coastal convective precipitation extremes to gradual SST increase. The increased lower tropospheric humidity provides a richer moisture source for convective precipitation and contributes to low-level instability. More importantly, the near-surface warming reduces static stability, allowing deep convection to be more easily triggered, increasing precipitation around Krymsk by over 300%. The strongly nonlinear nature of the precipitation response to incremental SST increase also suggests that the thermodynamical bounds of atmospheric moisture increase may not be a reliable predictor of changes in regional convective precipitation extremes; static stability and mesoscale dynamics clearly also play important roles. Extreme precipitation in coastal regions may instead be governed by regional tipping points, whereby SST thresholds favouring more powerful convective systems are key. The Black Sea may have exceeded one such threshold. With climate projections predicting increased SSTs [Kirtman et al., 2013] and summertime cyclone activity [Loeptian et al., 2008] in the BSM region, this suggests a corresponding increased risk of intense convective precipitation events. Other coastal regions with comparable geographical features may, where similar trends are projected, be similarly affected.

The Krymsk event was one of several recent meteorological extremes in which unusually intense precipitation was accompanied by anomalously high SSTs [Trenberth et al., 2015]. Using the methodology outlined in this chapter, the contribution of climatic changes to such events can be investigated at the high resolutions and range of forcings necessary to reveal the key physical mechanisms driving such events. This provides quite different information to that obtained from the probabilistic approach, where changes in likelihood are the focus. In addition to this, the methodology also allows past extreme events to be simulated under contemporary thermodynamical conditions, revealing how they would develop under present-day or near-future conditions, which should provide valuable information for local planners.

4.4 Appendix

4A

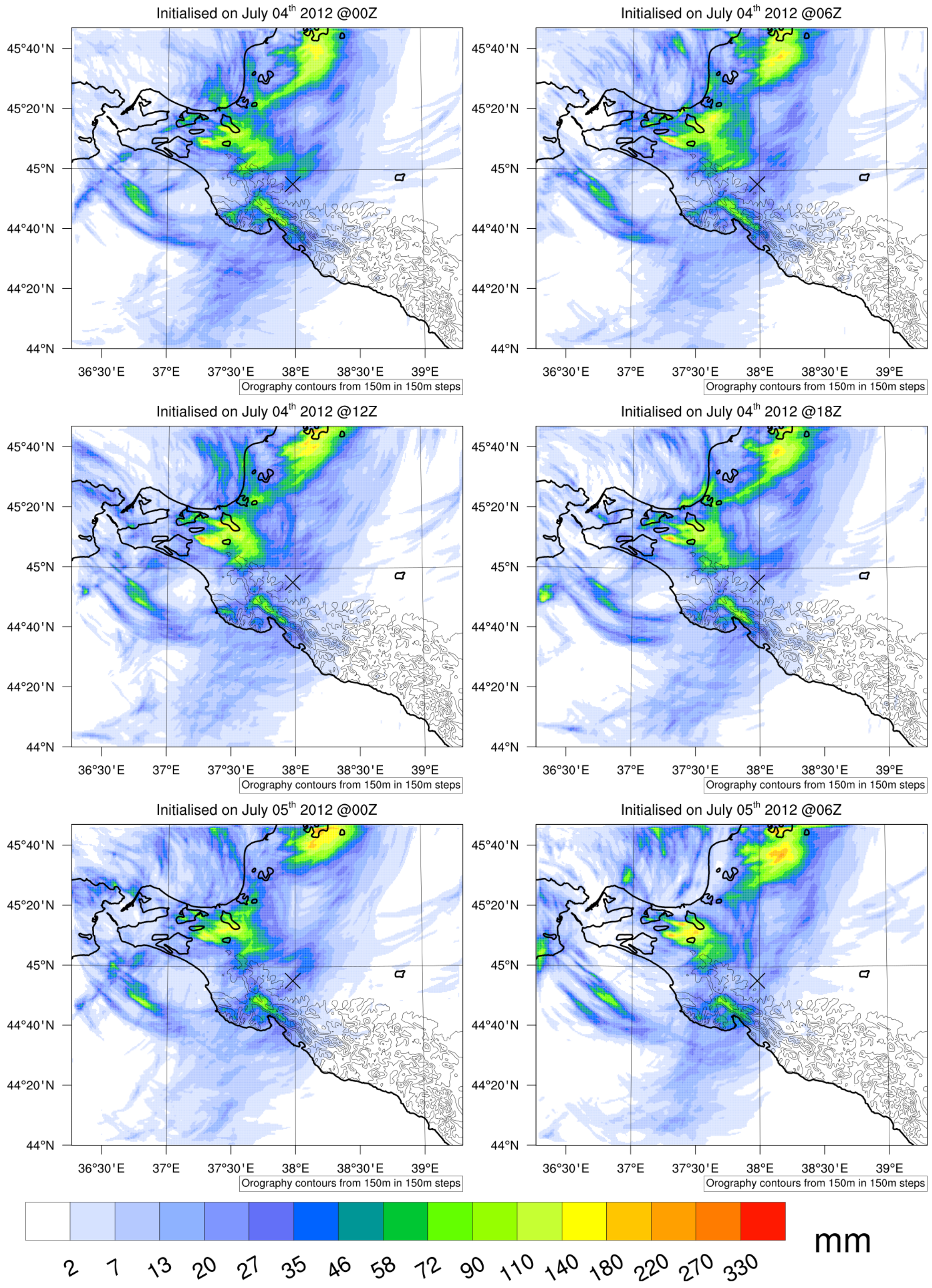

Figure 4.14: **$\mathbf{SST_{cold}}$ ensemble.** Simulated 24-hour precipitation totals as in Figure 3.11, except for the coldest SST state (SST_{cold})

4B

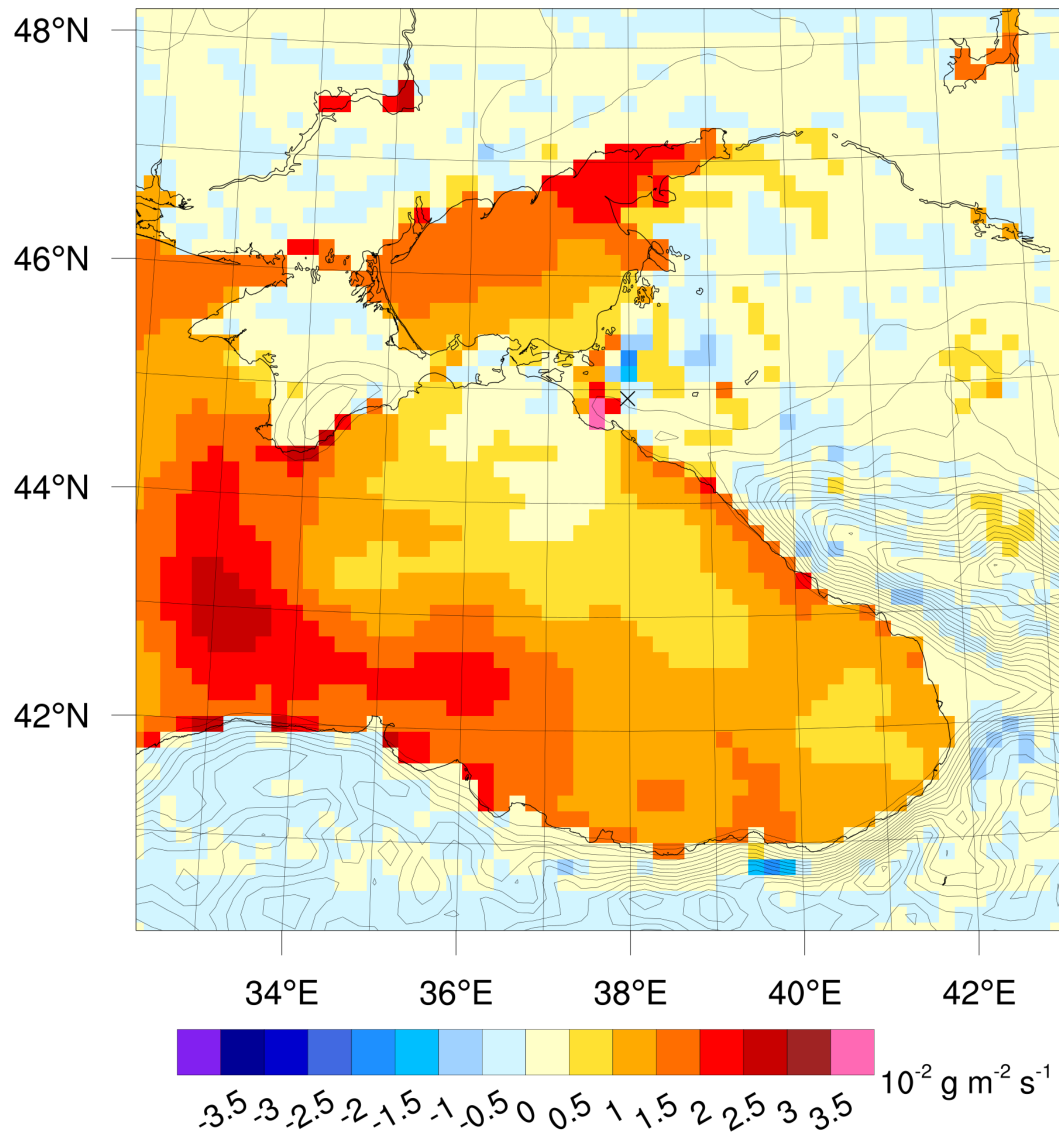

Figure 4.15: **Increased Surface Moisture Flux.** Difference in mean instantaneous surface moisture flux, for D15, between the SST_{obs} and SST_{cold} ensemble means. The temporal period is as in Fig. 4.8. Thin black lines show orography contours in 150 m steps.

5 Evidence for added value of convection-permitting models for studying changes in extreme precipitation

In this chapter, the Krymsk event is used to study the added-value of convection-permitting models. The response of the simulated precipitation intensity is compared between simulations with parametrized and explicit convection. Physical mechanisms behind differences in the responses are then identified. This chapter is based on the paper of the same name, by EP Meredith, D Maraun, VA Semenov and W Park, which has been accepted in *Journal of Geophysical Research: Atmospheres.*

5.1 Introduction

Precipitation extremes can strongly affect society. Understanding the response of extreme precipitation to a changing climate and how this is represented in climate models is thus an important challenge. The intensity of precipitation extremes is expected to increase in a warming climate [Allen and Ingram, 2002; Trenberth, 1999]. Such an increase has been detected in observational studies [Karl and Knight, 1998; Groisman, 2005; Seneviratne et al., 2012; Donat et al., 2013] and is also projected by global climate models [Semenov and Bengtsson, 2002; Kharin et al., 2007; Orlowsky and Seneviratne, 2011], primarily in the tropics and high latitudes. In particular, coastal precipitation extremes can be sensitive to sea surface temperature (SST) increase [Diffenbaugh et al., 2005; Meredith et al., 2015].

The representation of precipitation extremes in climate models, however, has been shown to be highly sensitive to model resolution, much more so than that of the mean [Volosciuk et al., 2015]. Additionally, there is a growing body of evidence [Kendon et al., 2012; Chan et al., 2014a; Ban et al., 2014] suggesting that convection-permitting resolution (O($\sim$2 km)) is essential for accurately capturing mid-latitude summertime convective extremes.

The lower the model resolution, the fewer the processes important for precipitation that can be resolved. Convective parametrization schemes help to address this. Such schemes were originally designed to prevent instability from building up over too long a period and too wide an area before triggering convection, which would lead to unrealistically intense large-scale convection and overly active low-level cyclogenesis, and to account for vertical motions and the associated latent heating. These aims are achieved by rearranging temperature and moisture in the atmospheric column, producing precipitation as a by-product. Convection schemes generally consider grid-box averages of meteorological variables to decide when convection is triggered. The Kain-Fritsch scheme [Kain, 2004], used in this study, identifies updraught source layers (USLs) based on the mean thermodynamical properties of low-level parcels. In simple terms, the parcel from the USL is then prescribed a perturbation temperature related to grid-resolved vertical velocity; if the sum of this plus the temperature at the lifting condensation level is greater than the environmental temperature, the parcel is considered for deep convection. A 1-dimensional Lagrangian model is then implemented to estimate the parcel's vertical velocity. If vertical velocity remains positive over a minimum cloud depth, deep convection is activated. The scheme then rearranges mass in the column via updraughts, downdraughts and environmental mass fluxes until at least 90% of CAPE is removed, producing precipitation as a by-product. CAPE removal is achieved through a combination of heating aloft and reduced equivalent potential energy in the USL. While convective parametrization schemes improve the representation of precipitation in coarser models, the low resolutions of such models make it inevitable that many of the localized effects which influence precipitation, in particular extreme precipitation, at mesoscales cannot be accounted for by the model or parametrization scheme.

In achieving higher resolutions that more faithfully resolve extreme precipitation events, dynamical downscaling can add value to general circulation model (GCM) output. When considering the added value (AV) of higher resolutions, a distinction should be drawn between adding fine scale detail and adding value at the spatial scale of the driving climate model. For precipitation, the potential AV of increased model resolution is greatest (i) at short temporal scales, (ii) during the warm season, i.e. when convection dominates, and (iii) in regions of complex topography, regardless of the season and temporal scale [Di Luca et al., 2012]. Further AV (for multiple variables) is achieved in coastal zones and in environments with high mesoscale variability [Feser et al., 2011]. Convection-permitting resolution yields additional AV through the improved representation of both the diurnal convective cycle and deep-convective processes [Hohenegger et al., 2008; Prein et al., 2013].

Importantly, AV not only refers to the representation of present day climate, but in particular to the representation of the corresponding climate change signal. GCM resolution, for example, is known to influence the strength of the response to warming of precipitation extremes [Kitoh et al., 2009; Li et al., 2011b; Yang et al., 2014]. Additionally, the need to parametrize convective processes in GCMs raises questions about how well the response to warming of convective precipitation extremes is captured in such models. Convection-permitting resolution is thus most likely essential to correctly capture the climate change signal of summertime convective extremes [Kendon et al., 2014; Ban et al., 2015].

The AV of higher resolution simulations, for example in regional climate models (RCMs), lies in their ability to simulate physically coherent process chains which may, or may not, modulate and improve the climate change signal [Di Luca et al., 2015], as has recently been demonstrated in convection-permitting simulations (CPSs) of summertime extreme sub-daily precipitation [Chan et al., 2014b; Kendon et al., 2014; Ban et al., 2015].

Due to high computational expense, however, differences in the sensitivity of extreme precipitation to boundary forcing enhancement between parametrized and convection-permitting models, and the underlying mechanisms, have not been studied in detail, for example over a spectrum of forcing strengths. In this respect, RCM sensitivity studies of individual extremes can be an instructive, yet inexpensive, tool. The traditional GCM or GCM-RCM approach to investigating precipitation extremes, requiring climate timescale simulations to create adequate statistics, would be hardly computationally feasible at convection-permitting resolution and over a wide range of SST states, each representative of different climate regimes.

Downscaling to convection-permitting resolution does come with its own caveats though, as the choice of convective parametrization in the coarse domain may strongly influence the development of convection in the inner convection-permitting domain(s) [Warner and Hsu, 2000; Lean et al., 2008].

As demonstrated in chapter 4, convection-permitting RCM simulations can reveal the potential for a highly nonlinear response of coastal extreme precipitation to SST increase [Meredith et al., 2015]. Here the devastating 2012 precipitation extreme near the Black Sea town of Krymsk (§3.2.1) is again taken as a recent showcase example, and used to explore the sensitivity of extreme precipitation to SST increase in ensemble simulations with parametrized and explicit convection, over a wide range of SST forcings. Focusing on the underlying mechanisms, evidence is presented for the AV of CPSs for studying changes in convective precipitation extremes.

5.2 Methods

Changes in precipitation extremes outside of the tropics are believed to be primarily influenced by thermodynamical changes [Emori and Brown, 2005], rather than changes in large-scale circulation. In this framework, it is assumed that for each precipitation extreme in the present climate there is an analogous event in a future climate, occurring under a comparable atmospheric circulation but in a warmer and hence moister environment [Lenderink and van Meijgaard, 2008]. Working within this paradigm, alternate storylines [Hazeleger et al., 2015] of the Krymsk event are created for a spectrum of SST regimes, and the sensitivity of the extreme precipitation to SST increase is compared between simulations with parametrized and explicit convection.

5.2.1 Model and Experiment

The model and experimental setup are identical to that described in chapter 4 and §3.2.2. The experiment differs only in how the model output is analysed. This setup allows the sensitivity of extreme coastal precipitation to enhanced SSTs to be compared between simulations with parametrized and explicit convection, while keeping computational expenses relatively low. For each domain, convective processes are handled in a manner appropriate to the horizontal resolution. Convection is thus parametrized in D15, while no convective parametrization is used in D3 or D0.6. D15 thus differs from the other simulations in its horizontal resolution and in its treatment of convection. In D15, five convective parametrization schemes were tested, leading the Kain-Fritsch scheme [Kain, 2004] (with default tuning parameters) to be selected to drive the convection-permitting domains, due to its superior simulation of the event. The extreme precipitation responses to increasing SSTs for the remaining convective parametrization schemes (D15 only), which lead to the same conclusions, are also presented.

For the analyses, the D15 and D0.6 simulations are compared over their common area, i.e. that of D0.6. Importantly, all data from the fine resolution simulations are aggregated to the coarse D15 grid *prior* to analysis; this involves taking the mean of all D0.6 grid cells that are located within the area of a given D15 grid cell, for each D15 grid cell covering the D0.6 domain. As such, the simulations are compared at the same spatial scales to assess the AV of CPSs, rather than simply the added small-scale detail. Differences in the simulations are attributed to differences in their treatment of convection, taking account of the resolution appropriate to each method of treating convection. For extreme precipitation, an objective method is used to identify and analyse the maximum local intensity of the precipitation event, at hourly intervals. This entails considering the spatial precipitation maximum each hour, i.e. the (15 km resolution) grid cell within the D0.6 area that has the highest hourly precipitation total. This is referred to as the '*hourly precipitation maximum*'. Physical changes associated with the hourly precipitation maximum serve as the clearest objective illustration of changes occurring in areas of the grid affected by intense precipitation. The two waves of convection are treated separately.

5.3 Results

The ability of the WRF model setup to reproduce the Krymsk event with observed forcings is validated in detail, for D0.6, in §3.2.3 and in Meredith et al. [2015]. Additional validation, provided in Appendix 5A, shows that the event magnitude is well captured by the D0.6 simulation. Intensities on the D0.6 native grid and their corresponding aggregation to D15 yield similar magnitudes, indicating that the highest intensities were spread over a relatively large area. D15, however, fails to fully capture the observed rainfall intensity. The compatibility of the D0.6 precipitation totals with observations gives confidence in the faithfulness of the simulation, allowing its modelled fields to be treated as a plausible reference to compare against. Here, the focus is on how the event responds to boundary forcing enhancement (in this case SST) under parametrized and explicit convection.

Area average precipitation (over the common D0.6 area) during the event is qualitatively similar in the parametrized and explicit convection simulations (Figure 5.1 a,b), and shows a broadly similar response to increasing SSTs. The clearest difference between the two simulations is in the duration of the precipitation event. The first wave of precipitation, in particular, is notably longer with parametrized convection. Looking at hourly precipitation maxima, however, order of magnitude differences in precipitation intensity are evident between the simulations with parametrized and explicit convection (Figure 5.1 c,d), even though the results of the D0.6 simulation have been aggregated to the D15 grid. These results highlight the well-known tendency for extreme precipitation events to be too temporally persistent, spatially widespread and not locally heavy enough in models with parametrized convection [Kendon et al., 2012], and point towards the AV of CPSs at local and sub-daily scales. The more realistic local precipitation intensities produced by CPSs result from improved representation of convective features when convection is explicitly resolved [Lean et al., 2008]. In the following, these features and how their improved representation modulates the precipitation response are investigated.

Temporally averaging over each wave of convection, the response shape of hourly precipitation maxima to increasing SST can be more clearly seen (Figure 5.2). Between

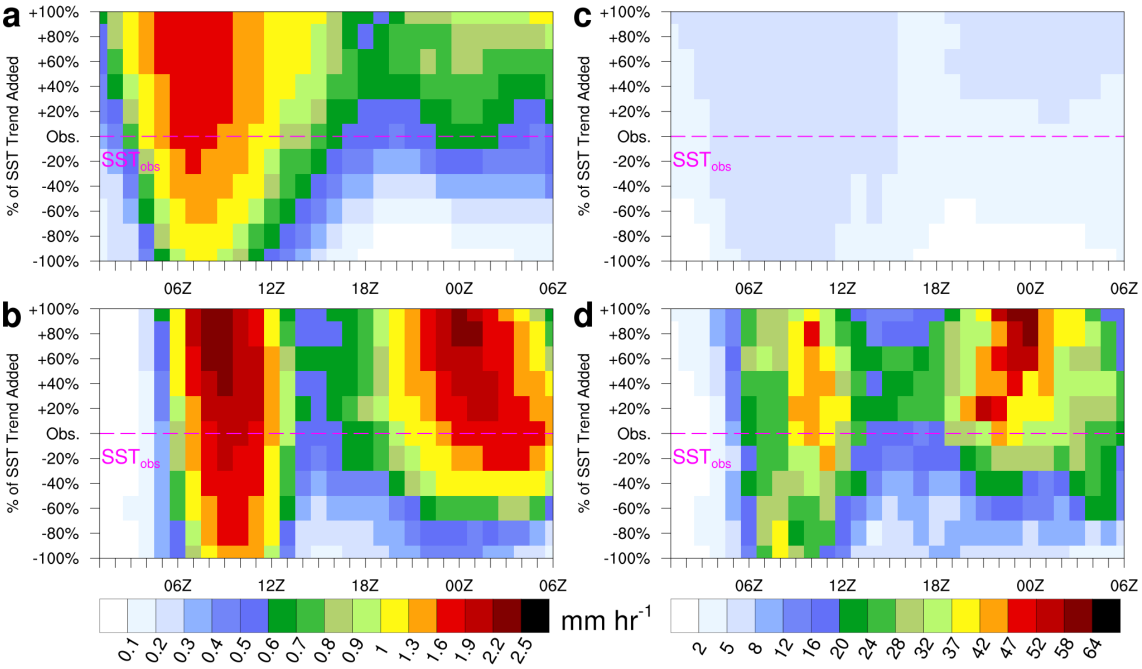

Figure 5.1: **Temporal evolution of precipitation event for different SST forcings.** Area average precipitation over inner domain area for (a) 15 km resolution simulation with parametrized convection and (b) 0.6 km resolution simulation with explicit convection. Panels (c) and (d) are as in (a) and (b), respectively, except for grid cell precipitation maxima. Results are based on ensemble means, all data are aggregated to the 15 km resolution grid, and only grid cells within the area of D0.6 are considered.

the parametrized and explicit convection simulations, the transition behaviour from the lowest to the highest SST notably diverges, despite the parametrized convection simulation driving the higher resolution domains. The CPSs respond overall more strongly to increasing SST, during both waves of convection. More importantly though, the CPSs exhibit a strongly nonlinear precipitation response to increasing SST, characteristic of a transition into a high precipitation regime [Meredith et al., 2015]. The nonlinear nature of the precipitation response to increasing SSTs is either strongly damped (first wave) or completely missed (second wave) in the simulations with parametrized convection. The nonlinear relationship also holds at the daily scale (Figure 5.2 c). The strong divergence of the convective response in the convection-permitting D0.6 from that of the coarse D15 suggests that, in order to maximize the AV of CPSs, suitably large convection-permitting grids can be used to negate the influence of the coarse grid convective parametrization on the inner domain's solution, as speculated by Warner and Hsu [2000]. Grid sizes of 156×131 and 391×321 are used here for D3 and D0.6, respectively.

In the remainder of this section, the physical mechanisms behind the different precipitation responses is investigated. To this end, the hourly precipitation maximum provides a measure of the maximum local intensity of the event, and the clearest illustration of the physical effects occurring in areas affected by intense precipitation. For brevity, the focus is on the second wave of convection, where the differences are more pronounced. Analysis of the first wave of convection, which leads to similar conclusions, can be found in the Appendix to this chapter (5C).

Increasing SSTs create a warmer and moister lower atmosphere, resulting in higher convective available potential energy (CAPE) and lower convective inhibition (CIN). To a first approximation, this should give the potential for precipitation intensity to increase in parallel. The strong differences in local precipitation intensity evident in Figure 5.1, however, also affect the local atmospheric profile. In particular, the more intense precipitation in the CPSs has a strong cooling effect on the PBL, which is neither evident in the parametrized convection simulations nor the colder SST states of the CPSs (Figure 5.3 a,b). Consequences of such low-level cooling are reduced CAPE and increased CIN in the PBL, which oppose the CAPE and CIN tendencies due to increased SSTs. This contributes to the flatter precipitation response seen in the CPSs once deep convection is established in the higher SST simulations. With parametrized convection, however, a net warming remains in the PBL as SSTs increase.

The enhanced local precipitation intensities evident in D0.6 result from the broader distribution of vertical motions, and hence vertical moisture transport, that can be captured at

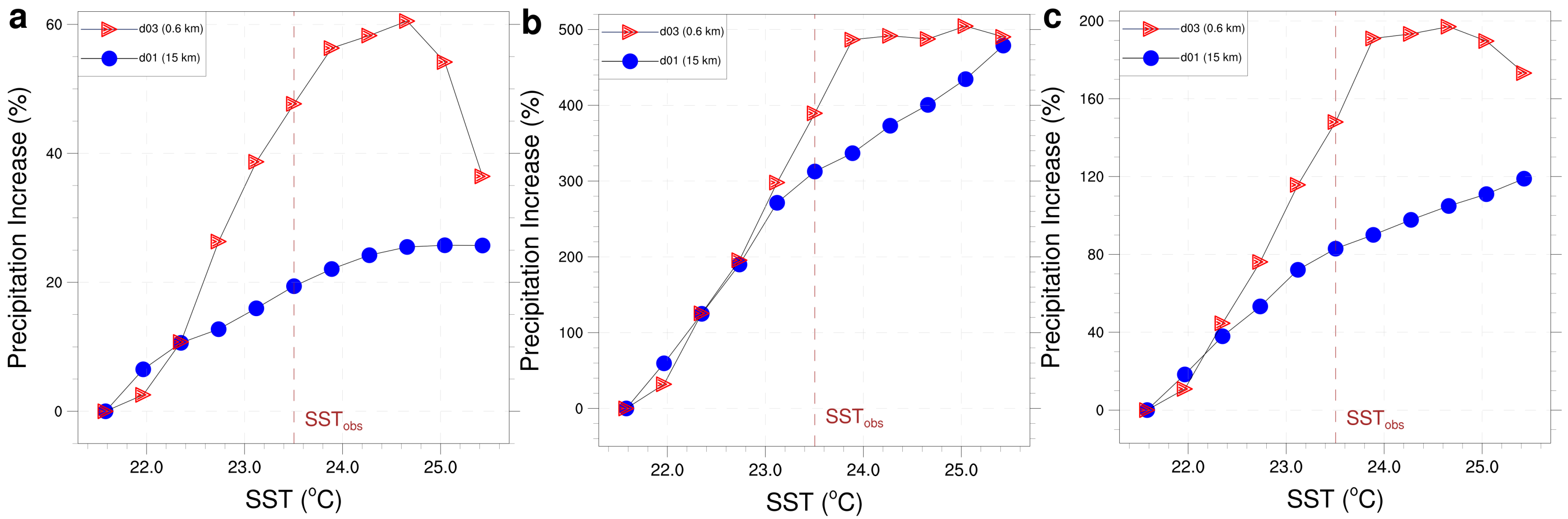

Figure 5.2: **Extreme precipitation response to enhanced SST forcing.** Increase in temporally averaged grid cell precipitation maxima during (a) the first and (b) the second waves of precipitation, and (c) from the start of the first to the end of the second wave of precipitation. All data are aggregated to the 15 km resolution grid and only grid cells within the area of D0.6 are considered.

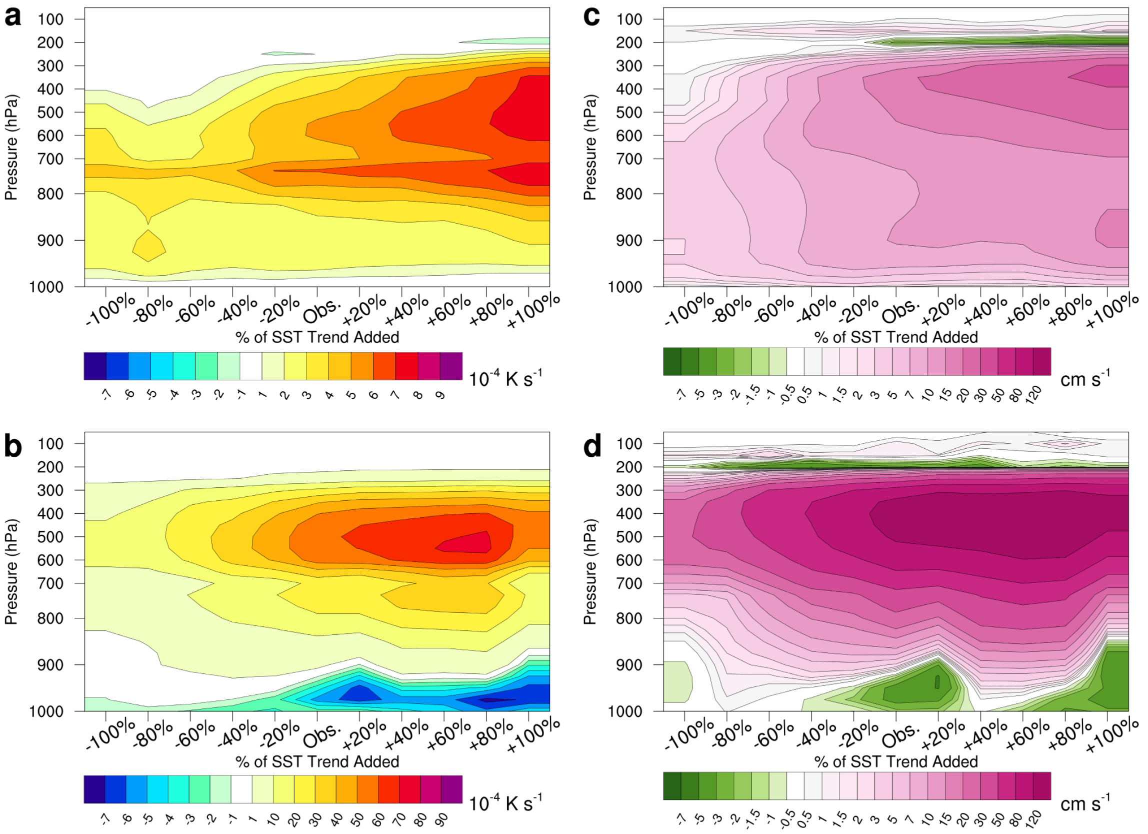

Figure 5.3: **Impact and cause of increased precipitation intensity.** Simulations with parametrized (top) and explicit (bottom) convection, during the second wave of convection. **(a,b)** Latent heating response for grid cell precipitation maxima. **(c,d)** Vertical velocity for grid cell precipitation maxima. All data are aggregated to the 15 km resolution grid and only grid cells within the area of D0.6 are considered. A precipitation threshold of 2.0 mm hr^{-1} is used for the grid cell precipitation maxima. Note the different color scales between rows.

higher resolution [Yang et al., 2014]. Vigorous convection is produced on the D0.6 native grid through (resolved) locally intense updraughts (Figure 5.3 c,d), which appear to be inadequately parametrized in the coarser D15 simulation. The higher resolution of the D0.6 native grid also allows a more detailed representation of surface topography, which can play a key role in orographic uplift and potential subsequent convection. Additional sensitivity studies applying the D15 topography field to D0.6, however, show that the more realistic surface topography in D0.6 is not a dominant factor in the triggering of deep convection or the nonlinear precipitation response (not shown).

Precipitation intensity also affects the strength of convective downdraughts. Convective downdraughts result from the evaporation of precipitation as it falls through the troposphere and, to a first approximation, can be thought of as scaling with precipitation intensity. Downdraughts play an influential role in convective systems. In the lower troposphere, they transport relatively low equivalent potential temperature (θ_{e}) air below the lifting condensation level, having a strongly stabilizing effect on the atmospheric profile [Kain, 2004]. If strong enough, downdraughts can also block low-level inflow [Schoenberg Ferrier et al., 1996], inhibiting further convection. To analyse downdraughts associated with the hourly precipitation maxima, the maximum downdraught in a 3x3 neighbourhood centred on the hourly precipitation maximum is considered each hour. As SSTs increase, a strong growth in the convective downdraughts associated with the hourly precipitation maxima is only evident in the CPSs (Figure 5.4 a,b). Importantly, though, it is not just the strength of the downdraughts that increases the depth to which downdraughts of a given strength penetrate also increases. For the coldest SST states, even the CPSs do not create strong downdraughts. Once deep convection develops in the CPSs though, the stronger downdraughts start penetrating to the surface, contributing to the flatter precipitation response. This results from increasing stability within the PBL, which can be seen by the cooling of the lower troposphere that accompanies the downdraughts in the CPSs (Figure 5.4 d). Additionally, the stronger the downdraughts that reach the surface, the more capable they are of blocking low-level inflow into the system. As it is expected that the coarser simulation with parametrized convection cannot generate grid scale vertical motions comparable to those under explicit convection, the convective parametrization scheme is intended to account for the unresolved vertical motions through environmental mass fluxes, redistributing heat and moisture throughout the column. Despite this, the parametrized convection simulations show no evidence of low-level latent cooling comparable to that when convection is explicitly resolved (Figure 5.4 c,d). Area averaged CIN upstream of the coastal orography (Figure 5.5 b) decreases monotonically as SSTs increase in the parametrized convection simulations, allowing precipitation intensity to increase with SSTs. In the CPSs, however, the decrease in CIN as SSTs increase first slows and then stops across the higher SST ensembles, i.e. in those ensembles where deep convection takes hold and causes enhanced low-level cooling (Figure 5.5 a). For the same reasons, the increasing CAPE due to higher SSTs, while not stopped, is considerably curbed in the CPSs relative to the parametrized convection simulations (Figure 5.5 c).

Ignoring momentum considerations, downdraughts will penetrate downwards until they are either warmer than their surroundings or they reach the surface. Lower relative humidity favours the generation of stronger downdraughts [Knupp and Cotton, 1985] through increased evaporation of precipitation in the lower troposphere and the resultant greater latent heat of evaporation. As such, differences in the relative humidity profiles between the parametrized and explicit convection simulations can contribute to differences in the representation of downdraughts, even those aggregated to the coarser 15 km resolution. The column relative humidity profiles one hour prior to the hourly precipitation maxima show marked differences between the simulations with parametrized and explicit convection. With parametrized convection, relative humidity is noticeably higher in the lower troposphere, as compared with the CPSs, and doesn't show the same clear tendency to decrease as SSTs increase (Figure 5.6). This may be due to the parametrized treatment of downdraughts during the preceding integration of the model, within D15. The Kain-Fritsch scheme derives humidity profiles based on a number of microphysical assumptions, one of which is a constant rate of decrease of downdraught relative humidity with distance beneath the cloud base, which may not be suitable for extreme precipitation. As such, cloud base height can strongly influence subsequent changes in the lower troposphere relative humidity profile. The decreased mid-tropospheric relative humidity simulated at higher SSTs, that is only evident in the CPSs, may also play an important role in inhibiting the development of secondary cells [Shepherd et al., 2001], contributing to the tipping-point nature of the precipitation response.

The described low-level cooling in the CPSs, due to more intense precipitation and convective downdraughts, also affects where and how subsequent convection is triggered. Assuming the presence of an adequate moisture source and conditional instability, the final ingredient required for convection is uplift [e.g. Doswell, 1987]. In this study, a consistent source of uplift is provided by the coastal orography, which presents an abrupt barrier roughly perpendicular to the onshore flow. This is key to the high local intensities [Kotlyakov et al., 2013] observed during the event. As the hourly precipitation intensity increases though, the outflow associated with the increased low-level cooling extends out over the sea, behaving like a gravity current [Corfidi, 2003] emanating from the coastal orography. The resulting presence of near-surface cold pools over the sea provides another source of uplift upstream of the coastal orography, and results in more convection being

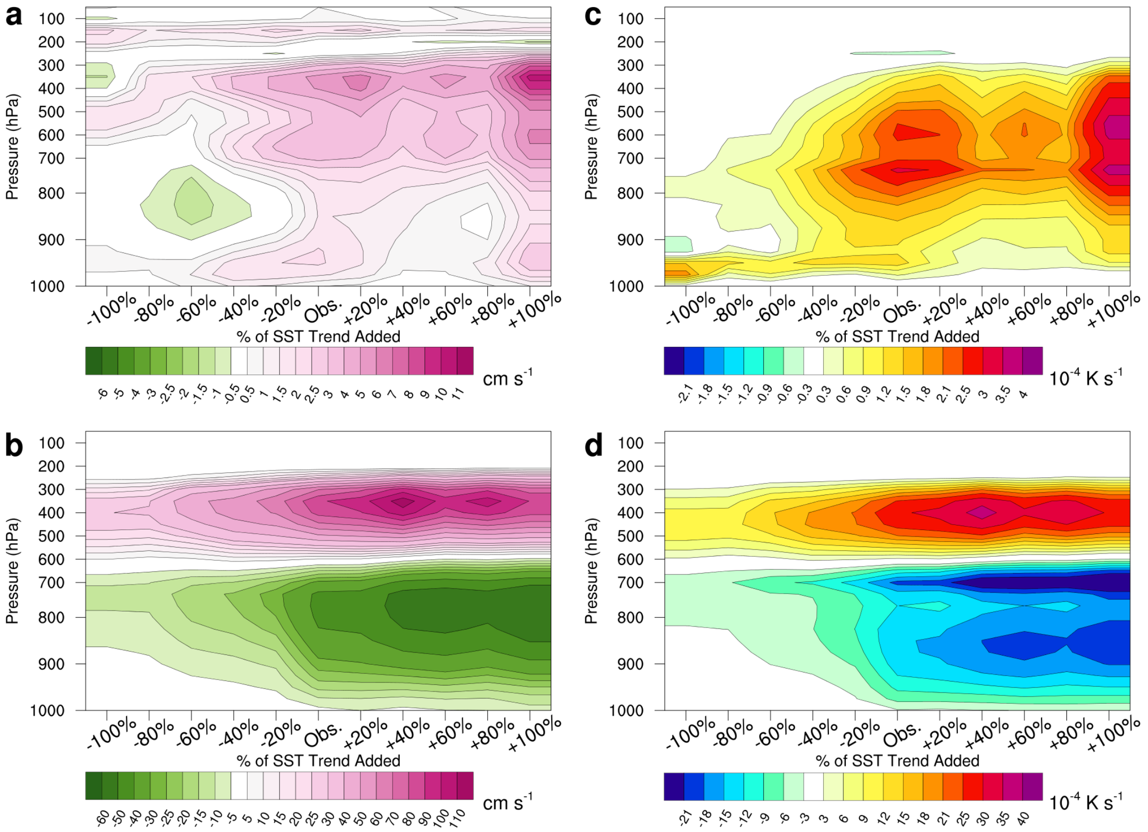

Figure 5.4: **Impact of increased precipitation intensity.** Simulations with parametrized (top) and explicit (bottom) convection, during the second wave of convection. **(a,b)** Downdraft response associated with grid cell precipitation maxima, based on the maximum downdraft either in or directly adjacent to the grid cell precipitation maximum. **(c,d)** Latent heating for (a,b). All data are aggregated to the 15 km resolution grid and only grid cells within the area of D0.6 are considered. A precipitation threshold of 2.0 mm hr^{-1} is used for the grid cell precipitation maxima. Additionally, to distinguish downslope winds from convective downdrafts, a modified version of *Jimenez and Dudhia's* [2012] nondimensional Laplacian operator is defined to exclude downdrafts over downward sloping land (relative to wind direction). This only impacts the results of the 15 km resolution simulation and is explained in detail in Appendix 5B. Note the different color scales between rows.

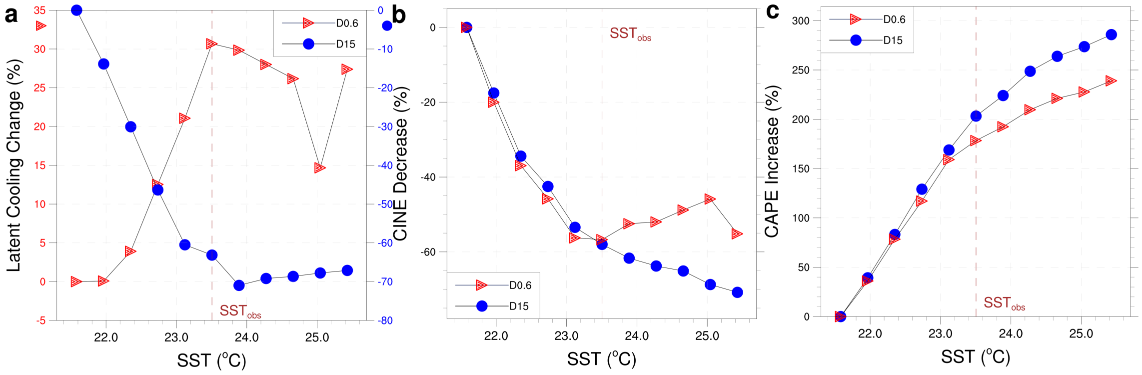

Figure 5.5: **Response to SST increase. (a)** Latent cooling **(note different y-axes)**, **(b)** Convective Inhibition, **(c)** CAPE. All values are averaged over the box marked in Figure 5.7 b, within the PBL, and over both waves of convection.

triggered over the sea in the warmer SST ensembles (Figure 5.7). The precipitation-cooled outflow associated with this new convection over the sea subsequently extends the outflow boundary even further from the coast. This is evident in the back-building of the mesoscale convective system that is simulated at warmer SST states and found in satellite observations of the event (not shown). The near-surface cold pools over the sea also provide a smoother and less vigorous uplift than the coastal orography, potentially limiting the precipitation intensity increase. As these air parcels continue downstream towards the coastal orography, they arrive drier and stabler due to the preceding convective processes which, in turn, limits the intensity of subsequent precipitation triggered by orographic uplift. The absence of low-level cold pools in the parametrized convection simulations means that this effect is only evident in the CPSs.

The same sensitivity experiments (for D15 only) carried out with four other convective parametrization schemes (Table 5.1) found precipitation responses ranging from essentially flat to strongly monotonic (Figure 5.8), highlighting the dependence of projections of convective precipitation extremes on the choice of parametrization scheme. None of the schemes were capable of reproducing the nonlinear response shown under explicit convection. This suggests that the results demonstrate an inherent limitation of convective parametrization schemes, rather than a peculiarity of the scheme that is focused on.

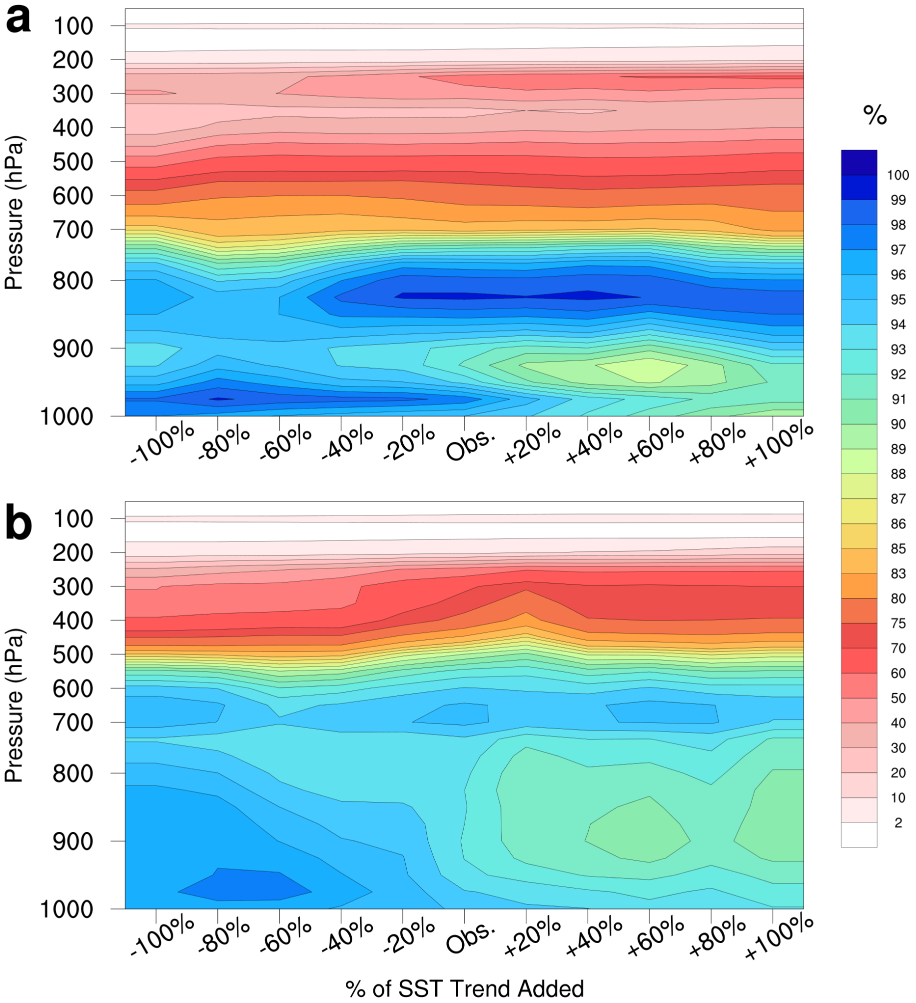

Figure 5.6: **Changes in Relative Humidity.** As in Fig. 5.3, except for relative humidity in the maximum *precipitation* column 1 hour prior to the downdraft. D15 is shown in panel **(a)**, D0.6 in panel **(b)**.

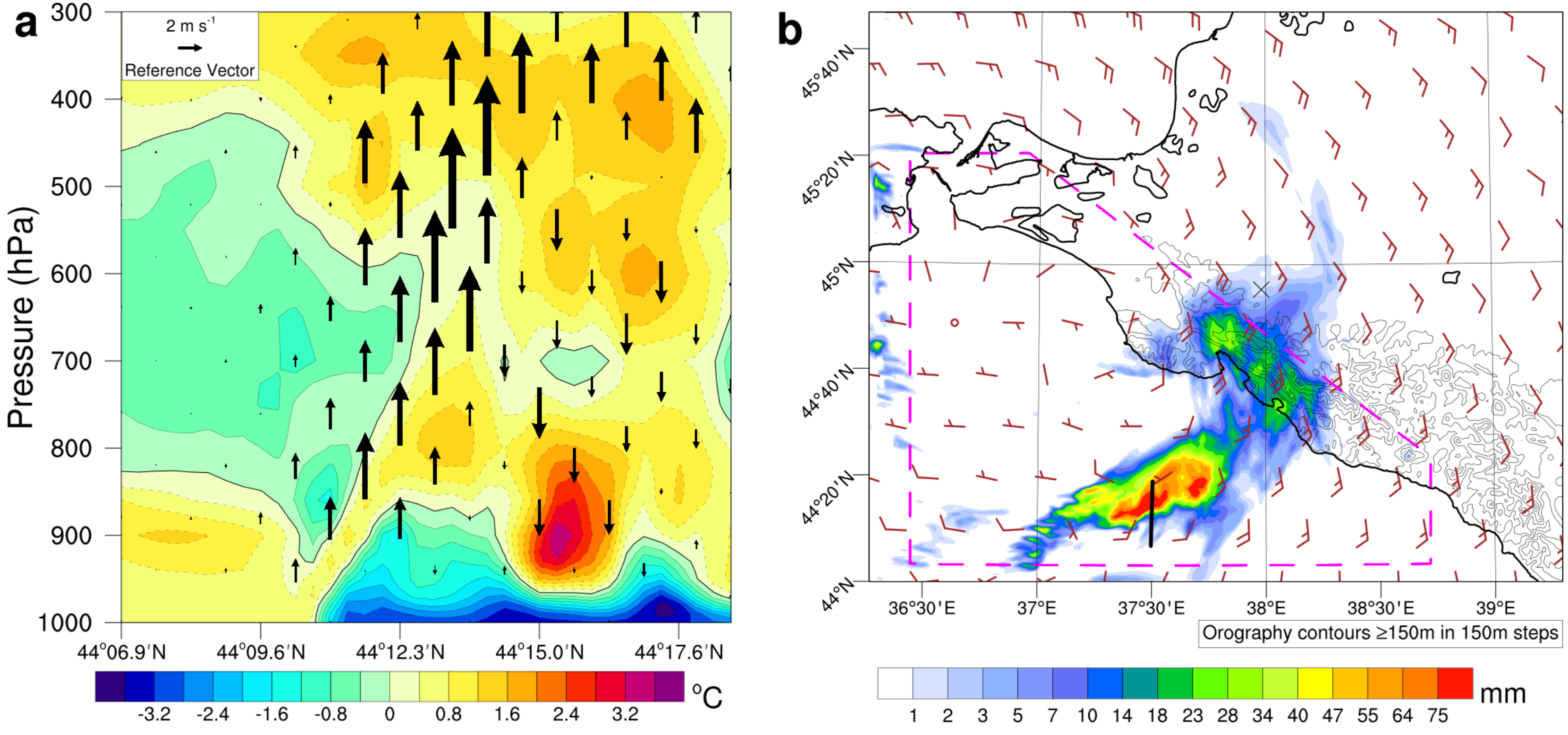

Figure 5.7: **Cold pool triggered convection.** **(a)** D0.6 cross-section (marked in (b)) showing instantaneous temperature anomaly and vertical motion for one member of the warmest SST ensemble, during the 2$^{\text{nd}}$ wave of convection. Convection can be seen initiating at the edge of the near-surface cold pool, before continuing in the direction of the flow (see panel (b)). The temperature anomaly is relative to the mean across the west-east dimension of D0.6, only considering points over the sea. The 0°C contour is marked with a thick black line. **(b)** Accumulated precipitation in the hour leading up to the snapshot in (a), with the cross-section along 37.5°E marked in black. Wind barbs illustrate the instantaneous flow at 850 hPa, in m s^{-1}. The dashed magenta line denotes the area over which the averages in Figure 5.5 are calculated.

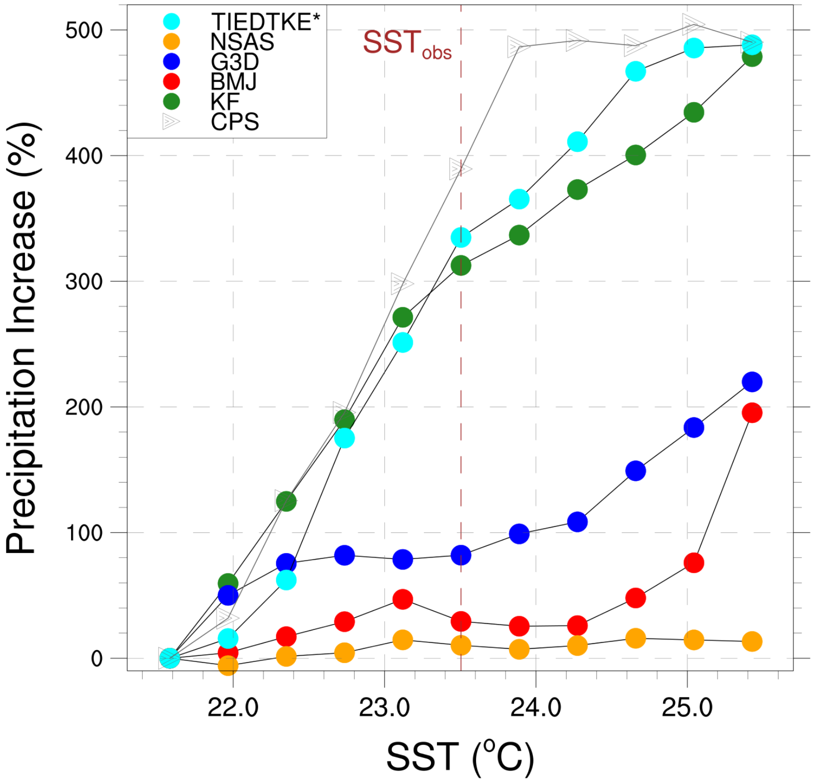

Figure 5.8: **D15 extreme precipitation response to enhanced SST with different convective parametrizations.** Increase in temporally averaged grid cell precipitation maxima during the second wave of precipitation. For illustration, the convection-permitting simulation is also shown in grey (CPS, triangles). ∗Note that the response of the Tiedtke scheme (cyan) has been scaled by a factor of 0.25 so that the shape of all response curves can be seen clearly in the same panel. The legend is explained in Table 5.1. As in Figure 5.2, results are based on ensemble means, all data are aggregated to the 15 km resolution grid, and only grid cells within the area of D0.6 are considered.

Abbreviation	Scheme name	Reference(s)
TIEDTKE	Tiedtke	Tiedtke [1989], Zhang et al. [2011]
NSAS	New Simplified Arakawa-Schubert	Han and Pan [2011]
G3D	Grell 3D Ensemble	Grell [1993], Grell and Devenyi [2002]
BMJ	Betts-Miller-Janjic	Janjic [1994]
KF	Kain-Fritsch	Kain [2004]

Table 5.1: Parametrization schemes used in Figure 5.8

5.4 Discussion and Conclusions

Taking the 2012 Krymsk precipitation extreme as a recent showcase example, it has been demonstrated over a large range of SST forcings that the response of extreme coastal precipitation to SST increase can be substantially different in CPSs than in coarser models with parametrized convection. Specifically, it has been shown how the fine-scale representation of precipitation intensity and vertical motions in CPSs can strongly modulate the extreme precipitation response to SST increase at both the daily and sub-daily timescale. Resolving these processes adds value by enabling key features, such as near-surface cooling and deeper penetrating downdraughts, to explicitly develop and affect the precipitation response. The tendency for reduced lower tropospheric relative humidity in the CPSs further contributes to the strong nonlinearity of the extreme precipitation response.

In GCM aquaplanet experiments with parametrized convection and relatively coarse resolutions, Yang et al. [2014] identified subgrid-scale variability of vertical moisture transport (primarily due to changes in vertical velocities) as explaining most of the resolution dependence of extreme precipitation. Here a detailed investigation of the physical mechanisms that can also lead to a different response to SST increase of extreme precipitation in models with parametrized and explicit convection is presented. The results highlight not only the AV of CPSs for better representing convective precipitation extremes, but crucially also their AV for studying changes in convective extremes, which stems primarily from the increased local precipitation intensities that parametrized convection cannot reproduce. These increased intensities result from the greater spatial variability of vertical motions that the fine-resolution grid can capture, and play a key role in the strongly nonlinear nature of the extreme precipitation response under explicit convection, for example by creating stronger downdraughts which transport relatively low θ_e air into the lower troposphere. The simulations with parametrized convection proved to inadequately represent the physical processes which can damp further convective intensification during extreme precipitation events.

While convective parametrization schemes can of course be tuned to better represent changes in particular extremes, a superseding requirement of climate models is for convective parametrization schemes that well represent the mean conditions across large scales, often to the detriment of regional extremes. Convective parametrization schemes which consider a much broader distribution of vertical velocities at the subgrid-scale, perhaps partly stochastically determined, may go some way towards bridging the gap with convection-permitting models and better recreating the locally intense precipitation exhibited during precipitation extremes in CPSs. As has been demonstrated, this can produce effects which strongly modify the local environment, and is key to the nonlinear response.

Eden et al. [2014] argue that it is difficult to demonstrate AV in RCMs for simulating present day local precipitation extremes, compared to GCMs, once relatively simple statistical postprocessing [Wong et al., 2014] to correct for biases and scale gaps has been applied to both simulations. For detecting the response to warming of extreme precipitation, though, bias correction methods suffer from essentially inheriting the wrong climate change trends from the climate model. As demonstrated here, CPSs are not limited in this way. Rather, the AV of CPSs is set apart from other downscaling methods by its origin in the simulation of independent, often highly localized, physical process chains.

Fine-scale processes are known to play an important role in modulating the response of daily precipitation extremes to climate change, particularly in coastal areas dominated by convective precipitation [Diffenbaugh et al., 2005]. The results presented here raise questions about the ability of models with parametrized convection to accurately represent the response of sub-daily to daily convective extremes to climatic changes in coastal regions. If the response to warming of convective extremes, particularly those in coastal regions, is of interest, then convective parametrization schemes would have to be substantially improved. Furthermore, one could conceive developing statistical postprocessing methods which include local-scale meteorological information. Absent such advances, CPSs are required not only to capture the magnitude of the response between individual states [Kendon et al., 2014], but also the shape of the response across multiple states, which can be highly nonlinear.

5.5 Appendix

5A. Further validation of model simulation, against observed precipitation.

The primary validation of the simulations is carried out in §3.2.3 and Meredith et al. [2015] (including supplementary information therein). Here, additional validation of 24 hour precipitation totals at Krymsk is conducted, using simulations D15 and D0.6, with the latter aggregated to the 15 km resolution grid.

To account for the simulated precipitation field potentially being (spatially) shifted from the observed field, the grid cell containing Krymsk is selected, and all precipitation simulated within one grid cell either side of this is then considered. This gives a 3x3 box centred on Krymsk, for each ensemble member. Box-and-whisker plots are created to analyse the distribution of 24 hour precipitation totals across all members and boxes. Whiskers represent the 5^{th} and 95^{th} percentiles, with the box representing the 25^{th} and 75^{th} percentiles, and the median.

Figure 5.9 shows box-and-whisker plots for (a) D15; (b) D0.6 aggregated to D15; (c) D0.6 on its native grid (0.6 km resolution), with a box covering the same area as the 3×3 boxes in (a) and (b); (d) D0.6 on its native grid (0.6 km resolution), except with a smaller box covering only 15 km × 15 km, i.e. equivalent to one grid cell in D15.

As can be seen in Figure 5.9 (a), the coarse resolution simulation with parametrized convection (D15) is not capable of reproducing the intense precipitation observed at Krymsk (yellow bars). Once convection is explicitly represented, however, the observed total at Krymsk fits well within the distribution of simulated 24 hour precipitation totals (b), even though the data have been aggregated to the 15 km resolution grid.

This is also true of the simulated totals on the D0.6 native grid (c, d). The reduced magnitude of the upper percentiles once D0.6 has been aggregated to D15, compared to those on the D0.6 native grid, illustrate the effect of aggregation on the precipitation field: the most intense localized precipitation is smoothed-out. Even with this scaling effect, however, the precipitation intensities in D0.6 are still compatible with observations and are not reduced to the level of those in D15, further suggesting that the results of the D15 experiment stem from the inadequate parametrization of convective processes associated with extreme precipitation.

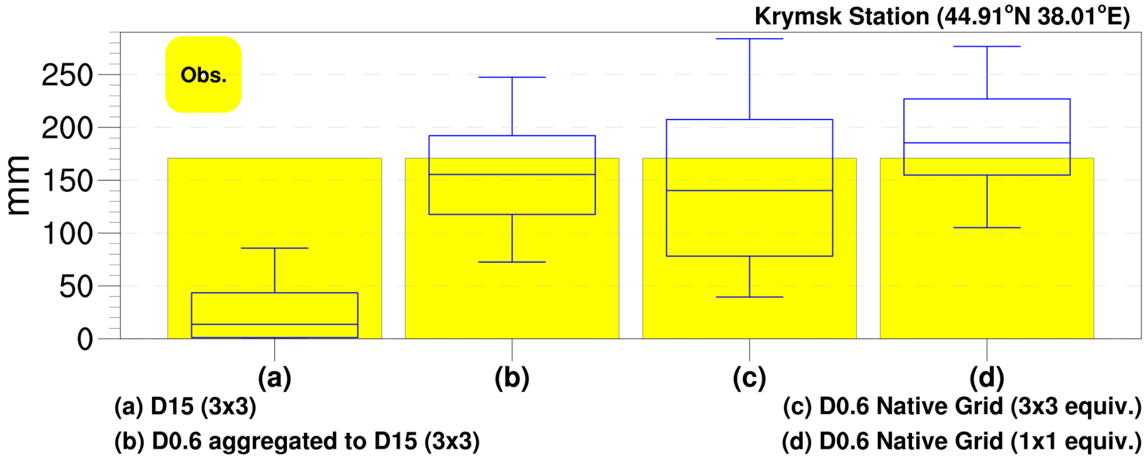

Figure 5.9: **Validation.** 24 hour precipitation observed (yellow) and simulated (box-and-whiskers) at Krymsk weather station.

While these results are good, it is important to add the caveat that there is a considerable degree of spatial randomness inherent in precipitation totals recorded at point locations, i.e. at the Krymsk weather station. As such, one cannot necessarily expect point totals to be representative of the broader precipitation field.

5B. Further information on the measurement of downdraughts from the model output.

As demonstrated in the main text, vertical motions due to convective activity are much smaller in D15 than in D0.6. As a result, the strongest downward motions simulated in D15 actually result from downslope winds, rather than convective downdraughts. To create Figure 5.4, it is first necessary to be able to distinguish between downslope winds and convective downdraughts.

This is achieved, firstly, by each time step only considering downward motions either in or directly adjacent to the maximum precipitation cell (on the D15 grid). Secondly, a modified version of Jiminez and Dudhia's [2012] nondimensional Laplacian operator is defined, to exclude grid cells with downward slopes (relative to the wind direction) over a certain threshold from consideration.

To distinguish topographic features in a regional model, Jiminez and Dudhia [2012] apply the following operator to the topographic field h:

$$\triangle^2 h_{i,j} = \frac{1}{4}(h_{i+1,j} + h_{i,j+1} + h_{i-1,j} + h_{i,j-1} - 4h_{i,j}) \tag{5.1}$$

which they term the nondimensional Laplacian operator and is related to the traditional Laplacian operator by $\bigtriangledown^2 h = \triangle^2 h/(\triangle x)^2$

Here equation (5.1) is modified to take account of wind direction, giving four different operators, to be used according to which quadrant (i.e. NE, SE, SW, NW) the wind direction vector is located in.

$$\text{NE: } \triangle^2 h_{i,j} = A^{-1}(h_{i+1,j} + h_{i+1,j} + \frac{1}{\sqrt{2}} h_{i+1,j+1} - Ah_{i,j}) \tag{5.2}$$

$$\text{SE: } \triangle^2 h_{i,j} = A^{-1}(h_{i,j-1} + h_{i+1,j} + \frac{1}{\sqrt{2}} h_{i+1,j-1} - Ah_{i,j}) \tag{5.3}$$

$$\text{SW: } \triangle^2 h_{i,j} = A^{-1}(h_{i,j-1} + h_{i-1,j} + \frac{1}{\sqrt{2}} h_{i-1,j-1} - Ah_{i,j}) \tag{5.4}$$

$$\text{NW: } \triangle^2 h_{i,j} = A^{-1}(h_{i,j+1} + h_{i-1,j} + \frac{1}{\sqrt{2}} h_{i-1,j+1} - Ah_{i,j}) \tag{5.5}$$

where A $= \frac{1+2\sqrt{2}}{\sqrt{2}}$

10 metre surface winds are used to determine the wind direction. Thus, for a northeastward wind, negative values of (5.2) would imply a downslope wind, with a similar argument applying to downslope winds in the remaining quadrants.

To exclude downslope winds from the calculation of downdraughts, a threshold slope value of -40 is set for equations (5.2) - (5.5). Thus, for a wind direction oriented towards a given quadrant, if the corresponding modified nondimensional Laplacian operator gives a value less than -40, then the grid point is not considered for calculation of convective downdraughts.

These considerations only impact the results in D15, as the downdraughts in D0.6 are far stronger than downslope winds within that domain. Considering downdraughts from D15 without the aforementioned specifications results in an almost constant downdraught magnitude across SST states, though decreasing slightly as higher SSTs warm the lower troposphere, giving weaker downslope winds (not shown).

Figure 5.10 shows the grid points which would be excluded from consideration for a wind orientated within the north-eastern quadrant (the most common orientation during the event).

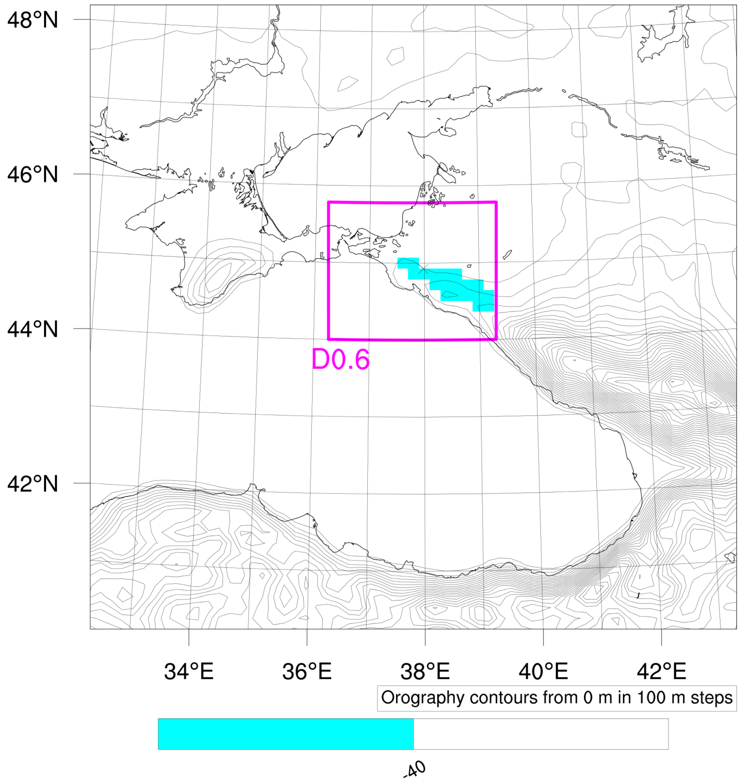

Figure 5.10: **Exclusion of downslope winds.** For a wind direction orientated in the north-eastern quadrant, the grid cells marked in blue would be excluded from consideration for calculating Figure 5.4.

5C. Same analysis for 1st wave of convevction.

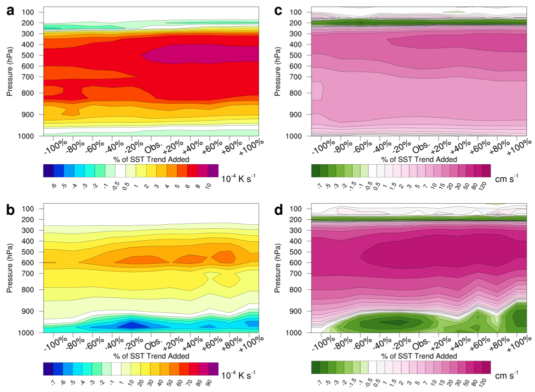

Figure 5.11: **As in Figure 5.3, except for the first wave of convection.**

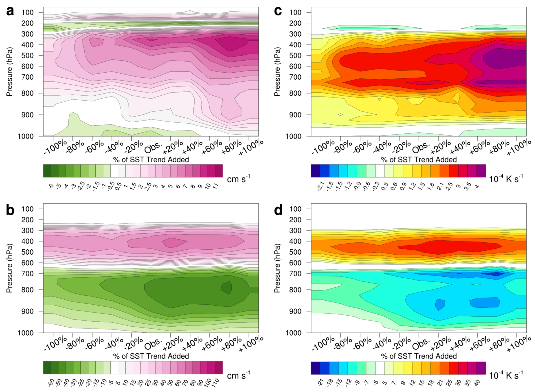

Figure 5.12: **As in Figure 5.4, except for the first wave of convection.**

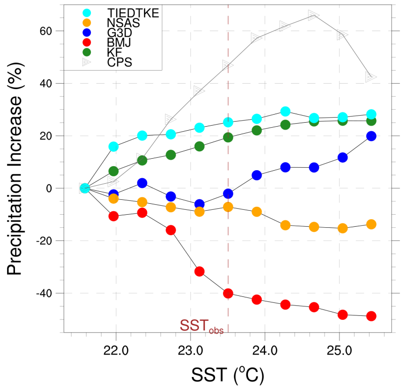

Figure 5.13: **As in Figure 5.8, except for the first wave of convection.** Note though, that in this figure the response of the Tiedtke scheme has not been scaled.

6 Conclusions

Extreme precipitation events are characterised by both their rarity and potential to strongly affect society. Extreme precipitation, particularly that of a convective nature, responds sensitively to climatic changes, much more so than mean precipitation. In a warmer climate, increased atmospheric moisture content gives the potential for more intense extreme precipitation. Understanding the mechanisms by which changes in extreme precipitation may occur is clearly an important challenge, though can be difficult using traditional approaches such as analysis of observations or climate model output. The former approach is often limited by a lack of data availability, while the latter can be limited by the coarse resolution of global climate models which cannot capture many of the localized processes behind mesoscale precipitation extremes, which intense convective events in the extratropics tend to be. Very-high resolution models offer promise of improved understanding of convective precipitation extremes and how they may respond to climatic changes, though the full extent of their added value is yet to be determined and they also come with increased computational expense.

As set out in the research foci in chapter 1, this thesis has sought to better understand mechanisms by which regional precipitation extremes respond to climatic changes, and how this response is represented in different resolution models, using a regionalized, event-based modelling approach. With a focus on the Black Sea and Mediterranean region, a recent high-impact extreme precipitation event was selected as a showcase example for further study. The sensitivity of the event's intensity to recent SST trends was examined using an ensemble of convection-permitting sensitivity experiments across 11 different SST states, representative of past, present, and extrapolated future SST regimes. In light of recent work showing the importance of convection-permitting resolution for capturing changes in intense summertime precipitation events [Kendon et al., 2014; Ban et al., 2015], the use of convection-permitting resolution was a crucial component of the study. The regionalized and event-based nature of the study allowed the event to be simulated across a spectrum of SST regimes while keeping the computational expense limited; using a wide range of forcings was crucial for investigating nonlinearities in the relationship between SST and the intensity of the precipitation event. The same set of sensitivity studies were then used to explore the added value of convection-permitting simulations for studying changes in extreme precipitation, with respect to the lower-resolution parent domain where convective processes needed to be parametrized. The added value was studied in particular with respect to the shape of the extreme precipitation response to SST increase across a range of SST states in parametrized and explicit convection simulations, with a focus on the mechanisms behind any differences in the response.

6.1 Summary and Implications

In this section, the research foci outlined in chapter 1 shall be returned to and the results of the thesis shall be discussed in their context.

The added value of RCMs for simulating observed extreme precipitation events

The first, minor, result presented in this thesis was a demonstration in chapter 3 of the added value of regional models for reproducing observed extreme precipitation events. This was done using two recent extreme precipitation events in Europe as test cases - the June 2013 Central Europe flooding and the July 2012 Krymsk precipitation extreme. For the former, the extreme precipitation accumulated over a 3-day period and was driven by a persistent synoptic-scale circulation pattern. As such, the event was already reasonably well reproduced in the global model which provided the lateral boundary conditions (ERA-Interim reanalysis). The 0.15° resolution regional model still exhibited added value compared to the driving model, though. This was found mostly in the mountainous areas of the northern Alps and the Ore Mountains (Erzgebirge), where simulated precipitation totals were able to match the intensities found in observations. Precipitation totals in the driving model were too low in mountainous areas, suggesting that for this extreme precipitation event the regional model's more accurate representation of topographic forcings was a key source of added value.

The second event tested was the July 2012 Krymsk precipitation extreme, this time in a triply-nested configuration with horizontal resolution increasing up to a convection-permitting 0.6 km. Unlike the Central Europe floods, this event was not well captured in global models and resulted from localized mesoscale processes. The 15 km resolution WRF simulation already added value, compared to the global models, but was unable to reproduce the locally intense precipitation observed at Krymsk (171 mm in 24 hours). In this respect, the convection-permitting 0.6 km resolution simulation added further value by realistically reproducing the high intensity precipitation found in observations. Separate sensitivity studies applying the 15 km resolution orography to the 0.6 km resolution domain (not shown) suggest that the improved topography in the 0.6 km resolution simulation was not a critical factor in the improved simulation. Rather, the improved representation of convective dynamics provided in the convection-permitting simulation were key, as found in Prein et al. [2013].

The inability of the 15 km resolution simulation, which is still relatively high resolution, to realistically reproduce the event intensity of the Krymsk precipitation extreme raises questions about the utility of models with parametrized convection for studying climate-related changes in mesoscale convective extremes.

Identification and understanding of mechanisms by which extreme precipitation events may be amplified

With a focus on the Black Sea and Mediterranean region, the July 2012 Krymsk precipitation extreme was taken as a showcase example to study the sensitivity of an extreme precipitation event to SST increase. Convection-permitting simulations using SST states ranging from those representative to the early 1980s to those representative of 30 years beyond the event (assuming a continued warming trend) showed the crucial role of recent Black Sea warming in amplifying the Krymsk event. From the ensemble with the coldest to the ensemble with observed SSTs, sensible heating of the lower atmosphere by the warmer Black Sea led moisture availability to increase at close to that which would be expected based on the Clausius-Clapeyron relation, roughly 15%. Precipitation across the Krymsk region increased by over 300% though, between the same ensembles. This suggests limitations of the thermodynamical bounds (i.e. the CC relation) for predicting changes in convective precipitation extremes in coastal regions. Changes in dynamical factors, such as static stability, clearly also play an important role. The highly nonlinear response of the event's intensity to SST increase - a sharp initial increase followed by a levelling-off - suggests that convective extremes in coastal regions may be governed by regional SST thresholds which favour more powerful systems. A warmer Black Sea acts as a store of heat, whose higher SSTs have the potential to increase instability and thus the probability of intense deep-convective events being triggered when suitable weather systems pass. SST increase is not a phenomenon unique to the BSM region; comparable regions undergoing SST increase could thus also be at risk of more intense convective extremes.

The regional modelling strategy employed in the study enabled the physical mechanisms behind the amplification of the precipitation event to be clearly identified. This is not always so straightforward using a global modelling approach, where the probability of similar events is compared between massive ensembles of present and past climates. The reduced computational expense of the regional modelling approach also allowed a nonlinear relationship across multiple SST states to be revealed. This approach, where appropriate, offers a promising way forward for future sensitivity studies of individual extreme events, which is of critical importance for isolating the mechanisms which can amplify extremes and providing regional-scale information to those affected by climate change.

Attribution of recent extreme precipitation events to changes in the climate system

Also in chapter 4, the intensity of the Krymsk event was conditionally attributed to the warming that has occurred in the Black Sea since the early 1980s. In other words, had the same cyclone passed over the Black Sea in the early 1980s, the intense precipitation observed in July 2012 would have been virtually impossible. Taking this and the preceding research focus together, the research presented in chapter 4 "*represents a crucial step towards combining the understanding of an event with an assessment of its likelihood of occurrence*" [Otto, 2015]. Conversely, it was shown in Appendix 3A that the 2013 Central Europe floods could not be attributed to anomalous SSTs or soil moisture. Rather, the persistence of the synoptic pattern appears to have been key. Whether such persistent patterns have become more likely due to climate change is a question that is not suited to the regional modelling strategy employed for the two aforementioned events. Such a question would need to be addressed with a global modelling experiment.

As stated, the attribution in chapter 4 is conditional on the given synoptic pattern. The method employed does not investigate how the likelihood of such a circulation pattern, airmass or temperature/moisture profile may have changed over the same period. To test changes in the likelihood of the Krymsk event given all possible weather, both at present and in the early 1980s, would require infeasibly large simulations. Separate research [Tilinina et al., 2013] does indicate an increase in summertime cyclonic activity over recent decades in much of the BSM region though, which may also have increased the likelihood of the event. Another approach would be that of Lackmann [2014], who also modified the temperature, humidity and geopotential in the lateral boundary conditions of a regional sensitivity experiment of Hurricane Sandy. The changes to the lateral boundary conditions were based on mean changes in the temperature field derived from reanalyses and climate model experiments (CMIP5). For the Krymsk event, such an approach would give a different answer to a different question, and would still fail to address the question of whether a cyclone like that responsible for the Krymsk event would have formed in the past or future climate.

The added value of convection-permitting models for studying changes in extreme precipitation

In chapter 5, the Krymsk regional sensitivity experiments were used to examine the added value of convection-permitting simulations for studying changes in convective extremes, as compared to lower-resolution models with parametrized convection. It was found that the nonlinear response of the precipitation intensity to SST increase that the explicit convection simulations exhibited could not be reproduced in the parametrized convection simulations, where the response was much more linear. The physical mechanisms behind the different responses were then explored. The failure of the parametrized convection simulations to reproduce the nonlinear response stemmed from the inadequate parametrization of vertical motions under extreme conditions. Insufficiently strong updraughts led to too weak precipitation, which in turn led to the under-representation of convective downdraughts and near-surface cooling from intense precipitation. These features were found to be key to the nonlinear response in the convection-permitting simulations, acting to stabilize the atmosphere locally and cause subsequent convection to be triggered by cold-pools over the sea rather than by orographic uplift near to Krymsk.

These findings imply that projections in convective extremes based on simulations using parametrized convection should be treated with caution. The mechanisms revealed suggest areas in which existing convective parametrization schemes could be improved. Convective parametrization schemes which allow a much broader range of vertical motions to be considered, perhaps stochastically determined, may perform much better under extreme conditions. Without such improvements, convection-permitting simulations offer the most promising approach for studying changes in convective precipitation extremes, though with obvious computational constraints.

6.2 Outlook

Understanding recent weather extremes, not just precipitation extremes, from a climate perspective remains an important endeavour, which can yield valuable information about the mechanisms by which a changing climate influences extreme events. The methodology utilised in this thesis offers a computationally inexpensive manner in which other weather extremes can be studied in detail and the roles of key forcings can be isolated. Trenberth et al. [2015], for example, identify four recent extremes in which anomalously high SSTs may have played a role in enriching the moisture supply to precipitating systems, aiding their intensification and bringing heavier rains. While convection-permitting simulations are most likely necessary for such studies of convective events, resolutions an order of magnitude lower should be sufficient for similar studies of extreme hot or cold events. In the context of event attribution, the 'conditional' approach provides more useful information about *how* an event may have been impacted by climate change, rather than simply the change in probability of the event due to climate change. Such information can be valuable for planners.

The added value of convection-permitting modelling has now been clearly demonstrated, with this thesis building on the work of others. Convection-permitting modelling is likely to become more and more common, especially as computational (and storage) capacity increases. There remain many challenges to be addressed in convection-permitting modelling though. To date CPMs have only been run over relatively short timescales, of the order of a decade, and over relatively small spatial scales, i.e. national or sub-continental. As such, CPMs are not fully tested on climate timescales or over large domains. Many of the parametrization schemes used in other components of atmospheric models were not originally designed for such high resolutions. Some of the assumptions within these parametrization schemes - radiation, turbulence, etc. - and how the schemes interact with one another may need to be reviewed for use at convection-permitting resolution. Such efforts are already under way. The latest version of the WRF model (v3.7.1), for example, now contains scale dependency in many of its parametrization schemes. An additional challenge facing the improvement and evaluation of convection-permitting models is a lack of sufficiently high-resolution datasets, particularly over longer time periods, to compare the model output against. In this respect, validation of individual observed events in CPMs is a useful substitute. None of the issues outlined here are insurmountable, though, and it is most likely only a matter of time before convection-permitting global climate simulations become a reality.

References

Allen, M. R., and W. J. Ingram (2002). Constraints on future changes in climate and the hydrologic cycle, Nature, 419, 224232.

Allen, M. (2003). Liability for climate change. Nature, 421(6926), 891-892.

Anthes, R. A. (1983). Regional models of the atmosphere in middle latitudes. Monthly weather review, 111(6), 1306-1335.

Ban, N., et al. (2014). Evaluation of the convection-resolving regional climate modeling approach in decade-long simulations, J. Geophys. Res. Atmos., 119, 78897907 , doi:10.1002/2014GL062588.

Ban, N., et al. (2015). Heavy precipitation in a changing climate: Does short-term summer precipitation increase faster?, Geophys. Res. Lett., 42: 11651172, doi:10.1002/2014JD021478.

Bayr, T. (2013). *Tropical atmospheric circulation changes under global warming* (Doctoral dissertation). Retrieved from http://macau.uni-kiel.de/.

Bougeault, P., et al. (2010). The THORPEX interactive grand global ensemble. Bulletin of the American Meteorological Society, 91(8), 1059-1072.

Berg, P., et al. (2013). Strong increase in convective precipitation in response to higher temperatures. Nature Geosci., 6, 181185.

Blöschl, G., et al. (2013). The June 2013 flood in the Upper Danube basin, and comparisons with the 2002, 1954 and 1899 floods. Hydrology and Earth System Sciences, 17(12), 5197-5212.

Brown, S. J., et al. (2008). Global changes in extreme daily temperature since 1950. Journal of Geophysical Research: Atmospheres (19842012), 113(D5).

Chan, S. C., et al. (2014a). The value of high-resolution met office regional climate models in the simulation of multihourly precipitation extremes, J. Clim., 27, 61556174.

Chan, S. C., et al. (2014b). Projected increase in summer and winter UK sub-daily precipitation extremes from high-resolution regional climate models, Clim. Dyn., 41, 14751495.

Christensen, O. B., et al. (2001). Internal variability of regional climate models. Climate Dynamics, 17(11), 875-887.

Coles, S. (2001). *An introduction to statistical modeling of extreme values.* Springer Series in statistics. Springer.

Collins, W. D., et al. (2004). Description of the NCAR Community Atmosphere Model (CAM 3.0). NCAR Tech. Note NCAR/TN464+STR. 214 pp.

Corfidi, S. F. (2003). Cold pools and MCS propagation: Forecasting the motion of downwind-developing MCSs, Weather and Forecasting 18, 6, 997-1017.

Cortesi, N., et al. (2012) Daily precipitation concentration across Europe 19712010, Nat. Hazards Earth Syst. Sci., 12, 2799-2810.

Coumou, D., and Rahmstorf, S. (2012). A decade of weather extremes. Nature Climate Change, 2(7), 491-496.

Crétat, J., and Pohl, B. (2012). How physical parameterizations can modulate internal variability in a regional climate model. Journal of the Atmospheric Sciences, 69(2), 714-724.

Dai, A. (2006). Recent climatology, variability, and trends in global surface humidity. Journal of Climate, 19(15), 3589-3606.

Davies, H. C., and Turner, R. E. (1977). Updating prediction models by dynamical relaxation: An examination of the technique. Quarterly Journal of the Royal Meteorological Society, 103(436), 225-245.

Dee, D. P., with 35 co-authors (2011). The ERA-Interim reanalysis: configuration and performance of the data assimilation system. Quart. J. R. Meteorol. Soc., 137, 553-597.

Denis, B., et al. (2003). Sensitivity of a regional climate model to the resolution of the lateral boundary conditions. Climate Dynamics, 20(2-3), 107-126.

Di Luca, A., et al. (2012). Potential for added value in precipitation simulated by high-resolution nested regional climate models and observations. Climate Dynamics 38.5-6:1229-1247.

Di Luca, A., et al. (2015). Challenges in the Quest for Added Value of Regional Climate Dynamical Downscaling. Current Climate Change Reports 1.1:10-21.

Diaconescu E. P., et al. (2007). The impact of lateral boundary data errors on the simulated climate of a nested regional climate model. Climate Dynamics, 28(4), 333350.

Diaconescu, E. P., and Laprise, R. (2013). Can added value be expected in RCM-simulated large scales?. Climate Dynamics, 41(7-8), 1769-1800.

Diffenbaugh, N. S., et al. (2005). Fine-scale processes regulate the response of extreme events to global climate change. Proceedings of the National Academy of Sciences of the United States of America, 102.44:15774-15778.

Donat, M. G., et al. (2013). Updated analyses of temperature and precipitation extreme indices since the beginning of the twentieth century: The HadEX2 data-set, J. Geophys. Res. Atmos., 118, 20982118, doi:10.1002/jgrd.50150.

Doswell III, C. A. (1987). The distinction between large-scale and mesoscale contribution to severe convection: A case study example, Weather and Forecasting, 2, 1, 3-16.

Eden, J. M., et al. (2014). Comparison of GCM- and RCM-simulated precipitation following stochastic postprocessing, J. Geophys. Res. Atmos., 119, 11,04011,053, doi:10.1002/2014JD021732.

EM-DAT: The OFDA/CRED International Disaster Database - www.emdat.be, Universit Catholique de Louvain, Brussels (Belgium).

Emori, S., and S. J. Brown (2005). Dynamic and thermodynamic changes in mean and extreme precipitation under changed climate, Geophys. Res. Lett., 32, L17706, doi:10.1029/2005GL023272.

Feser, F., et al. (2011). Regional climate models add value to global model data: a review and selected examples. Bulletin of the American Meteorological Society 92.9:1181-1192.

Fischer, E.M., at al. (2007). Soil moisture-atmosphere interactions during the 2003 European summer heat wave. Journal of Climate, 20(20), 5081-5099.

Fogarty, C. T., et al. (2006). The role of anomalously warm sea surface temperatures on the intensity of Hurricane Juan (2003) during its approach to Nova Scotia. Monthly weather review, 134(5), 1484-1504.

Funatsu, B. M., et al. (2009). Comparison between the Large-Scale Environments of Moderate and Intense Precipitating Systems in the Mediterranean Region. Mon. Wea. Rev., 137, 39333959.

Giorgi, F. (1990). Simulation of regional climate using a limited area model nested in a general circulation model. Journal of Climate, 3(9), 941-963.

Giorgi, F., and Mearns, L. O. (1999). Introduction to special section: Regional climate modeling revisited. Journal of Geophysical Research: Atmospheres (19842012), 104(D6), 6335-6352.

Grams, C. M., et al. (2014). Atmospheric processes triggering the central European floods in June 2013. Natural Hazards and Earth System Science, 14(7), 1691-1702.

Grell, G. A. (1993). Prognostic Evaluation of Assumptions Used by Cumulus Parameterizations. Mon. Wea. Rev., 121, 764787.

Grell, G. A. and D. Devenyi (2002). A generalized approach to parameterizing convection combining ensemble and data assimilation techniques. Geophys. Res. Lett., 29, 1693.

Groisman, P. Y. et al. (2005). Trends in Intense Precipitation in the Climate Record. J. Clim., 18, 13261350.

Han, J. and H. L. Pan (2011). Revision of convection and vertical diffusion schemes in the NCEP Global Forecast System. Wea. Forecasting, 26, 520533.

Hardwick Jones, R., et al. (2010). Observed relationships between extreme sub-daily precipitation, surface temperature, and relative humidity, Geophys. Res. Lett., 37, L22805.

Hazeleger, W., et al. (2015). Tales of future weather. Nat. Clim. Change 5(2), 107-113.

Heikkilä, U., et al. (2011). Dynamical downscaling of ERA-40 in complex terrain using the WRF regional climate model. Climate dynamics, 37(7-8), 1551-1564.

Held, I. M., and Soden, B. J. (2006). Robust responses of the hydrological cycle to global warming. Journal of Climate, 19(21), 5686-5699.

Herring, S. C., et al. (2014). Explaining extreme events of 2013 from a climate perspective. Bulletin of the American Meteorological Society, 95(9), S1-S104.

Hohenegger, C., et al. (2008). Towards climate simulations at cloud-resolving scales. Meteorologische Zeitschrift, 17(4), 383-394.

Hong, S.Y. and J.O. J. Lim (2006). The WRF singlemoment 6class microphysics scheme (WSM6). J. Korean Meteor. Soc., 42, 129151.

Hong, S.Y., Yign, N., and Dudhia, J. (2006). A new vertical diffusion package with an explicit treatment of entrainment processes. Mon. Wea. Rev., 134, 23182341.

Iacono, M. J., et al. (2008). Radiative forcing by longlived greenhouse gases: Calculations with the AER radiative transfer models. J. Geophys. Res., 113, D13103.

Janjic, Z. I. (1994). The StepMountain Eta Coordinate Model: Further developments of the convection, viscous sublayer, and turbulence closure schemes. Mon. Wea. Rev., 122, 927945.

Jimnez, P. A. and J. Dudhia (2012). Improving the Representation of Resolved and Unresolved Topographic Effects on Surface Wind in the WRF Model, J. Appl. Meteor. Climatol., 51, 300316.

Jones, R. G., et al. (1995). Simulation of climate change over europe using a nested regionalclimate model. I: Assessment of control climate, including sensitivity to location of lateral boundaries. Quarterly Journal of the Royal Meteorological Society, 121(526), 1413-1449.

Kain, J. S. (2004). The KainFritsch convective parametrisation: An update. J. Appl. Meteor., 43, 170181.

Karl, T. R., and R. W. Knight (1998). Secular Trends of Precipitation Amount, Frequency, and Intensity in the United States. Bull. Amer. Meteor. Soc., 79, 231241.

Kendon, E., et al. (2012). Realism of rainfall in a very high resolution regional climate model. J. Clim. 25, 57915806.

Kendon, E., et al. (2014). Heavier summer downpours with climate change revealed by weather forecast resolution model, Nat. Clim. Change, 4, 570576.

Kharin, V., et al. (2007). Changes in temperature and precipitation extremes in the IPCC ensemble of global coupled model simulations. J. Clim., 20(8), 1419-1444.

Kirtman, B., et al. Near-term Climate Change: Projections and Predictability. In: *Climate Change 2013: The Physical Science Basis.* Contribution of Working Group I to the Fifth Assessment Report of the Intergovernmental Panel on Climate Change [Stocker, T.F., D. Qin, G.-K. Plattner, M. Tignor, S.K. Allen, J. Boschung, A. Nauels, Y. Xia, V. Bex and P.M. Midgley (eds.)]. Cambridge University Press, Cambridge, United Kingdom and New York, NY, USA (2013).

Kitoh, Akio, et al. (2009). Projection of changes in future weather extremes using super-high-resolution global and regional atmospheric models in the KAKUSHIN Program: Results of preliminary experiments. Hydrological Research Letters 3:49-53.

Klein Tank, A. M. G., and Können, G. P. (2003). Trends in indices of daily temperature and precipitation extremes in Europe, 1946-99. Journal of Climate, 16(22), 3665-3680.

Knupp, K. R., and W. R. Cotton (1985). Convective cloud downdraft structure: An interpretive survey. Reviews of Geophysics 23.2:183-215.

Kotlyakov, V. M. et al. (2013). Flooding of July 67, 2012, in the town of Krymsk, Regional Research of Russia 3.1: 32-39, doi:10.1134/S2079970513010061.

Lackmann, G. M. (2014). Hurricane Sandy before 1900, and after 2100. Bulletin of the American Meteorological Society, 96, 547560.

Lean, H. W., et al. (2008). Characteristics of high-resolution versions of the Met Office Unified Model for forecasting convection over the United Kingdom. Monthly Weather Review 136.9:3408-3424.

Lenderink, G. and E. van Meijgaard (2008). Increase in hourly precipitation extremes beyond expectations from temperature changes. Nature Geosci., 1, 511514.

Li, F., et al. (2011a). Response of precipitation extremes to idealized global warming in an aquaplanet climate model: towards a robust projection across different horizontal resolutions. Tellus A 63.5:876-883.

Li, F., et al. (2011b). Impact of horizontal resolution on simulation of precipitation extremes in an aquaplanet version of Community Atmospheric Model (CAM3). Tellus A 63.5:884-892.

Loeptien, U., et al. (2008). Cyclone life cycle characteristics over the Northern Hemisphere in coupled GCMs. Climate Dynamics, 31(5), 507-532.

Lott, F. C., et al. (2013). Can the 2011 East African drought be attributed to humaninduced climate change?. Geophysical Research Letters, 40(6), 1177-1181.

Lucas-Picher, P., et al. (2008). Investigation of regional climate models internal variability with a ten-member ensemble of 10-year simulations over a large domain. Climate dynamics, 31(7-8), 927-940.

Lynch, P. (2006). *The emergence of numerical weather prediction: Richardson's dream.* Cambridge University Press.

Maraun, D., et al. (2010). Precipitation downscaling under climate change: Recent developments to bridge the gap between dynamical models and the end user. Reviews of Geophysics, 48(3).

Meredith et al. (2015). Crucial role of Black Sea warming in amplifying the 2012 Krymsk precipitation extreme, Nature Geosci., 8, 615-619.

Mesinger, F., et al. (2002). Limited area predictability: can upscaling also take place. Research Activities in Atmospheric and Oceanic Modelling, (32), 5-30.

MiguezMacho, G., et al. (2004). Spectral nudging to eliminate the effects of domain position and geometry in regional climate model simulations. Journal of Geophysical Research: Atmospheres (19842012), 109(D13).

Miguez-Macho, G., et al. (2005). Regional climate simulations over North America: Interaction of local processes with improved large-scale flow. Journal of climate, 18(8), 1227-1246.

Min, S.-K., et al. (2011). Human contribution to more intense precipitation extremes. Nature, 470(7334), 378-381.

Moberg, A., et al. (2006). Indices for daily temperature and precipitation extremes in Europe analyzed for the period 19012000. Journal of Geophysical Research: Atmospheres (19842012), 111(D22).

National Centers for Environmental Prediction/National Weather Service/NOAA/U.S. Department of Commerce. 2000, updated daily. NCEP FNL Operational Model Global Tropospheric Analyses, continuing from July 1999. Research Data Archive at the National Center for Atmospheric Research, Computational and Information Systems Laboratory. http://dx.doi.org/10.5065/D6M043C6. Accessed 20 Nov 2013.

Neu, U. et al. (2013). IMILAST: A community effort to intercompare extratropical cyclone detection and tracking algorithms. Bull. Amer. Meteor. Soc., 94, 529547.

Oguz, T., et al. (2006) Climatic regulation of the Black Sea hydro-meteorological and ecological properties at interannual-to-decadal time scales, Journal of Marine Systems, 60(3-4), 235-254, ISSN 0924-7963.

Orlowsky, B. and S. I. Seneviratne (2011). Global changes in extreme events: Regional and seasonal dimension. Climatic Change.

Otte, T. L., et al. (2012). Does nudging squelch the extremes in regional climate modeling? J. Clim. 25(20), 7046-7066.

Otto, F. E. (2015). Climate change: Attribution of extreme weather. Nature Geoscience, 8, 581582.

Pall, P. et al. (2011). Anthropogenic greenhouse gas contribution to flood risk in England and Wales in autumn 2000. Nature, 470(7334). 382-385.

Peterson, T. C., et al. (2012). Explaining extreme events of 2011 from a climate perspective. Bulletin of the American Meteorological Society, 93(7), 1041-1067.

Peterson, T. C., at al. (2013). Explaining extreme events of 2012 from a climate perspective. Bulletin of the American Meteorological Society, 94(9), S1-S74.

Petoukhov, V., and Semenov, V. A. (2010). A link between reduced BarentsKara sea ice and cold winter extremes over northern continents. Journal of Geophysical Research: Atmospheres (19842012), 115(D21).

Prein, A. F., et al. (2013). Added value of convection permitting seasonal simulations. Climate Dynamics 41.9-10, 2655-2677.

Prein, A. F., et al. (2015). A review on regional convectionpermitting climate modeling: demonstrations, prospects, and challenges. Reviews of Geophysics, 53, 323-361.

Rayner, N. A.. et al. (2003) Global analyses of sea surface temperature, sea ice, and night marine air temperature since the late nineteenth century, J. Geophys. Res.Vol. 108, No. D14, 4407.

Reynolds, R. W., et al. (2007). Daily High resolution Blended Analyses for sea surface temperature. J. Clim., 20, 5473-5496.

Rinke, A., and Dethloff, K. (2000). On the sensitivity of a regional Arctic climate model to initial and boundary conditions. Climate Research, 14(2), 101-113.

Roberts, N. (2008). Assessing the spatial and temporal variation in the skill of precipitation forecasts from an NWP model. Meteorological Applications, 15(1), 163-169.

Roeckner, E., e al. (2003). The atmospheric general circulation model ECHAM 5. PART I: Model description.

Rummukainen, M. (2010). Stateoftheart with Regional Climate Models. Wiley Interdisciplinary Reviews: Climate Change, 1(1), 82-96.

Schär, C., and Jendritzky, G. (2004). Climate change: hot news from summer 2003. Nature, 432(7017), 559-560.

Schoenberg Ferrier, B., et al. (1996). Factors responsible for precipitation efficiencies in midlatitude and tropical squall simulations. Monthly weather review 124.10:2100-2125.

Semenov, V. A. and L. Bengtsson (2002). Secular trends in daily precipitation characteristics: greenhouse gas simulation with a coupled AOGCM, Clim. Dyn., 19, 123140.

Semenov, V. A., and Latif, M. (2015). Nonlinear winter atmospheric circulation response to Arctic sea ice concentration anomalies for different periods during 19662012. Environmental Research Letters, 10(5), 054020.

Seneviratne, S.I. et al. (2012). Changes in climate extremes and their impacts on the natural physical environment. In: Managing the Risks of Extreme Events and Disasters to Advance Climate Change Adaptation [Field, C.B., V. Barros, T.F. Stocker, D. Qin, D.J. Dokken, K.L. Ebi, M.D. Mastrandrea, K.J. Mach, G.-K. Plattner, S.K. Allen, M. Tignor, and P.M. Midgley (eds.)]. A Special Report of Working Groups I and II of the Intergovernmental Panel on Climate Change (IPCC). Cambridge University Press, Cambridge, UK, and New York, NY, USA, pp. 109-230.

Seth, A., and Giorgi, F. (1998). The effects of domain choice on summer precipitation simulation and sensitivity in a regional climate model. Journal of Climate, 11(10), 2698-2712.

Shepherd, J. M., et al. (2001). Rainfall morphology in Florida convergence zones: A numerical study. Monthly weather review 129.2:177-197.

Shuman, F. G. (1989). History of numerical weather prediction at the National Meteorological Center. Weather and Forecasting, 4(3), 286-296.

Skamarock, W. C., et al. (2008). A description of the Advanced Research WRF version 3. NCAR Tech. Note NCAR/TN-475+STR, 125 pp.

Stott, P. A., et al. (2004). Human contribution to the European heatwave of 2003. Nature, 432(7017), 610-614.

Stott, P. A., et al. (2013). Attribution of weather and climate-related events. In *Climate Science for Serving Society* (pp. 307-337). Springer Netherlands.

Tewari, M. et al. (2004). Implementation and verification of the unified NOAH land surface model in the WRF model. *20th conference on weather analysis and forecasting/16th conference on numerical weather prediction, pp. 1115.*

Tiedtke, M. (1989). A comprehensive mass flux scheme for cumulus parameterization in largescale models. Mon. Wea. Rev., 117, 17791800.

Torma, C., Giorgi, F., and Coppola, E. (2015). Added value of regional climate modeling over areas characterized by complex terrainPrecipitation over the Alps. Journal of Geophysical Research: Atmospheres, 120, 39573972..

Trenberth, K. E. (1999). Conceptual framework for changes of extremes of the hydrological cycle with climate change. In Weather and Climate Extremes (pp. 327-339). Springer Netherlands.

Trenberth, K. E., et al. (2003). The changing character of precipitation. Bulletin of the American Meteorological Society, 84(9), 1205-1217.

Trenberth, K. E. (2011). Changes in precipitation with climate change. Climate Research, 47(1), 123.

Trenberth, K. E. (2012). Framing the way to relate climate extremes to climate change. Climatic change, 115, 283-290.

Trenberth, K. E., et al. (2015). Attribution of climate extreme events. Nature Climate Change, 5, 725730.

Tilinina, N., et al. (2013) Comparing cyclone life cycle characteristics and their interannual variability in different reanalyses. Journal of Climate 26(17), 6419-6438.

Veljovic, K., et al. (2010). Regional climate modeling: Should one attempt improving on the large scales? Lateral boundary condition scheme: Any impact?. Meteorologische Zeitschrift, 19(3), 237-246.

Volosciuk, C., et al. (2015). Extreme Precipitation in an Atmosphere General Circulation Model: Impact of Horizontal and Vertical Model Resolution. J. Clim., 28(3), 11841205.

von Storch, H., et al. (2000). A spectral nudging technique for dynamical downscaling purposes. Monthly weather review, 128(10), 3664-3673.

Waldron, K. M., et al. (1996). Sensitivity of a spectrally filtered and nudged limited-area model to outer model options. Monthly weather review, 124(3), 529-547.

Warner, T. T., et al. (1997). A tutorial on lateral boundary conditions as a basic and potentially serious limitation to regional numerical weather prediction. Bulletin of the American Meteorological Society, 78(11), 2599-2617.

Warner, T. T., and H-M Hsu (2000). Nested-model simulation of moist convection: The impact of coarse-grid parameterized convection on fine-grid resolved convection. Monthly weather review 128.7:2211-2231.

Weisman, M. L., et al. (2008). Experiences with 0-36-h explicit convective forecasts with the WRF-ARW model. Weather and Forecasting, 23(3), 407-437.

Wong, G., et al. (2014). Stochastic model output statistics for bias correcting and downscaling precipitation including extremes. J. Clim. 27(18), 6940-6959.

Yang, Qing, et al. (2014). Atmospheric moisture budget and spatial resolution dependence of precipitation extremes in aquaplanet simulations. J. Clim. 27(10), 3565-3581.

Ye, H., and Fetzer, E. J. (2010). Atmospheric moisture content associated with surface air temperatures over northern Eurasia. International Journal of Climatology, 30(10), 1463-1471.

Zhang, C., et al. (2011). Improved representation of boundary layer clouds over the southeast pacific in ARWWRF using a modified Tiedtke cumulus parameterization scheme. Mon. Wea. Rev., 139, 34893513.

Zhang, X., et al. (2007). Detection of human influence on twentieth-century precipitation trends. Nature, 448(7152), 461-465.

MM5 similarity scheme references:

Paulson, C. A. The mathematical representation of wind speed and temperature profiles in the unstable atmospheric surface layer. J. Appl. Meteor., 9, 857861 (1970).

Dyer, A. J., and Hicks, B. B. Fluxgradient relationships in the constant flux layer. Quart. J. Roy. Meteor. Soc., 96, 715721 (1970).

Webb, E. K. Profile relationships: The log-linear range, and extension to strong stability. Quart. J. Roy. Meteor. Soc., 96, 6790 (1970).

Beljaars, A.C.M. The parametrisation of surface fluxes in large-scale models under free convection. Quart. J. Roy. Meteor. Soc., 121, 255270 (1994).

Zhang, D.L., and Anthes, R.A. A highresolution model of the planetary boundary layer sensitivity tests and comparisons with SESAME79 data. J. Appl. Meteor., 21, 15941609 (1982).

Abbreviations

AGCM	Atmospheric General Circulation Model
AV	Added Value
BSM	Black Sea and Mediterranean
CAPE	Convective Available Potential Energy
CC	Clausius-Clapeyron
CIN	Convective Inhibition
CPM	Convection-permitting Model
CPS	Convection-permitting Simulation
DFG	Deutsche Forschungsgemeinschaft
GEV	Generalized Extreme Value
IV	Internal Variability
LAM	Limited Area Model
NWP	Numerical Weather Prediction
PBL	Planetary Boundary Layer
RCM	Regional Climate Model
SST	Sea Surface Temperature
USL	Updraught Source Layer
WRF	Weather Research and Forecasting model

List of Figures

List of Tables

Publications

Crucial role of Black Sea warming in amplifying the 2012 Krymsk precipitation extreme, EP Meredith, VA Semenov, D Maraun, W Park and AV Chernokulsky, and published in Nature Geoscience, Vol. 8, pp. 615-619 (2015).

Evidence for added value of convection-permitting models for studying changes in extreme precipitation, EP Meredith, D Maraun, VA Semenov and W Park, Journal of Geophysical Research: Atmospheres. (Accepted)

Acknowledgements

So many people to thank...

Being a PhD student at GEOMAR has been an extremely enjoyable experience. However, without my supervisors Douglas Maraun and Wonsun Park giving me the opportunity to become a member of the Eurex project, it wouldn't have been possible. So for that, I shall be forever grateful. In addition to that, the quality of supervision provided during my time in GEOMAR was excellent, and allowed me to learn many new and interesting things. While he wasn't my supervisor, another person who I learnt so many new things from was Vladimir Semenov, who like DM and WP always had lots of good advice, suggestions and time. All three were instrumental in creating the Eurex project in which I was lucky to participate. Also thanks to the Helmholtz Foundation for funding the project.

I would also like to thank Claudia Volosciuk, my Mitdoktorandin in the Eurex project, who provided assistance with things too numerous to list and was also very nice to share an office and trips to Russia with. On that topic, all the people I shared the office with made for a nice working environment, so thanks also to Geraldine, Emanuele, Ana, Julian, Tom, Nadine, Rosanna, Jan, and all the short-term visitors.

I would also like to thank all of my other Russian colleagues from the Eurex project, who really treated us well whenever we visited Russia. So thanks to Mirseid, Sergey Gulev, Natalia, Maxim, and Slava. Special thanks are reserved for Alexander Chernokulsky and Alexander Gavrikov.

Other people who provided great assistance were Jan Harlaß and Guidi Zhou.

A big thanks also to all the people in the ME department, present and past, at GEOMAR for being very nice colleagues and always helpful. Also thanks to ISOS for running a great programme.

Finally, I would like to thank Professors Daniela Domeisen, Mojib Latif, Katja Matthes and Martin Wahl for agreeing to serve on my PhD committee.

Eidesstattliche Erklärung

Hiermit erkläre ich, dass die vorliegende Doktorarbeit selbständig unter Befolgung der Regeln guter wissenschaflicher Praxis der Deutschen Forschungsgemeinschaft (DFG) verfasst wurde und keine über die angegebenen Quellen hinausgehenden Hilfsmittel verwendet wurden. Ich versichere, dass diese Arbeit noch nicht zur Erlangung eines Doktorgrades an anderer Stelle vorgelegen hat.

Kiel im Oktober 2015

(Edmund Meredith)